THESE

Présentée pour obtenir le titre de
DOCTEUR DE L'UNIVERSITE LOUIS PASTEUR DE STRASBOURG
Ecole doctorale Mathématiques, Sciences de l'Information et de l'Ingénieur

Frequency-comb stabilized laser sources for absolute distance metrology at the Very Large Telescope Interferometer

par
Nicolas Schuhler

Soutenue le 27 novembre 2006 devant la commision d'examen:

Pr. P. Meyrueis, Examinateur, Directeur de Thèse
Directeur du Laboratoire de Systèmes photoniques, Strasbourg

Pr. Joël Fontaine, Rapporteur Interne
Professeur á l'Institut National des Sciences Appliquées, Strasbourg

Pr. E. Wagner, Rapporteur Externe
Leiter des Fraunhofer Institut für Physikalische Messtechnik, Freiburg

Pr. Y. Renotte, Rapporteur Externe
Professeur au laboratoire de Physique Générale, Université de Liège

Dr. P. Pfeiffer, Co-superviseur
Laboratoire de Systèmes photoniques, Strasbourg

Dr. S. Lévêque, Co-superviseur
European Southern Observatory, Garching beï München

Acknowledgements

I would like to thank P. Meyrueis for agreeing to supervise this thesis and for his valuable comments.

This thesis would not have been possible without the continuous and invaluable support provided by S. Lévêque who guided my work throughout the last three years. His patience and his experience have been indispensable to carry out this thesis.

I would also like to thank A. Glindeman and all the members of the VLTI group at the European Southern Observatory (ESO) for their welcome and collaboration.

I would like to express my special thanks to M. Accardo, G. Fischer and R. Frahm who always kindly provided me with the support I needed.

I am also very grateful to Y. Salvadé for welcoming me in his laboratory for one month (Laboratory of Metrology, Haute Ecole ARC, St-Imier, Switzerland), sharing his experience on metrology and exchanging many interesting ideas.

My acknowledgments are also directed to R. Holzwarth (Insitüt für Quantum Optik, Garching beï München and Menlo Systems GmbH, Martiensried, Germany) for his support with the optical frequency comb generator. The help of P. Kubina (Menlo Systems GmbH) is gratefully acknowledged.

Finally, I would like to thank the members of the Examination Board for agreeing to referee this dissertation and for their constructive comments.

Abstract

The forthcoming instrument of the Very Large Telescope Interferometer (VLTI), called Phase-Referenced Imaging and Micro-arcsecond Astrometry facility (PRIMA), uses a laser metrology system to monitor the variations of internal path lengths. This dissertation addresses the development, integration and test of frequency stabilized laser sources for the PRIMA Metrology system (PRIMET).

In the first part, we present in the context of PRIMA and the VLTI the specifications of PRIMET. We recall the basics of single-wavelength laser interferometry and introduce the problems raised by its application to PRIMET. We present the need for the absolute frequency stabilization of PRIMET laser and the interest for an upgrade of PRIMET towards absolute distance measurements.

In the second part, we present our contribution to the absolute frequency stabilization of PRIMET Nd:YAG laser on a transition of iodine. We characterize the system and measure precisely its performance with a self-referenced optical frequency comb. We improve the system to reach the specifications in terms of accuracy and stability of the locking frequency.

The third part addresses the upgrade of PRIMET towards absolute distance measurements by the use of two-wavelength interferometry. We propose a new concept of two-wavelength laser source frequency stabilized on an optical frequency comb. This permits the generation of an unprecedented large choice of synthetic wavelength with a relative accuracy better than 10^{-11} in vacuum. We validate the concept on a prototype and shows that it can be used to resolve an optical wavelength. Finally, we propose to apply this concept to the upgrade of PRIMET.

Keywords : laser metrology, absolute distance measurements, two-wavelength interferometry, laser frequency stabilization, optical frequency comb, heterodyne interferometry, Very Large Telescope Interferometer

Résumé

Le très grand télescope interférométrique européen (VLTI) sera bientôt équipé d'un nouvel instrument, appelé instrument pour l'imagerie à référence de phase et l'astrométrie micro-arcseconde (PRIMA). Cet instrument utilise un système de métrologie laser pour mesurer les variations de chemins optiques internes au VLTI. L'étude présentée dans ce mémoire porte sur le développement, l'intégration et le test de sources lasers stabilisées en fréquence pour le système de métrologie de PRIMA (PRIMET).

Dans une première partie, nous présentons le cahier des charges de PRIMET dans le contexte de PRIMA et du VLTI. Nous rappellons les bases de l'interférométrie laser à une longueur d'onde et introduisons les problèmes qu'impose son application à PRIMET. Nous en déduisons la nécessité de stabiliser la longueur d'onde du laser de PRIMET sur une référence absolue et expose l'intérêt de transformer ultérieurement PRIMET en un système de mesure de distances absolues.

Dans une seconde partie, nous décrivons notre contribution à la stabilisation en fréquence du laser Nd:YAG de PRIMET sur une raie d'absorption de l'iode. Nous mesurons précisément les performances du système avec un peigne de fréquences optiques auto-référencé. Nous améliorons le système pour satisfaire aux exigences du cahier des charges.

La troisième partie est consacrée à la transformation de PRIMET en un système de mesure de distances absolues par l'utilisation de l'interférométrie à deux longueurs d'onde. Nous proposons un nouveau concept de source laser qui utilise un peigne de fréquences optiques comme référence de fréquence. Cette source permet de générer un choix sans précédent de longueurs d'onde synthétiques avec une précision relative dans le vide meilleure que 10^{-11}. Nous validons le concept sur un prototype et montrons qu'il peut être utilisé en interférométrie à deux longueurs d'onde pour résoudre une longueur d'onde optique. Enfin, nous appliquons ce concept au design d'une nouvelle version de PRIMET.

Mots clés : métrologie laser, mesure de distance absolue, peigne de fréquences optiques, interférométrie hétérodyne, Very Large Telescope Interferometer

Symbols

- OPL: Optical Path Length
- OPD: Optical Path Difference
- c: speed of light, 299792458ms^{-1}
- λ: wavelength
- ν: frequency
- k=$\frac{2\pi}{\lambda}$: wave number
- τ: time delay
- $\mathbf{B}$: baseline of the interferometer
- $\Delta\Phi$: phase difference between two signals
- $\langle . \rangle$: time average
- $\mathcal{F}\{.\}$: denotes the Fourier transform
- $.^{\star}$: denotes the complex conjugate
- $E(\mathbf{r}, t)$:electric field considered at a point $\mathbf{r}$ at time t
- $A(\mathbf{r}, t)$: complex amplitude of a wave considered at a point $\mathbf{r}$ at time t
- ϵ: permittivity of the medium
- μ: permeability of the medium
- δA: differential atmospheric piston in dual-feed interferometry
- ΔL: difference of OPD seen by the stellar light in a dual-feed interferometer

- $\mathbf{\Delta S}$: difference of the two vectors pointing towards the two objects of a dual feed interferometer
- I: intensity
- n: refractive index
- λ: wavelength in a vacuum
- L: length difference between the two arms of a Michelson interferometer in a "vacuum"
- M: fringe order
- f(M): fractionnal part
- Φ: phase of the an interferometric signal (taken between $[-\pi;\pi]$)
- $\Phi_{unwrapped}$: unwrapped phase of the interferometric signal (with the phase equal to zero at zero OPD
- $\Delta\nu$: heterodyne frequency
- η: polarization cross-talk phase error in heterodyne interferometry
- ρ: cross-talk ratio, amplitude of the leakage wave over amplitude of the desired wave
- $\mathcal{V}$: fringe visibility

Acronyms

- ADC: Analog-to-Digital Converter
- AMBER: Astronomical Multi-BEam combineR
- AOM: Acousto Optic Modulator
- AT: Auxiliary Telescope
- BS: Beam Splitter
- DAC: Digital-to-Analog Converter
- DDL: Differential Delay Lines
- DL: Delay Line
- EOM: Electro-Optic Modulator
- EMC: Electro-Magnetic Compatibility
- ESO: European Southern Observatory
- FSU: Fringe Sensor Unit
- FWHM: Full Width at Half Maximum
- IMT: Institute of Microtechnology of Neuchâtel
- LP: Linear Polarizer
- LCU: Local Control Unit
- MACAO: Multi Application Curvature Adaptive Optics
- MIDI:Mid-Infrared Interferometric Instrument
- MPQ: Max Planck institute for Quantum optics

- NAR: Non Ambiguity Range
- Nd:YAG: Neodymium-doped Yttrium Aluminum Garnet
- NPRO: Non Planar Ring Oscillator
- OFCG: Optical Frequency Comb Generator
- OPD: Optical Path Difference
- OPL: Optical Path Length
- PBS:Polarizing Beam Splitter
- PD: PhotoDiode
- PID: Proportional-Integral-Derivative corrector
- PLL:Phase Lock Loop
- PRIMA: Phased-Referenced Imaging and Micro-arcsecond Astrometry
- PRIMET: PRIMA Metrology System
- RAM: Residual Amplitude Modulation
- SH: Second Harmonic
- SHG: Second Harmonic Generation
- SM-PM: Single Mode - Polarization Maintaining
- SNR: Signal to Noise Ratio
- StS: Star Separator
- TAC: Tools for Advanced Control library
- UT: Unit Telescope
- VCM: Variable Curvature Mirror
- VLTI: Very Large Telescope Interferometer

Contents

List of Figures

List of Tables

Introduction

The context of the thesis

The European Southern Observatory (ESO), is developing a new instrument for its Very Large Telescope Interferometer (VLTI) with the aim of detecting extra-solar planets and characterizing their orbits. This new instrument, called the Phase-Referenced Imaging and Micro-arcsecond Astrometry facility (PRIMA), will use a laser interferometer to monitor in real time the internal optical path variations introduced between several telescopes by vibrations and atmospheric turbulence. The most challenging astronomical observations demand an accuracy better than 5 nm over a stroke of 60 mm. In order to achieve the instrument main scientific goal, i.e the detection of extra-solar planets, such measurements carried out over half an hour must be repeatable over several years. This sets high specifications on the accuracy and on the stability of the laser interferometer wavelength.

The two problems addressed by the thesis

This thesis addresses two problems related respectively to the laser source of the PRIMA metrology system (PRIMET) and to its future upgrade.

The absolute frequency stabilization system of the PRIMA metrology system laser was delivered to ESO by the institute of Micro-technology of Neuchâtel. At the delivery, the system was not fully functional and its performance had not been measured. That is why our characterize it precisely and improve it to reach the specifications.

The first version of PRIMET will require a time consuming calibration due to its incremental approach. Consequently an upgrade of PRIMET toward absolute distance measurements is considered. As a result, a new concept of accurate and tunable multiple-wavelength light source based on the use of an optical frequency comb is proposed and validated by means of a prototype. The experimental results are used to propose a design for PRIMET upgrade.

Outline of the thesis

Part I

The first part recalls the context of the thesis. The origins of the two problems addressed in this manuscript are presented. Some classical results and some concepts more specific to PRIMA, used throughout the whole thesis, are addressed in this part.

The first chapter presents the Very Large Telescope Interferometer and its instrument PRIMA. PRIMA uses simultaneously two interferometers to observe two different astronomical objects. The two interferometric signals are tied together by the difference of optical path travelled by the stellar light between the telescopes. A subsystem of PRIMA, called PRIMET, is used to measure the difference of optical path differences between the two interferometers. A brief description of PRIMA and of its functions is given to justify the specifications of PRIMET.

The second chapter recalls the basics of single-wavelength laser interferometry. It presents the principle of laser interferometry and underlines the limited measurement range when it is not operated incrementally. Phase measurement based on heterodyne interferometry is addressed. The error sources in single-wavelength interferometry are analyzed. A general equation is given to estimate the magnitude of polarization cross-talk error in heterodyne interferometry. Finally, the importance of the wavelength calibration and stability is emphasized to stress the need of an absolute frequency stabilization system for PRIMET. This system is the subject of Part II.

The third chapter describes the design of PRIMET to highlight its differences with common laser interferometers and explain some specific technical choices. In particular, it explains the principle of superheterodyne interferometry which allows to measure directly and in real time the OPD difference between two interferometers. Various subsystems of PRIMET used in experiments described in this thesis are briefly described in this chapter. Finally the limitations of the incremental implementation of PRIMET are discussed to justify an upgrade of the system towards absolute distance measurement. This upgrade is the subject of Part III.

Part II

The stability and the calibration of the wavelength of PRIMET laser interferometer play a major role in the accuracy of the measurements. In this part we test the frequency stabilization system delivered to ESO and we improve some of its performance to reach the specifications.

PRIMET laser wavelength must be known with a relative accuracy of 10^{-8} over several years. Therefore, it must be stabilized on an absolute frequency reference provided by an atomic absorption line. In Chapter 4, we recall the basics of laser frequency stabilization and present our contribution to the development of the PRIMET laser frequency stabilization. The Nd:YAG laser is stabilized on a transition of iodine (I_2) at 659.5 nm using the Pound-Drever-Hall method. We have carried out preliminary studies on the frequency doubling of the laser light and on the iodine spectrum to help defining the hardware components used in the final system. The design and integration of the absolute frequency stabilization system was subcontracted to the Institute of Micro-Technology of Neuchâtel (IMT). We modified the control loop of the system delivered by IMT to enable the frequency locking on long time scales by the use of a second frequency actuator.

The difficulty of locking the frequency of Nd:YAG lasers emitting at 1.3 microns, such as PRIMET laser, is to find a frequency reference and an accurate frequency sensor. These problems apply similarly to the tests of the laser stability. In Chapter 5, we describe the experiments we carried out to characterize the system and improve it when it was feasible and relevant. We have first modeled the error signal generated by the Pound-Drever-Hall method. The model is compared to experimental results and is used to estimate the performance of the system in closed loop. In order to investigate the presence of detection noise in the stabilization system, we have used a self-referenced optical frequency comb as an independent frequency sensor. Furthermore, we took advantage of the high accuracy of the comb to calibrate the locking frequency of the laser and its repeatability over a few days. From these results, we propose and validate some possible improvements of the set-up. Finally, we compare the performance of the system to the specifications

Although the atomic transition provides an absolute reference, environmental conditions may alter the set-up. Therefore, it is required to calibrate the locking frequency of the system in its final environment. It may even be interesting to calibrate periodically the laser locking frequency to take into account some possible long term drifts due to the aging of the set-up. In Chapter 6, we study the feasibility of the calibration of PRIMET wavelength by comparison with a stabilized laser interferometer available at the observatory.

Part III

The initial version of PRIMET, based on classical incremental laser metrology requires a time consuming calibration before every observation. Part III addresses the problem of a possible upgrade of PRIMET which would reduce the calibration time.

In Chapter 7, we recall the principle of two-wavelength interferometry to measure a distance with a larger synthetic wavelength. We describe the algorithm used to link two-wavelength and single-wavelength measurements. In order to be applied this algorithm requires that the two-wavelength measurement is more precise than half an optical wavelength. We analyze the sources of error to show the role of the calibration and stabilization of the synthetic wavelength in the two-wavelength measurement error.

The state of the art given about the laser sources used for two-wavelength interferometry shows that the main limitations of these sources are the range of available synthetic wavelengths and the wavelength accuracy. In order to overcome these problems, we propose to stabilize two lasers over wide frequency ranges on an optical frequency comb generated by a femtosecond pulsed laser. In Chapter 8, we describe the principle of such a source which can generate an unprecedented choice of synthetic wavelengths with high accuracy. We have build and tested a two-wavelength source prototype. Experimental results are presented on the calibration of the synthetic wavelength. A two-wavelength interferometer based on this source is compared to a commercial laser interferometer to demonstrate that it can resolve an optical wavelength.

Finally, Chapter 9 describes an upgrade of PRIMET based on the new concept of two-wavelength laser source and on the experimental results obtained with the prototype. The two-wavelength interferometer used in the previous chapter is modified to permit differential OPD measurement. The system uses an external cavity laser diode to generate a chain of decreasing synthetic wavelength used to calibrate the differential OPD in a few seconds instead of a few minutes. We calculate the characteristics of the wavelength chain that could be used to calibrate PRIMET.

Conclusion

All the results obtained in the thesis are summarized in the thesis conclusion. Finally an overview of the continuations of this work is presented.

Part I

Context and problems : frequency stabilised laser sources for distance metrology inside the VLTI

Forewords

This first part aims at setting the background of the work presented in this thesis, the Phase-Referenced Imaging and Micro-arcsecond Astrometry instrument of the European Southern Observatory, and at defining its two objectives : the development of an absolutely stabilized laser source for incremental superheterodyne interferometry and its upgrade toward a stabilized multiple-wavelength laser source for absolute metrology .

Chapter 1 introduces briefly the Very Large Telescope Interferometer of the European Southern Observatory and its forthcoming instrument PRIMA. The specifications of its laser metrology system will serve as a basis through the whole thesis.

Such specifications can be met only by the use of single-wavelength interferometry which is the subject of *Chapter 2*. The principle of this technique and its main drawback, known as the Non Ambiguity Range limitation, are presented. In particular, the need of this technique for an absolutely frequency stabilized laser source for large OPD measurement, which forms the first axis of research of this thesis, is addressed.

In *Chapter 3* all the elements described in the first two chapters are used to explain the technical choices made for the PRIMA incremental metrology system. The limitations of this system, which lead to the development of an absolute metrology system, are presented. The technical constraints presented in this chapter apply also to the upgrade of PRIMET that we propose in Part III.

Outline of Part I

Chapter 1

Context : why does the VLTI need a new laser metrology system?

This thesis addresses the problem of frequency stabilized laser sources for single wavelength and ultimately multiple-wavelength metrology. The general concepts used or developed during this work are applied to the particular case of the metrology system of PRIMA a forthcoming instrument of the European Southern Observatory Very Large Telescope Interferometer.

This chapter presents the framework of this thesis. It recalls the reason why a new metrology system is required for the VLTI and it insists on its specifications which make its particularity.

1.1 The Very Large Telescope Interferometer

At the beginning of the eighties the European Southern Observatory started the project of a 16 m telescope called the Very Large Telescope. After several delays and modifications the project was shifted into an array of four big telescopes and several smaller telescopes that could be applied to long baseline stellar interferometry [Law00].

The Very Large Telescope Interferometer (VLTI), last described in [Ga04], is part of the Paranal Observatory which is build on top of the Cerro Paranal (2635 m, latitude -25.62 °) in the Atacama desert, Chile.

At the time being the complete VLTI is expected to have access to the four 8 m diameter telescopes, Unit Telescopes (UT), and to use four 1.8 m diameter telescopes, Auxiliary Telescopes (AT), completely devoted to interferometry and relocatable in 30 different stations. The four UTs and the

Figure 1.1: The Paranal Observatory home of the Very Large Telescope Interferometer

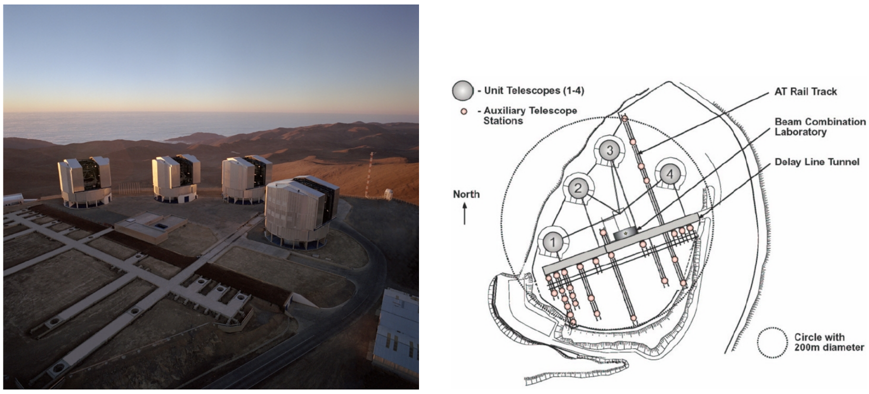

ATs stations are shown on Figure 1.1. The maximum distance between the two telescopes of the interferometer, which defines the theoretical angular resolution of the system, is 128 m with two UTs and 200 m with two ATs. The four UTs and the 30 stations that can receive an AT are linked together by a network of tunnels. These tunnels accommodate the delay lines which compensate for the optical path difference and relay the beam to the interferometric laboratory. The beams coming from the telescopes are recombined in the laboratory using different instruments, Figure 1.2.

The first stellar fringes have been obtained in March 2001 with two UTs, [PRf01], and in March 2005 with two ATs, [PRf05]. First scientific results with two UTs were achieved in November 2001, [Sci01]. Since then several articles have been published based on VLTI data, most of them are listed in the Publications section of [Law] along with articles based on other interferometers measurements.

The VLTI is currently equipped with 3 instruments VINCI, MIDI and AMBER. The last instrument of the first generation, PRIMA, whose metrology system is the framework of this thesis, is described briefly in the next section. In addition to these instruments the VLTI is equipped with several facilities to compensate for the effects of the atmospheric or internal turbulence : adaptive optics systems for all the UTs ([Aa04]), fringe trackers and a tip-tilt sensor placed after the delay lines.

Figure 1.2: Top: simplified sketch of the VLTI optical train. Bottom: map of the VLTI laboratory with the test instrument VINCI, the first generation instruments (VINCI, MIDI, AMBER and PRIMA) and the different facilities.

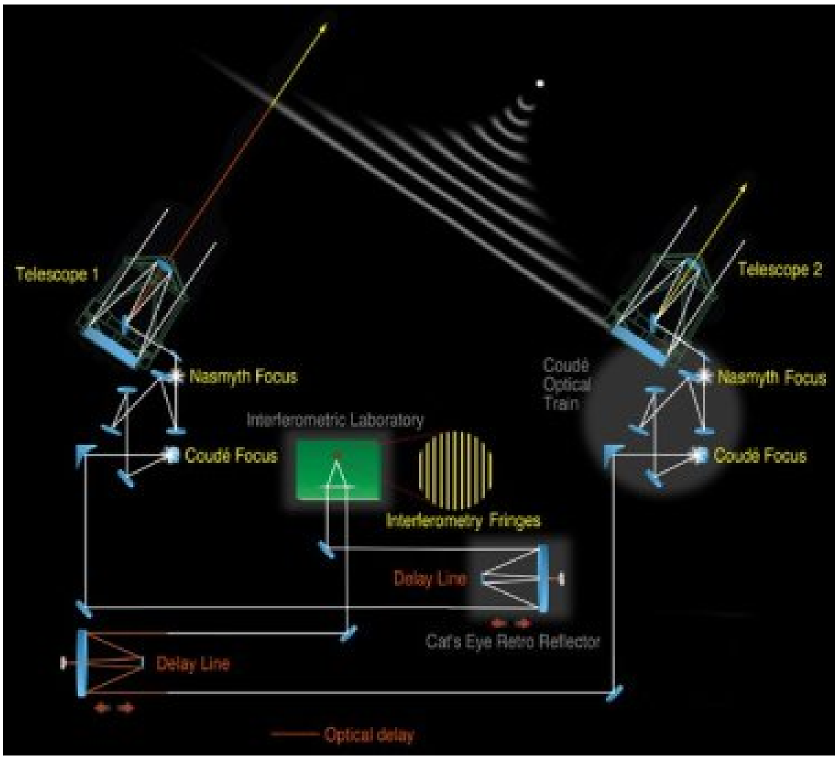

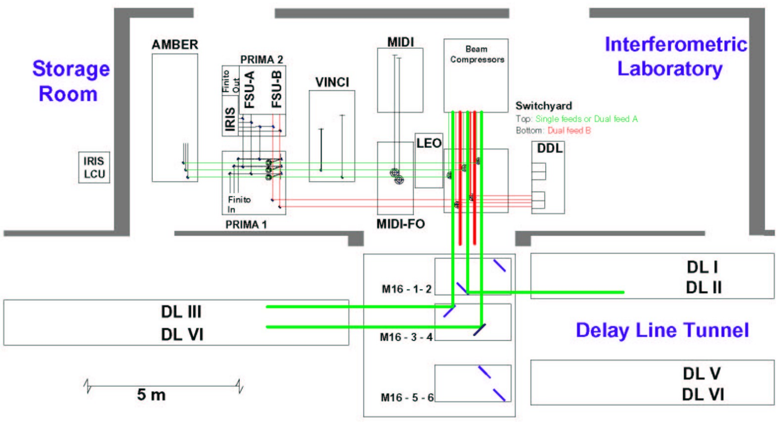

1.2 The Phase-Referenced Imaging and Micro-arc-second Astrometry facility

The "Phase-Referenced Imaging and Micro-arc-second Astrometry" (PRIMA) facility of the VLTI is based on the simultaneous coherent observation of two celestial objects in which the two interferometric signals are tied together by an internal metrology system, [DLK+00]. The role of this metrology system is to monitor the PRIMA instrumental optical path errors to reach a final instrumental phase accuracy limited by the atmospheric piston anisoplanatism (defined in [ERF00]). Such a system, called dual feed interferometer, is used for phase-referenced imaging (described in [Law00]) and for narrow angle astrometry (as proposed by Shao in [SM92]). Scientific objectives of PRIMA are described in [PDD+03].

The PRIMA facility will be installed on the UTs and on the ATs. It will be optimized for phase-referenced imaging on faint objects from $1\,\mu$m to $10\,\mu$m on the UTs and for micro-arc-second astrometry, between $1.5\,\mu$m and $2.2\,\mu m$ on the ATs. At the moment PRIMA is expected to work with two UTs or two ATs.

General scheme

PRIMA should fulfill the following general requirements:

- pick up two stars at the Coudé focus of both telescopes and follow them accurately;
- redirect both collimated beams parallel to each other, through the VLTI light ducts and the delay lines, down to the interferometric laboratory;
- introduce an accurate and variable differential delay between both star lights;
- track the fringes on the brightest star in order to co-phase the telescopes, and measure the fringe phase residuals;
- detect and measure the faint star fringes on the second feed;
- measure the total differential delay between both star light paths in the interferometer.

To perform these tasks PRIMA is constituted of four subsystems distributed all over the VLTI. The *star separators* (StS, described in [DNdM+03]) at the Coudé foci of the telescopes pick up the two stars and their surrounding field and inject the beams toward the VLTI main delay lines. In the laboratory *differential delay lines* are installed to tune the differential delay between the light coming from the two stars. Two *fringe sensors/trackers*, Fringe Sensors Units (FSU), (one of which used as the astrometric camera) recombine the two pairs of stellar beams to measure the movement of the stellar fringes so as to compensate for it with the delay lines. Finally a *laser metrology system* is used to measure the difference of OPD created in the VLTI between the two interferometers. The laser beam is injected in the optical train at the level of the FSU and its end points are located in the StS. PRIMA general scheme is summarized in Figure 1.3.

Figure 1.3: General principle of PRIMA.

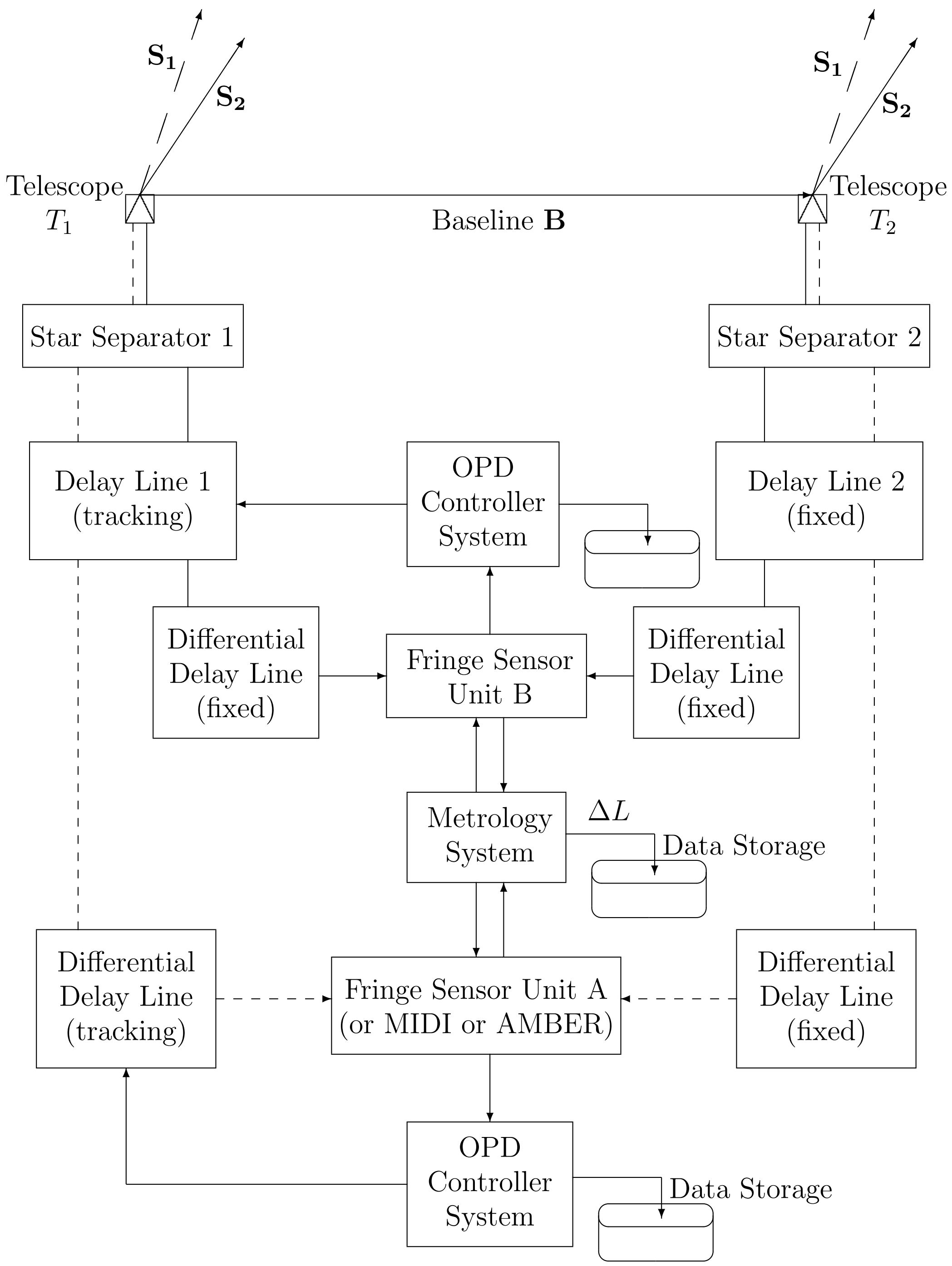

1.3 Specifications of the PRIMA Metrology System

A highly accurate metrology system is required to monitor the PRIMA instrumental optical path errors to reach a final instrumental phase accuracy limited by the atmospheric piston anisoplanetism. The metrology system shall measure the internal differential delay seen by the stellar light, ΔL, between both channels with a 5 nm (standard deviation) accuracy goal (or $\lambda/200$ for λ=1 μm), over typically 30 min. The accuracy requirement is driven by the astrometric mode, but can be relaxed by a factor 50 to 100 in the imaging mode, and depending on the observing parameters. In addition to an ambitious accuracy objectives, the metrology system has to cope in particular with a long and air filled light path. The sampling frequency is set by the FSU which works at 8 kHz.

In observing conditions, the amplitude of ΔL can reach about 60 mm. However, the metrology system must monitor the entire internal path of the VLTI, along hundred of meters, to obtain an accurate estimation of ΔL by eliminating equivalent dead path error.

Table 1.1: Specifications for PRIMET.

Observable	Differential optical path length seen by the stellar light
Maximum differential OPD (single way), ΔL	60 mm
Distance of propagation	500 m for each interferometer
Resolution	1 nm
Accuracy	5 nm
Sampling frequency	$\geq$ 8 kHz

Chapter 2

First problem : Single Frequency Laser Interferometry and need for an absolutely frequency stabilized laser source

The PRIMA metrology system has an ambitious goal of 5nm (standard deviation) accuracy over 30 minutes along a maximum stroke of 60 mm. Its design is based on single-wavelength laser interferometry. The performance of this method depends mostly on the light source and on the signal detection and processing. In order to reach such specifications, all sources of error have to be carefully budgeted. In particular the accuracy of such a system over ranges large compared to the optical wavelength is limited by the calibration and stability of the light source optical frequency. Furthermore, as single-wavelength interferometry uses the optical wavelength as a yardstick, it cannot determine distances longer than half of the optical wavelength with a single measurement point.

This chapter recalls the principle of single-wavelength interferometry and points out its intrinsic limitation known as the Non Ambiguity Range. Heterodyne interferometry which is used regularly in this thesis is presented. Next, the issue of temporal coherence is addressed. Finally the sources of error in single-wavelength laser metrology are tackled and the need for a stable and calibrated wavelength is highlighted.

2.1 Principle and notion of Non Ambiguity Range

2.1.1 The interference phenomenon

The phenomenon of interference is specific to the physics of waves and may appear when several waves are superimposed. It is by achieving interferences with light that Young showed for the first time the wave nature of light. Light can be described as electro-magnetic waves. In a medium of permittivity ϵ and permeability μ, the electric field vector associated to a monochromatic plane lightwave of frequency ν can be described by:

$$\mathbf{E}(\mathbf{r},t) = \Re e\left\{\mathbf{A}(\mathbf{r})\exp(i2\pi\nu t)\right\} \tag{2.1}$$

where:

$$\mathbf{A}(\mathbf{r}) = \begin{cases} a_x(\mathbf{r})\exp(i(\mathbf{k}\cdot\mathbf{r}-\phi_x)) \\ a_y(\mathbf{r})\exp(i(\mathbf{k}\cdot\mathbf{r}-\phi_y)) \\ a_z(\mathbf{r})\exp(i(\mathbf{k}\cdot\mathbf{r}-\phi_z)) \end{cases} \tag{2.2}$$

is a complex vector of three cartesian components where $\mathbf{k}$ is the propagation vector, and ϕ_x, ϕ_y and ϕ_z are constant phase offsets. The intensity of such a wave is given by:

$$I = \frac{c}{\pi}\sqrt{\frac{\epsilon}{\mu}}\left\langle \mathbf{E^2}\right\rangle \tag{2.3}$$

where $\langle\rangle$ denotes the time average. The intensity is proportional to the time average of the square electric field because detector bandwidths are much smaller than the frequency of the optical electric field (around 10^{15}Hz in the visible). If all the intensities are considered in the same medium one can consider only the $\langle\mathbf{E^2}\rangle$ term to compare them.

For the sake of simplicity and because it is most of the time sufficient, *in this thesis waves are considered to be scalar waves propagating in a homogeneous and isotropic medium.*:

$$E(\mathbf{r},t) = \Re e\left\{a(\mathbf{r})\exp(i(\mathbf{k}\cdot\mathbf{r}-\phi))\exp(i2\pi\nu t)\right\} \tag{2.4}$$

Let's consider two monochromatic plane scalar waves of same frequency propagating in the same direction. Assuming there is no loss in the medium their complex amplitudes can be written:

$$\mathbf{A}_1(\mathbf{r}) = \sqrt{I_1}\exp(i(\mathbf{k}\cdot\mathbf{r}-\phi_1)) \tag{2.5}$$
$$\mathbf{A}_2(\mathbf{r}) = \sqrt{I_2}\exp(i(\mathbf{k}\cdot\mathbf{r}-\phi_2)) \tag{2.6}$$

where I_1 and I_2 are respectively the intensities of the wave 1 and of the wave 2. The intensity of the wave resulting from the superposition of these two waves is:

$$\begin{aligned} I(\phi_1, \phi_2) &= \left\langle (E_1 + E_2)^2 \right\rangle && (2.7) \\ &= I_1 + I_2 + 2\sqrt{I_1 I_2} \\ &\quad \times \langle \cos(\phi_1 - \phi_2) + \cos(2\pi 2\nu t + \phi_1 + \phi_2) \rangle . && (2.8) \end{aligned}$$

Due to the limited bandwidth of optical detectors the time average of the term of frequency 2ν is averaged to zero and the detected intensity is:

$$I(\phi_1 - \phi_2) = (I_1 + I_2)\left[1 + 2\frac{\sqrt{I_1 I_2}}{I_1 + I_2}\cos(\phi_1 - \phi_2)\right]. \tag{2.9}$$

The visibility, $\mathcal{V}$ of the fringes is:

$$\mathcal{V} = \frac{I_{Max} - I_{Min}}{I_{Max+I_{Min}}} = 2\frac{\sqrt{I_1 I_2}}{I_1 + I_2}. \tag{2.10}$$

Figure 2.1: Normalized intensity of the wave resulting from the superimposition of two scalar monochromatic waves of same frequency and equal intensities. The intensity is periodic with the phase difference between the two interfering waves.

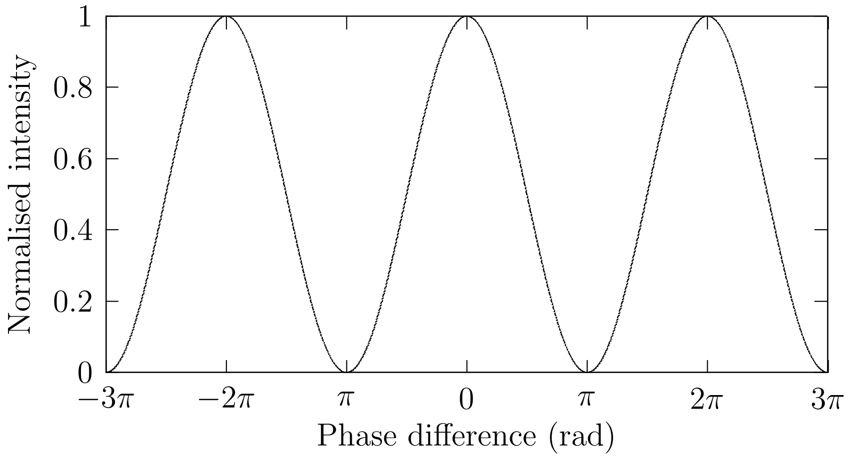

The intensity is a function of the phase difference of the two waves, Figure 2.1. When the two waves are in phase the intensity is maximal. On the contrary when one wave is retarded by π the intensity is minimal (even equal to zero if the two waves have the same intensity).

This result has been derived for monochromatic waves. However purely monochromatic light sources cannot exist because of the quantum nature of light emission. The phase of a real wave is not a constant but is varying quickly in time. The phenomenon of interference appears only if the phases of the two waves are correlated which is usually not the case if the two waves are not emitted by the same source (although Magyar and Mandel showed that it is possible, [MM63]). In that case no interferences arise and the superposition of the two waves is said to be incoherent, the intensity of the resulting wave is then the sum of the individual intensities of the two waves. Nevertheless when the two waves are emitted by the same source their phases can be correlated, at least on a small time scale, and interferences arise. The superimposition of the two waves is then called coherent or partially coherent depending on the degree of correlation of the two electric field. This is described by the theory of partial coherence [BW01]. The coherence of lasers is addressed in more details in Section 2.3.

2.1.2 The Michelson interferometer

The interference equation, Equation 2.9, shows that the intensity resulting of the superposition of two monochromatic waves of same frequency depends on the phase difference between these two waves. The phase difference can be seen as a time delay between the arrival of the two waves. If the waves left a same point, the phase difference at the level of the detector is due to a difference of distance of propagation. This is well shown in the Michelson interferometer, the optical set-up that Albert Abraham Michelson used in 1887 to exhibit the first strong evidence against the theory of the so called luminuferous ether, [MM87]. In a Michelson interferometer, Figure 2.2, an optical

Figure 2.2: Basic Michelson interferometer set-up. BS: Beam Splitter. PD: Photo Diode.

monochromatic wave is divided by a beam splitter in two waves propagating in perpendicular directions. Both waves are retroreflected by mirrors and are superimposed again by the beam splitter. Each wave has traveled along one arm of the interferometer at the speed of light. If one arm is longer than the other by a distance L the wave which has traveled in this arm arrives at the beam splitter with a time delay $\tau = 2nL/c$, where n is the refractive index of the medium (assumed to be homogenous and isotropic) and c the speed of light. After the beam splitter the interference equation, Equation 2.9, can be rewritten:

$$I(L) = I_1 + I_2 + 2\sqrt{I_1 I_2}\cos\left(2\pi\frac{2nL}{\lambda}\right). \tag{2.11}$$

Assuming the beam splitter divides the wave in two waves of equal intensity $I_0/2$ the previous equation becomes:

$$I(L) = \frac{I_0}{2}\left(1 + \cos\left(2\pi\frac{2nL}{\lambda}\right)\right). \tag{2.12}$$

The intensity at the output of the interferometer varies with the cosine of the quantity 2nL called the Optical Path Difference, OPD, of the interferometer. Consequently the phase, Φ, of the interference signal is linked to the interferometer OPD through the equation:

$$\Phi = 2\pi\frac{OPD}{\lambda}. \tag{2.13}$$

Provided the intensities of the two interfering waves are known Equation 2.11 can be inverted and information on the OPD can be obtained. However the inversion of the cosine gives a quantity known modulo 2π yielding an infinite number of values for the OPD:

$$\Phi = \mathrm{Arccos}\left(\frac{I - (I_1 + I_2)}{2\sqrt{I_1 I_2}}\right) + 2m\pi, m \in \mathbb{Z} \tag{2.14}$$

$$OPD_{real} = \frac{\lambda}{2\pi}\mathrm{Arccos}\left(\frac{I - (I_1 + I_2)}{2\sqrt{I_1 I_2}}\right) + 2m\lambda, m \in \mathbb{Z}. \tag{2.15}$$

This limitation of interferometry is known as the problem of the Non Ambiguity Range, NAR. With a single measurement of the phase the real value of the OPD can be determined only if it is known a priori with an accuracy better than λ. This problem can be avoided if the OPD of the interferometer varies continuously at a reasonable speed from a reference position. This position is in general determined by illuminating the interferometer with a broad spectrum source. Indeed as it can be deduced from Equation 2.11 the positions of maxima and minima of the interference signal are wavelength dependent except at the zero OPD where there is a maximum for every wavelength. By detecting this one maximum of the interferogram, called the "white fringe",

Figure 2.3: Normalized intensity of the interference signal and corresponding unwrapped phase and phase mod 2π.

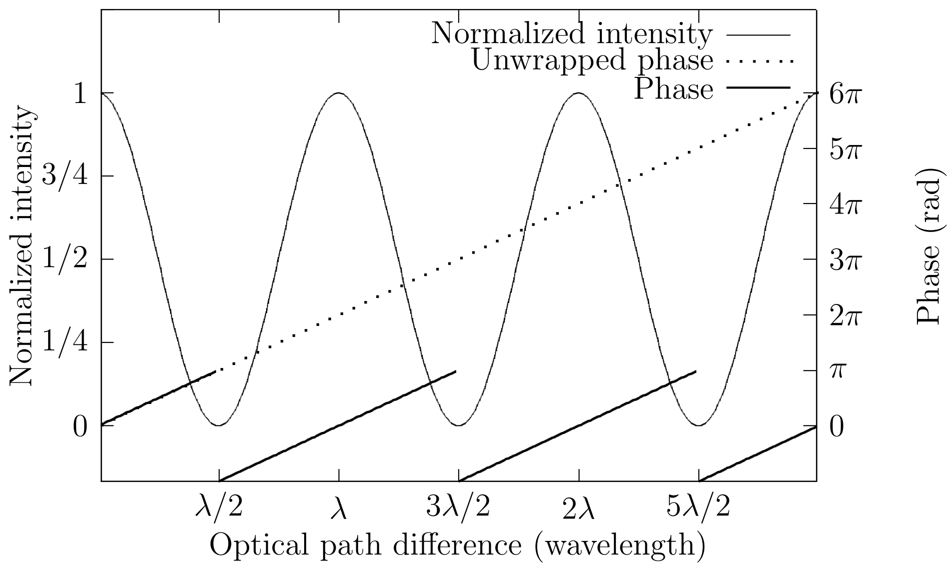

one can determine the zero OPD with high precision. Starting from this reference position and changing slowly the OPD, it is possible to count the fringes and get an unwrapped value of the phase of the interferometric signal, i.e the real value of the OPD, Figure 2.3. The unwrapped phase is written:

$$\Phi_{unwrapped} = 2M\pi + \Phi, M \in \mathbb{Z} \tag{2.16}$$

where M is called the fringe order and Φ the wrapped phase is taken between $[-\pi;\pi]$. Consequently the OPD is given by:

$$\begin{aligned} OPD &= \frac{\Phi_{unwrapped}}{2\pi}\lambda &(2.17)\\ &= (M + f(M)) \times \lambda &(2.18)\end{aligned}$$

where f(M) is called the fractional part and is given by :

$$f(M) = \Phi/\pi. \tag{2.19}$$

Single wavelength laser metrology is said to be incremental because the measurement of an OPD larger than the NAR (λ) requires to count fringes. This puts several limits to the measurements, in particular between two phase measurements the OPD must not change by more than one wavelength, otherwise the fringe order is not updated correctly. Moreover each loss of the signal requires a calibration of the system and the restart of the measurement at the zero OPD or at any other reference position of the interferometer.

2.2 Phase measurement, heterodyne interferometry

The OPD of the interferometer is computed from the phase of the interferometric signal. Two techniques are used to measure the phase.

2.2.1 Phase-stepping

The traditional technique called phase stepping consists in interpolating the phase from a few values of the interference signal taken for the OPD modulated by well known steps (typically 4 steps of $\lambda/2$). Phase stepping techniques and the different interpolation algorithms (ABCD, five points, etc...) are well described in [Cre88]. This technique is used in PRIMA Fringe Sensor Unit as explained in Figure 2.4. Phase stepping suffers from several flaws:

- a limited detection bandwidth;
- a limited resolution, typically around $2\pi/200$.

2.2.2 Heterodyne interferometry

The second technique is called heterodyne interferometry and is based on heterodyne detection. The principle is to send waves of slightly different frequencies in the two arms of the interferometer and measure the phase of the beat signal obtained after superimposition of the two waves. The phase of this signal contains the information about the OPD as explained below.

Let's derive the intensity of the wave resulting from the superimposition of two waves of same intensity I, phases ϕ and ϕ' and slightly different frequencies ν and $\nu + \Delta\nu$:

$$
\begin{aligned}
I(\phi_1, \phi_2) &= \Big\langle \Big(\sqrt{I} \exp\left(i\left(2\pi\nu t + \phi\right)\right) \\
&\qquad + \sqrt{I} \exp\left(i\left(2\pi\left(\nu + \Delta\nu\right) t + \phi'\right)\right)\Big)^2 \Big\rangle && (2.20) \\
&= we\left(1 + \langle \cos\left(2\pi\Delta\nu t + \phi' - \phi\right)\rangle\right. \\
&\qquad \left. + \langle \cos\left(2\pi\left(2\nu + \Delta\nu\right) t + \phi + \phi'\right)\rangle\right) && (2.21)
\end{aligned}
$$

The time average of the cosine term with a frequency equal to $2\nu + \Delta\nu$ is zero as its frequency is much higher than the bandwidth of an optical detector. However the frequency difference $\Delta\nu$ between the two waves may be small enough to be detected. In such a case one observes a "beat signal" which

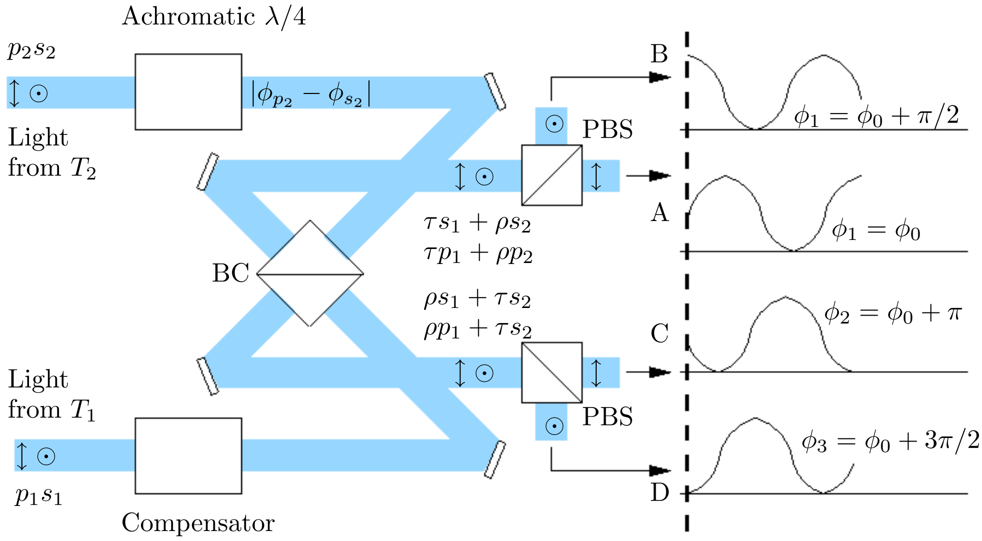

Figure 2.4: The PRIMA fringe sensor units use the phase stepping technique to measure the position of the fringes. The $\pi/2$ phase delay due to a reflection is used to generate achromatic phase shift between the two linear orthogonal components of the polarization in each beam. The result is that it is possible to measure simultaneously the intensity of the interferometric signal for four phases separated by $\pi/2$. The phase ϕ_0 is interpolated from the intensity measurements A,B,C and D.

is the sum of a DC level and a cosine oscillating at the frequency difference of the two optical waves with a phase equal to the phase difference of the two waves. The phase of this signal can be measured by comparison with a reference signal.

This result can be applied to distance measurement using a Michelson interferometer, Figure 2.5. Let's consider a light beam composed of two monochromatic waves with slightly different frequencies and orthogonal linear polarization states. This beam goes through a first beamsplitter. At one output a linear polarizer is used to create the reference beat signal between the two waves of orthogonal polarization's. Assuming that after the linear polarizer the interfering waves have the same intensity, the signal detected is:

$$S_{ref}(t) \propto (1 + \cos(2\pi\Delta\nu t + \phi_{H,ref} - \phi_{V,ref})), \qquad (2.22)$$

where $\phi_{H,ref}$ and $\phi_{V,ref}$ are the phases of the two waves (with respectively linear horizontal and linear vertical polarization state) at the beamsplitter. The beam coming out of the second output of the beamsplitter propagates

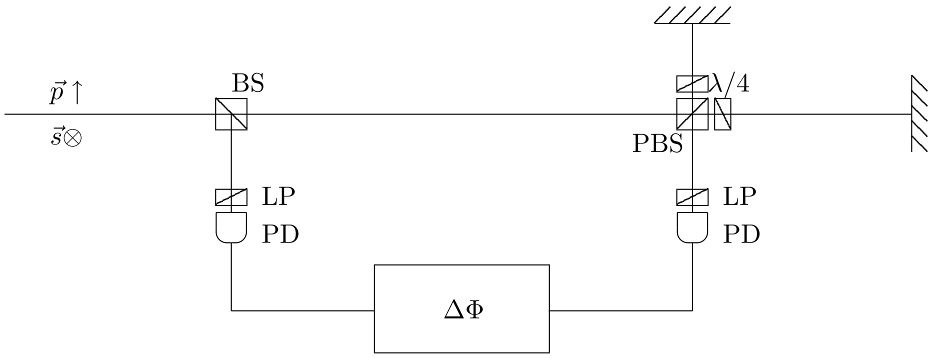

Figure 2.5: Basic polarization based heterodyne Michelson interferometer set-up. A beam composed of two waves with orthogonal linear polarization state is split in two by a beamsplitter (BS). At one output of the BS a linear polarizer (LP) is used to create the reference beat signal detected by a photo-diode (PD). The second beam propagates toward a polarization beam splitter (PBS). Each polarization propagates into one arm of the interferometer and is rotated by π after passing twice through a quarter-wave plate ($\lambda/4$. At the output of the interferometer the two waves are made to interfere in order to create the measurement beat signal. A phasemeter measures the phase difference $\Delta\Phi$ between the two signal.

to a polarizing beamsplitter where the two waves are separated and sent into each arm of the interferometer. After a round trip in the interferometer and two ways through a quarter-wave plate the two waves are superimposed on the polarizing beamsplitter and a linear polarizer creates the measurement beat signal (assuming the interfering waves have the same intensity):

$$S_{meas}(t) \propto (1 + \cos(2\pi\Delta\nu t + \phi_{H,meas} - \phi_{V,meas})) . \tag{2.23}$$

Both signals are fed to a phasemeter which, after a proper signal processing, computes the phase difference, $\Delta\phi$, of the two beat signals:

$$\begin{aligned} \Delta\phi &= (\phi_{H,meas} - \phi_{V,meas}) - (\phi_{H,ref} - \phi_{V,ref}) \\ &= (\phi_{H,meas} - \phi_{H,ref}) - (\phi_{V,meas} - \phi_{V,ref}) . \end{aligned} \tag{2.24}$$

The first term of the difference is proportional to the optical path length, OPL, seen by the horizontally polarized wave between the first beam splitter and the second pass in the polarizing beam splitter:

$$\phi_{H,meas} - \phi_{H,ref} = \frac{OPL_H}{\lambda_H} . \tag{2.25}$$

Similarly, for the vertically polarized wave:

$$\phi_{V,meas} - \phi_{V,ref} = \frac{OPL_V}{\lambda_V}. \tag{2.26}$$

Moreover, assuming that $\lambda_V \approx \lambda_H \approx \lambda$ (which is verified since $\Delta\lambda \ll \lambda$), and inserting the last two equations in Equation 2.24, one deduces that the phase difference is proportional to the difference of optical length seen by the two waves. Since the two wave paths are superimposed everywhere but in the interferometer arms the difference of OPL reduces to the OPD of the interferometer. The phase difference given by the phasemeter is equivalent to the phase of the interferometric signal that would be obtained with a single wavelength:

$$\Delta\phi = \Phi = 2\pi\frac{OPD}{\lambda} \tag{2.27}$$

Several technologies can be used to generate the two waves with orthogonal polarization and slightly different frequencies. Commercial systems are usually based on dual mode Zeeman laser (He:Ne) which produce directly two frequencies with quasi orthogonal linear polarization state. The output of a single mode laser can also be split in two, the two beams being frequency shifted with different frequencies by the use for instance of Acousto Optic Modulators (AOM), [ST91]. As the heterodyne frequencies are in general not larger than a few megahertz no high-speed detectors are required.

Heterodyne interferometry presents interesting features and good performances such as:

- insensitivity to intensity fluctuations (outside of the heterodyne bandwidth);
- high sampling frequency (easily up to several kilohertz);
- high accuracy and high resolution on the phase measurement (up to $2\pi/1000$).

However, compared to phase-stepping, heterodyne interferometry suffers from an additional source of error which is the crosstalk between the two waves in the interferometer arms. This problem, that should be taken care of carefully, is explained in more details in Section 2.4.1.

2.3 Coherence length of single mode lasers

The results of Section 2.1.2 have been derived for monochromatic waves. As mentioned in Section 2.1.1, real sources cannot produce monochromatic waves. Consequently the two waves used in single wavelength interferometry are coherent only over a given time, i.e a given length. The decorrelation of the two waves decreases the contrast of the fringes. Therefore it is possible to define a threshold for the contrast below which the two waves are considered incoherent.

At the output of a Michelson interferometer a wave interferes with a time delayed copy of itself. The intensity is a function of the time and of the delay τ created by the OPD of the interferometer:

$$\begin{aligned} I\left(\tau = \frac{2nL}{c}\right) &= \left\langle (E(t) + E(t+\tau))^2 \right\rangle && (2.28) \\ &= \langle E(t)E^\star(t)\rangle + \langle E(t+\tau)E^\star(t+\tau)\rangle \\ &\quad +2\Re e\left\{\langle E(t)E^\star(t+\tau)\rangle\right\} && (2.29) \end{aligned}$$

As the wave intensity is assumed to be constant:

$$\langle E(t)E^\star(t)\rangle = \langle E(t+\tau)E^\star(t+\tau)\rangle = I. \tag{2.30}$$

Equation 2.29 can then be rewritten:

$$I\left(\tau = \frac{2nL}{c}\right) = 2I\left(1 + \frac{\Re e\left\{\langle E(t)E^\star(t+\tau)\rangle\right\}}{I}\right) \tag{2.31}$$

Assuming the electric field is stationary the second term of the sum which is equal to the real part of the autocorrelation function of the electric field depends only on the delay τ. The autocorrelation function of the electric field is also known as the complex degree of temporal coherence, denoted $\gamma(\tau)$, and is the key tool of the partial coherence theory, [BW01]. According to this theory, the contrast of the interference signal, called visibility and denoted $\mathcal{V}$, is given by the modulus of the autocorrelation function normalized by the intensity :

$$\mathcal{V} = |\gamma(\tau)| = \frac{\langle E(t)E^\star(t+\tau)\rangle}{I}. \tag{2.32}$$

Applying the Wiener-Khintchine theorem ([BW01]), the contrast of the interference signal is related to the spectrum of the light source:

$$\mathcal{V} = |\gamma(\tau)| = \frac{|\mathcal{F}\{S(P,\nu)\}|}{I} \tag{2.33}$$

where S is the spectral density of the electric field. Laser spectra are usually described by a gate function or with more accuracy by a Gaussian or a Lorentzian distribution. For a given FWHM the shape of the spectrum modifies the coherence length (Table 2.1). For a solid state laser with a Lorentzian linewidth a FWHM smaller than 95 kHz is required to reach a coherence length of 1 km!

Table 2.1: Normalized power spectrum density (ν_0 central frequency, $\Delta\nu$ FWHM), corresponding contrast as a function of the time delay and coherence time for a contrast equal to 1/e.

Normalized power spectrum density $S(\nu)$	Contrast as a function of the time delay $\lvert\gamma(\tau)\rvert$	Coherence time τ_c ($\lvert\gamma(\tau_c)\rvert = e^{-1}$)
Gate function: $\begin{cases} 1/\Delta\nu & \text{if } \nu \in [\nu_0 - \Delta\nu/2; \nu_0 - \Delta\nu/2] \\ 0 & \text{otherwise} \end{cases}$	$\left\lvert \frac{\sin(\pi\Delta\nu\tau)}{\pi\Delta\nu\tau} \right\rvert$	$\frac{0.7}{\Delta\nu}$
Gaussian: $\frac{2\sqrt{\ln 2/\pi}}{\Delta\nu} \exp\left(-4\ln 2 \frac{(\nu-\nu_0)^2}{\Delta\nu^2}\right)$	$\exp\left(-\left(\frac{\pi\Delta\nu\tau}{2\sqrt{\ln 2}}\right)^2\right)$	$\frac{2\ln 2}{\pi\Delta\nu}$
Lorentzian: $\frac{\frac{\Delta\nu}{2\pi}}{(\nu-\nu_0)^2 + \left(\frac{\Delta\nu}{2}\right)^2}$	$\exp(-\pi\Delta\nu\lvert\tau\rvert)$	$\frac{1}{\pi\Delta\nu}$

2.4 Sources of error in single wavelength interferometry

In single wavelength interferometry the distance is derived from a phase measurement and from the value of the wavelength of the light source using Equation 2.17. There are obviously two sources of error: the measurement of the phase and the calibration and stability of the wavelength:

$$\begin{aligned} OPD_{measured} &= \frac{\Phi + \delta\Phi}{2\pi}(\lambda + \delta\lambda) \\ &= OPD + \frac{\Phi}{2\pi}\delta\lambda + \frac{\delta\Phi}{2\pi}\lambda + \frac{\delta\Phi}{2\pi}\delta\lambda \end{aligned} \tag{2.34}$$

where $\delta\Phi$ is the phase error and $\delta\lambda$ the error on the knowledge of the wavelength. The second order error term can usually be neglected.

2.4.1 Phase error

The error made on the estimation of the phase depends on the phase measurement technique. Only errors related to heterodyne interferometry will be discussed in this section (see [Cre88] for more details about error in phase stepping). Phase error in heterodyne interferometry can be divided in two independent contributions: an electronic contribution arising in the phasemeter and an optical contribution due to crosstalk between the two heterodyne waves.

Phasemeter error

Heterodyne interferometry uses usually zero-crossing phasemeters. On the rising zero-crossing of the reference signal a fast counter is started and is then stopped on the next rising zero-crossing of the measurement signal. The time measured by the counter is divided by the period of the heterodyne signal to obtain the phase shift between the two signals. The resolution of the process is directly given by the ratio between the heterodyne frequency and the frequency of the counter yielding a typical phase resolution of $2\pi/1000$. The accuracy of the phasemeter is decreased by phase delays introduced between the signals by the electronics of the system (amplifiers, filters, etc...). Digital electronics is added to count fringes and unwrap the phase of the signal. Section 3.2.6 presents briefly the phasemeter used in PRIMET and its performance.

Crosstalk error

The crosstalk error is classical in heterodyne interferometry and creates an error of period λ. This error is caused by a non perfect separation of the two heterodyne waves at the beam splitter and has been extensively studied ([HZ94], [DF00], [WLD99], [YDC$^+$99], [HW92], [TYN89]). In the next paragraph we propose a general derivation of the crosstalk error as a function of the crosstalk amplitude. The result can be applied for small crosstalk to compute the induced crosstalk error caused by the different sources described in the previously cited references.

Let's consider what happens in a heterodyne Michelson interferometer when the two heterodyne waves are not perfectly separated by the beam splitter. In the arm 1, in which only the wave at frequency ν_1 should be present, there is a leakage of the second wave at frequency ν_2. A symmetrical situation is assumed in the second arm. The electric fields in the two arms after a round trip in the interferometer arms are:

$$\begin{aligned} E_1(t) &= A\cos(2\pi\nu_1 t + \phi_1) + \beta\cos(2\pi\nu_2 t + \phi_1) && (2.35)\\ E_2(t) &= B\cos(2\pi\nu_2 t + \phi_2) + \alpha\cos(2\pi\nu_1 t + \phi_2)\,. && (2.36)\end{aligned}$$

After detection and bandpass filtering around the heterodyne frequency $\Delta\nu = \nu_2 - \nu_1$, the heterodyne signal becomes:

$$\begin{aligned} S(t) &= A\beta\cos(2\pi\Delta\nu t) + B\alpha\cos(2\pi\Delta\nu t)\\ &\quad + AB\cos(2\pi\Delta\nu t + \Delta\phi) + \alpha\beta\cos(2\pi\Delta t\nu + \Delta\phi)\,. && (2.37)\end{aligned}$$

If one assumes a small crosstalk the last term of the equation can be neglected and the signal can be rewritten:

$$\begin{aligned} S(t) &= AB\cos(2\pi\Delta\nu t + \Delta\phi) + (A\beta + B\alpha)\cos(2\pi\Delta\nu t)\\ &= (AB + (A\beta + B\alpha)\cos(\Delta\phi))\cos(2\pi\Delta\nu t + \Delta\phi)\\ &\quad + (A\beta + B\alpha)\sin(\Delta\phi)\sin(2\pi\Delta\nu t + \Delta\phi)\\ &= \left((AB)^2 + 2AB(A\beta + B\alpha)\cos^2(\Delta\phi) + (A\beta + B\alpha)^2\right) \times\\ &\quad \left\{\frac{1}{\sqrt{1+X^2}}\cos(2\pi\Delta\nu t + \Delta\phi) + \right.\\ &\quad \left.\frac{X}{\sqrt{1+X^2}}\sin(2\pi\Delta\nu t + \Delta\phi)\right\} && (2.38)\end{aligned}$$

with:

$$X = \frac{(A\beta + B\alpha)\sin(\Delta\phi)}{AB + (A\beta + B\alpha)\cos(\Delta\phi)}. \qquad (2.39)$$

Using the fact that:

$$\begin{aligned} \cos(\arctan(u)) &= \frac{1}{\sqrt{1+u^2}}, && (2.40)\\ \sin(\arctan(u)) &= \frac{u}{\sqrt{1+u^2}}, && (2.41)\end{aligned}$$

Equation 2.38 transforms into:

$$\begin{aligned} S(t) &= \left((AB)^2 + 2AB(A\beta + B\alpha)\cos^2(\Delta\phi) + (A\beta + B\alpha)^2\right) \times\\ &\quad \cos(2\pi\Delta\nu t + \Delta\phi - \eta) && (2.42)\end{aligned}$$

where:

$$\eta = \arctan\left(\frac{(A\beta + B\alpha)\sin(\Delta\phi)}{AB + (A\beta + B\alpha)\cos(\Delta\phi)}\right). \qquad (2.43)$$

η is the phase error induced by the crosstalk between the two waves in the interferometer. η is a function of the phase difference $\Delta\phi$ which is a function of the OPD and is periodical with a period equal to λ. Assuming the crosstalk is small and is the same in the two arms the error can be approximated by:

$$\eta \approx 2\rho \sin\phi \tag{2.44}$$

with $\rho \approx \alpha/A \approx \beta/B$. The resulting amplitude of the OPD error is given by:

$$\delta OPD_{crosstalk} = \frac{2\rho}{2\pi}\lambda \tag{2.45}$$

The crosstalk between the two waves can appear at the beamsplitter for different reasons and with different magnitudes (Table 2.2). Usually crosstalk limits the accuracy of heterodyne systems to a few nm. More precise measurements require an extremely careful management of the polarization. Another alternative is to operate in a vacuum with heterodyne waves that are not superimposed thus avoiding crosstalk.

Table 2.2: Possible sources of polarization crosstalk and their impact on the phase and OPD error

Origin of the error	Maximum phase error (rad)	Amplitude of the OPD error (for $\lambda = 1.3\mu m$)
Angular misalignment of the polarization's with respect to the beam splitter axis (angle θ)	$\eta_{max} \approx 2\tan\theta$	θ=1°: δOPD=7.3nm
Nonorthogonality of the two incoming polarization states (angle (2α))	$\eta_{max} \approx 2\tan\alpha$	α=1°: δOPD=7.3nm
Finite extinction ratio of the beam splitter ($\rho \approx r_p t_s/T_p R_s$)	$\eta_{max} \approx 2\rho$	ρ=1/1000: δOPD=0.42nm
Ellipticity (ϵ) of the two incoming polarization states	$\eta_{max} \approx 2\epsilon$	ϵ=1/100: δOPD=4.2nm

2.4.2 Wavelength stability and calibration

The second source of error is the calibration and the stability of the wavelength:

$$\begin{aligned} \delta OPD &= \frac{\Phi}{2\pi}\delta\lambda & (2.46)\\ &= OPD\frac{\delta\lambda}{\lambda} & (2.47)\end{aligned}$$

Equation 2.47 shows that the error is proportional to the OPD and to the relative knowledge of the wavelength $\delta\lambda/\lambda$. For a given accuracy the requirement on the knowledge of the frequency increases with the OPD to be measured.

Moreover, one can easily show that:

$$\left|\frac{\partial\Delta L}{\Delta L}\right| = \left|\frac{\partial OPD}{OPD}\right| = \left|\frac{\partial\Phi}{\Phi}\right| = \left|\frac{\partial\lambda}{\lambda}\right| = \left|\frac{\partial\nu}{\nu}\right|. \tag{2.48}$$

If the specifications are given as a maximum standard deviation $\sigma_{\Delta L}$ assumed to be small compared to the maximal ΔL, one can derive the following equation that gives the relation between the maximal standard deviation of the wavelength or of the frequency as a function of the required relative accuracy ϵ_R:

$$\left|\frac{\sigma_{\Delta L}}{\Delta L}\right| = \left|\frac{\sigma_{OPD}}{OPD}\right| = \left|\frac{\sigma_\Phi}{\Phi}\right| = \left|\frac{\sigma_\lambda}{\lambda}\right| = \left|\frac{\sigma_\nu}{\nu}\right| = \epsilon_R. \tag{2.49}$$

Chapter 3

Second problem: the incremental PRIMA Metrology System design and its intrinsic limitations, interest for an absolute metrology system

The aim of the PRIMA Metrology system is to monitor the differential OPD seen by the stellar light and occurring in the VLTI between the two channels of PRIMA. The specifications for PRIMET derived in Section 1.3 have lead to particular technical choices for the implementation of PRIMET.

This last introductory chapter describes the design of the first version of PRIMET. A quick overview of PRIMET is given to provide a better understanding of the necessity of an upgrade but also of our proposal to implement an absolute metrology system (described in the third part of the thesis).

3.1 From the specifications to the design

Being part of a larger stellar interferometer PRIMET must fulfill many specifications uncommon to classical laser metrology systems. This section synthesizes the consequences of the specifications on the design. In many cases the constraints due to the presence of stellar light have increased the complexity of PRIMET.

3.1.1 Real-time differential OPD measurement with superheterodyne interferometry

Single wavelength heterodyne interferometers provide the OPD of one interferometer only whereas PRIMET requires the measurement of the difference of two OPDs. Nevertheless the differential OPD can be directly measured using superheterodyne interferometry developed by Dändliker for two wavelength interferometry, [DTP88].

The output of a heterodyne interferometer is a beat signal with a phase proportional to the OPD of the interferometer. Superheterodyne interferometry adds another heterodyne layer by mixing the beat signals of two heterodyne interferometers. Let's consider two heterodyne interferometers of optical path differences OPD_1 and OPD_2, wavelength λ_1 and λ_2 and heterodyne frequencies $\Delta\nu_1$ and $\Delta\nu_2$. After bandpass filtering around $\Delta\nu_1$ and $\Delta\nu_2$ respectively the heterodyne signals are:

$$\left\{ \begin{array}{lcl} S_1(t) & \approx & \cos\left(2\pi\Delta\nu_1 t + \Phi_1\right) \\ S_2(t) & \approx & \cos\left(2\pi\Delta\nu_2 t + \Phi_2\right) \end{array} \right. \tag{3.1}$$

with the phases:

$$\left\{ \begin{array}{lcl} \Phi_1 & = & 2\pi\frac{OPD_1}{\lambda_1} \\ \Phi_2 & = & 2\pi\frac{OPD_2}{\lambda_2} \end{array} \right. . \tag{3.2}$$

If ones multiplies the two signals and applies to the result a bandpass filter at frequency $\Delta\nu = \Delta\nu_1 - \Delta\nu_2$ one gets a new beat signal:

$$S(t) \approx \cos\left(2\pi\Delta\nu t + \Phi\right) \tag{3.3}$$

with :

$$\begin{aligned} \Phi &= \Phi_1 - \Phi_2 \\ &= 2\pi\left(\frac{\Delta OPD}{\lambda_1} - \Delta\nu \times OPD_2\right) \end{aligned} \tag{3.4}$$

where $\Delta OPD = OPD_1 - OPD_2$. Thus the phase of the new beat signal is almost proportional to the difference of OPD between the two interferometers, the slight difference coming from the fact that the wavelengths used in the two interferometers are not identical. Provided the phase, i.e the OPD, of one of the interferometer is measured from its heterodyne signal, the second term of Equation 3.4 is known and the differential OPD can be deduced. As in heterodyne interferometry the phase measurement is done between a reference and a measurement signal, Figure 3.1.

Figure 3.1: Simplified sketch of a single wavelength superheterodyne interferometer

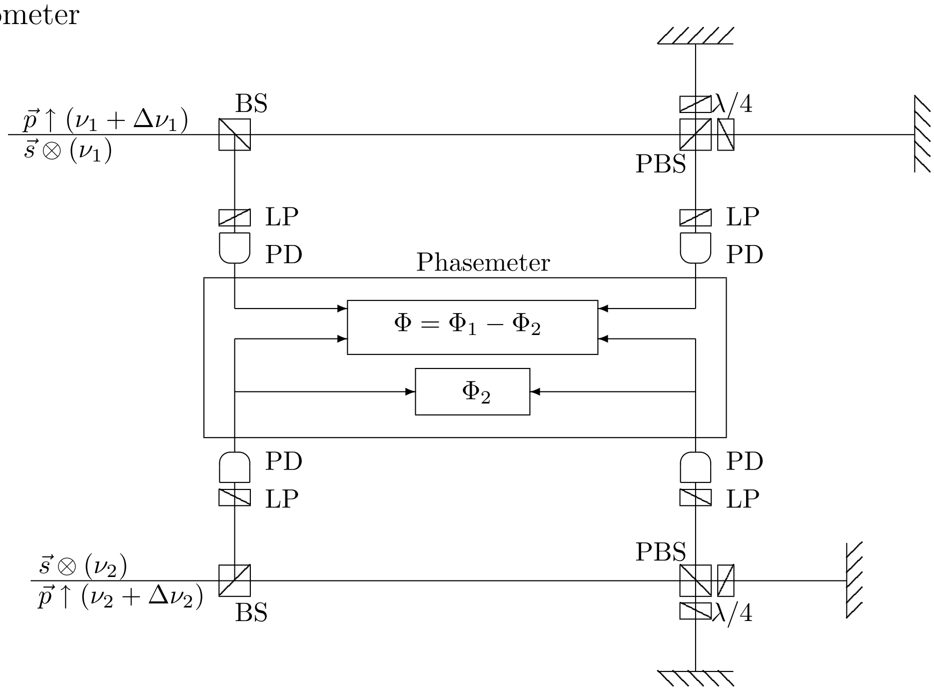

3.1.2 Accuracy

The required 5 nm (standard deviation) accuracy along 60 mm maximum differential OPD seen by the stellar light requires to superimpose the metrology and the stellar beams. Indeed the VLTI optical train is not evacuated which creates differential OPD between two parallel beams due to air turbulence or thermal inhomogeneities. The superimposition of the beams has several repercussions on the design of PRIMET.

Light source wavelength

The beam superimposition restricts the choice of the light source wavelength as every science detector will see straylight from the metrology laser. Consequently the visible part of the spectrum cannot be used as it is already used by the avalanche photodiodes of the MACAO adaptive optics system. Moreover it is not possible to dim the laser light with filters if the process causes at the same time the loss of stellar photons. The only possibility is to operate at a wavelength where no astronomical photons are available, i.e in the atmospheric absorption bands, so that it is possible to use notch filters to prevent the laser light from saturating the scientific detectors. The telecom

O band around 1.3 μm is the only choice. Laser diodes and solid-state lasers (Nd:YAG, Nd:YVO_4, Nd:YLF) are available at these wavelengths.

Beam combiners

As the stellar and the metrology beams are superimposed the optics has to be carefully design to superimpose and extract the metrology beam without deteriorating the astronomical signal (straylight, power loss) or the metrology signal (polarization crosstalk).

Frequency stabilization and calibration of the light source

As explained in Section 2.4 the uncertainty on the value of the wavelength of the light source is a significant part of the measurement error. The accuracy of 5 nm over 60 mm single way OPD requires a relative wavelength knowledge of $\delta\nu/\nu$=10^{-8} which is not reached naturally by any laser. An external frequency stabilization system using an absolute reference must be added to the light source.

3.1.3 Coherence length

PRIMET specifications imply the use of superheterodyne interferometry. In this case both heterodyne interferometers used in the system require an interference signal. Consequently the light source must have a coherence length larger than the maximum OPD of a single interferometer. That is why in the case of PRIMET the coherence length is not given by the maximum differential OPD (60 mm) but by the maximum OPD of the VLTI which is 250 m. According to Section 2.3, the maximum linewidth of the light source with a lorentzian shaped spectrum is 380 kHz. Such narrow linewidths at 1.319 μm are achieved without phase-locking by solid state laser (Non Planar Ring Oscillator (NPRO) Nd:YAG, FWHM≈5 kHz) or External Cavity Laser Diode (FWHM≈120 kHz).

3.1.4 Distance of propagation, VLTI throughput

The laser metrology beam propagates at maximum over 500 m and sees twice the VLTI optical train. This results in significant power loss. The estimated required power for one heterodyne component of PRIMET at the entrance of the VLTI train is 15 mW. Considering a single laser source and the loss due to the generation of the proper heterodyne waves more than 100 mW are required at the output of the laser. Moreover a good polarization extinction ratio is required to avoid the power loss due to the polarization separation of the heterodyne waves.

3.2 Design of PRIMET

3.2.1 Overall description

To fulfill the specifications several technological choices have been made for PRIMET. The system is a superheterodyne interferometer based on a NPRO Nd:YAG laser emitting at 1.319 μm. The metrology beams are superimposed to the stellar beams. The whole system can be divided into five subsystems some of them having interfaces with the rest of the VLTI, Figure 3.2.

The light source generates two pairs of linearly polarized heterodyne waves absolutely stabilized in frequency. The waves are fed through optical fibers to two beam launchers (one for each PRIMA channel) which superimpose the two waves of each heterodyne pair with orthogonal linear polarization states. The beam coming out of each beam launcher is directed toward a beam combiner. On the first pass the beam combiner separates the two orthogonal polarisations and send each of them in one arm of the VLTI toward a telescope. After retroreflection and superimposition to the stellar light in the StS, the two beams coming back from the telescopes are superimposed at the beam combiner and the metrology beams are extracted from the stellar beams. Part of the metrology beam is then fed to quad cells detectors which measure the lateral displacement of the beam of each heterodyne wave. The displacement is corrected by a control loop and a mirror located in the StS. The rest of the beam is coupled into a multimode (MM) fiber feeding the superheterodyne phasemeter. The phasemeter receives four light signals, one reference and one measurement signal for each pair of heterodyne waves, i.e for each channel of PRIMA. The phasemeter processes the signals and sends the phase difference to the PRIMET Local Control Unit (LCU) which derives the differential OPD. The LCU is also in charge of all the hardware control. All the electronics, including the light source, is located in the storage room to avoid heat dissipation, mechanical vibration and acoustic noise in the interferometric laboratory. The beams are propagated from the storage room to the laboratory (and conversely) through optical fibers.

Figure 3.2: PRIMET configuration and interfaces with PRIMA and VLTI. The Local Control Unit and its connexion to other PRIMET subsystems is not shown for clarity.

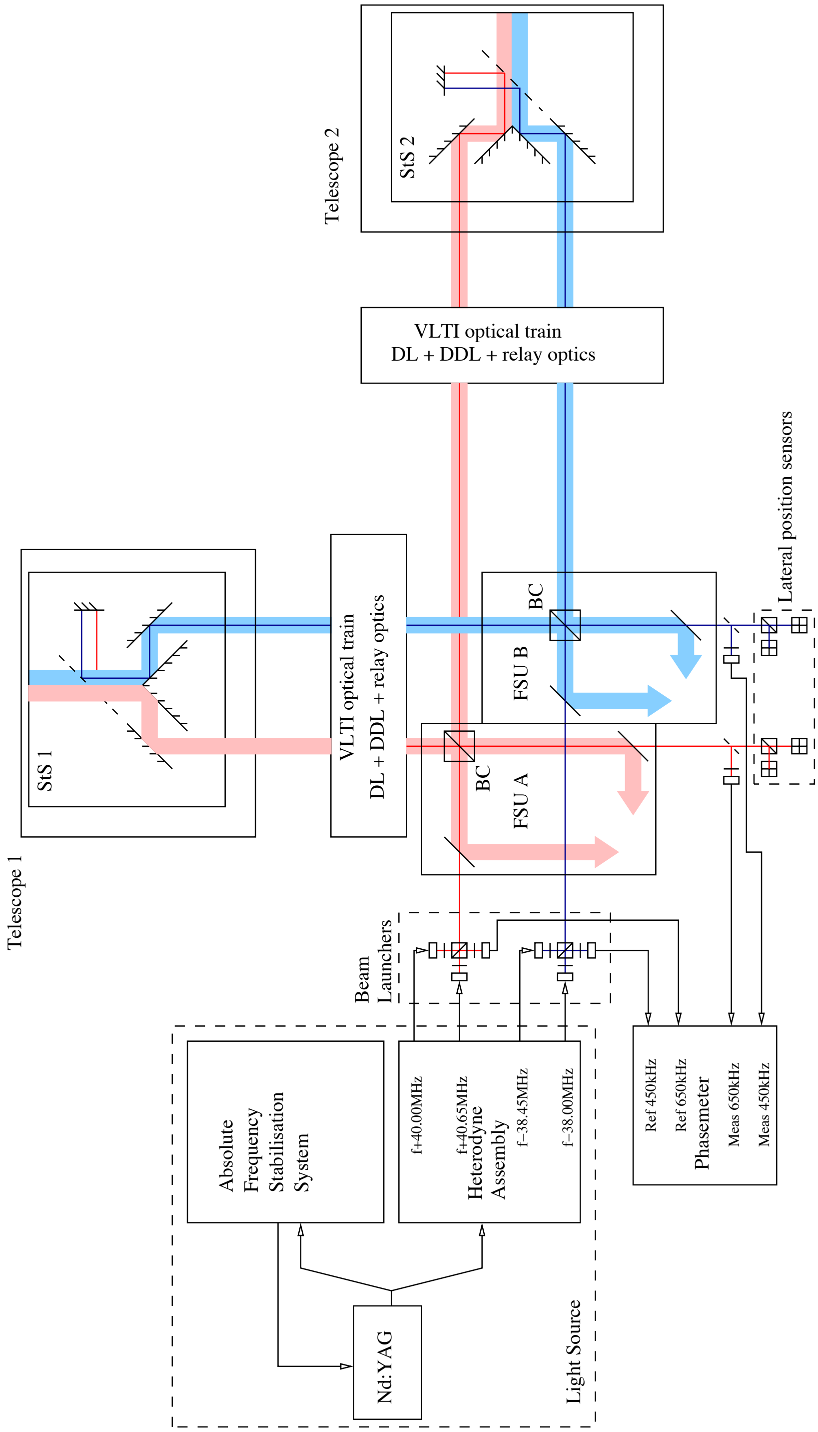

3.2.2 Light source

This subsystem, located in the storage room next to the interferometric laboratory is made of two independent parts, the absolute frequency stabilization system (detailed design, tests and performances are presented in Part II) and the heterodyne assembly, which are fed by a single Nd:YAG laser emitting at $1.319\,\mu$m. The NPRO Nd:YAG is the only laser source providing at the same time the required power and linewidth at the desired wavelength. Besides it is intrinsically a frequency stable laser and it features two actuators to correct for the frequency noise.

Absolute frequency stabilization

Emphasis is put on this key subsystem of PRIMET in Part II, as it represents a major contribution of this thesis.

Heterodyne assembly

The heterodyne assembly should deliver from the Nd:YAG single mode emission two pairs of heterodyne linearly polarized waves. The input power is split in four by a 2 by 4 Single-Mode polarization Maintaining, (SM-PM), fiber coupler with FC-APC connectors. Every output of the coupler is connected to a fiber pigtailed AOM which shifts the optical frequency. Two outputs are shifted respectively by +38.65 MHz and +38.00 MHz creating a 650 kHz heterodyne frequency. The other two outputs are shifted respectively by -40 MHz and -39.55 MHz to generate a 450 KHz heterodyne frequency. Each AOM is connected to a 30 m SM-PM fiber which propagates the light to the interferometric laboratory. The two pairs of heterodyne waves have been frequency shifted from each other by around 80 MHz to prevent any crosstalk between the two interferometers.

3.2.3 Beam launchers

The role of a beam launcher is to superimpose two heterodyne waves, launch them in the VLTI and generate the reference heterodyne signal. There are in total four beam launchers (PRIMA FSU-A, PRIMA FSU-B, AMBER, MIDI) but only two will be used at a time. Each beam launcher is located in the interferometric laboratory on the table of the instrument it will be used with (the goal is to reduce as much as possible the non common path between the stellar and the metrology light).

A beam launcher is a small optical set-up mounted on a 5 axis stage used to align the beam with respect to the VLTI optical train. Each heterodyne wave is fed to the beam launcher via a SM-PM fiber connected to the heterodyne assembly. The output beam of the fiber is collimated with a 1 mm diameter. Linear polarizers are used to set one polarization state linear horizontal and the other linear vertical. The two beams are superimposed using a PBS. However as the polarization states are not perfectly linear and as the PBS has a finite extinction ratio there is a leakage at the output of the PBS. The leaking beam is coupled into a multimode fiber and fed to one reference input of the phasemeter. The main part of the beam propagates toward the beam combiner. The whole beam launcher can be rotated around the optical axis so as to match the axis of the PBS with the axis of the beam combiners in order to reduce the polarization crosstalk.

Figure 3.3: Beam launchers and beam combiners mounted on a FSU at Alenia Spazio (Torino). Left: the beam launching system is seen from the back. On the left is the beam launcher with its two single mode fiber for the injection and its multimode fiber for the reference signal. The probe signal is collected on the right. In the middle one can see the beam combiner and the folding mirrors all equipped in their centre with a 2 mm patch for the metrology beam. Right: the same system seen from the side. The stellar beams arrive from the left. The metrology beams are extracted by the two folding mirrors situated between the cube and the K prism and the delay compensator.

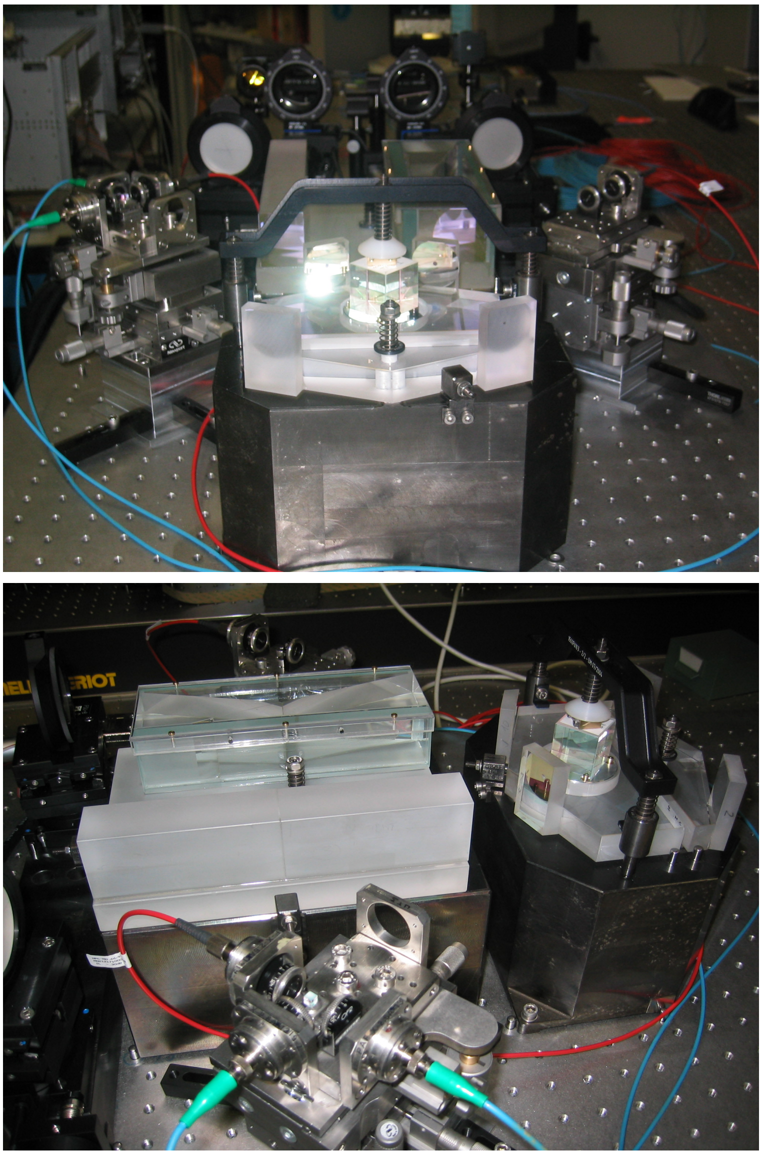

3.2.4 Beam combiners

At the first transmission, from the beam launcher toward the telescopes, the two heterodyne waves are separated thanks to their different polarization state and each one is sent to one telescope through the VLTI optical train. After being retroreflected by a mirror of the StS each metrology beam is superimposed to the center of the stellar beam. The resulting beam travels back to the beam combiner where it is superimposed to the beam coming from the other telescope. The metrology beam is then extracted from the stellar beam by the use of dichroic mirrors.

The metrology beam collimated by the beam launcher with a diameter of 1 mm is positioned at the center of the 18 mm diameter stellar beams (in the laboratory). The beam combiners are custom made beam splitters with a 2.5 mm patch at the center of each surface to accommodate the metrology beam. This patch, small compared to the size of the stellar beam, does not deteriorate significantly the stellar light.

3.2.5 Lateral displacement correction system

After a round trip in the VLTI the metrology beams are likely to present a lateral displacement due for example to thermal gradients in the tunnels. Such displacements provoke signal losses due to the decrease of the coupling efficiency in the fiber or to the decrease of the fringe contrast because of a non perfect overlapping of the two beams. After recombination of the beams a part of the power is picked by a beam splitter and is used to monitor the lateral displacement of each heterodyne wave. The two heterodyne components are separated by a polarizing beam splitter and the two beams are send to InGaAs four quadrants detectors. The vertical and horizontal beam displacements are computed by the LCU which runs a control loop and sends the correction signal to the field mirror located in the StS.

3.2.6 Superheterodyne phasemeter

The role of the phasemeter is to detect and process the interference signals to determine the phase difference related to the differential OPD. It has been developed and build at IMT. It is composed of an analogical stage responsible for the detection, amplification, mixing, filtering and conversion of the interference signals into TTL signals. The analogical stage outputs four signals: a reference and a measurement signal for the differential OPD and a reference and a measurement signal for the OPD of the science channel (used for the frequency mismatch compensation, see Equation 3.4 in Section

3.1.1). The digital phasemeter uses a zero crossing phasemeter to determine precisely the phase shift between the two signals for the differential OPD. In addition a fringe counter is used to provide to the LCU the complete unwrapped phase. A simple fringe counter is used with the two other signals for the frequency mismatch compensation. Programmable logic is used to send all the data (measurements and status) in 32 bits words to the LCU.

Figure 3.4: Schematic of PRIMET phasemeter (Institute of Microtechnology of Neuchâtel).

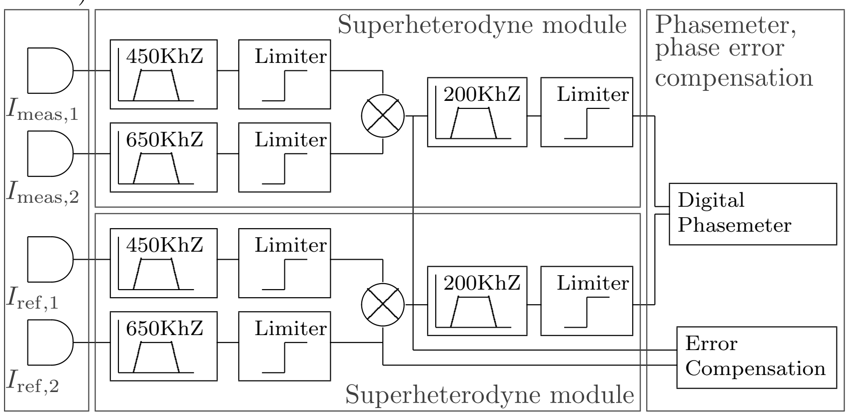

The following performances apply to the photodetection and phase measurement chain:

- resolution: $2\pi/1024$ rad;
- internal sampling frequency: 200 kHz;
- accuracy: $2\pi/800$ rad for an optical power of 20 nW per interferometric arm, a fringe visibility of $\mathcal{V}$=70 % and a 50 kHz bandwidth;
- bandwidth: B=110 kHz for each interferometric channel (i.e $\pm$55 kHz centered on their respective heterodyne frequency) and B=55 kHz for the differential OPD.

3.2.7 Local Control Unit

The Local Control Unit is in charge of all the software tasks including the computation of the differential OPD from the phasemeter data, the execution of the frequency stabilization control loop, the execution of the lateral displacement control loop and of all the control of the hardware. It is composed of two CPUs organized in a master/slave architecture, a TIM board defining a common time for all systems, analogic and digital input/output boards and a reflective memory board.

3.3 Limitations: interest of an upgrade to absolute metrology

As any other incremental metrology system PRIMET suffers from its limited NAR. In the case of PRIMET the NAR is equal to 659.5 nm, half of the metrology wavelength, as the OPD is considered for the stellar light (the OPD seen by the metrology beam is twice the OPD seen by the stellar light, back and forth, and the corresponding NAR is $\lambda = 1.319\,\mu$m as defined in Section 2.1.2). Thus it requires to be calibrated before each measurement, which means that the differential OPD has to be tuned from a reference position. In the case of PRIMET it has been decided that the reference position would be the zero OPD determined by observing the same star in both channels and tuning the DDL until the central fringe is observed for both channels.

This procedure sets constraints on the design of the StS and on the quality of its optics, mainly on the roof mirror that separates the field of view in two. The main difficulty is to have enough flux in both channels. This reduces the limit magnitude of the instrument. Moreover the whole procedure is time consuming as it requires to first acquire fringes with both FSUs, then move the field mirror to acquire the light from the second fainter object and finally change slowly the differential OPD until fringes are seen for these second object on the faint channel. Meanwhile during the whole procedure the differential OPD is monitored with PRIMET. Once this is done the observation can start. The calibration procedure is expected to last more than 15 min which represents half of the typical observing time (30 min). Furthermore this calibration procedure will have to be repeated if there are any signal loss. The time efficiency of observation with PRIMA is severely limited by the calibration procedure. As a consequence an upgrade of the system that allows to skip or to accelerate the calibration procedure is required.

An absolute laser metrology system would provide almost instantly the differential OPD. The calibration procedure required by a multiple wavelength metrology system such as the one proposed in the this part of this thesis is expected to last a few tens of second and is limited by the wavelength tuning speed of the laser source. At the time the design of PRIMA was made it was decided that it was less risky to implement first an incremental metrology with a calibration system than to build directly an absolute metrology system as no multiwavelength laser sources were commercially available. Since then the choice and the performances of laser sources have increased a lot and such a project seems now feasible. In particular, the development of optical frequency comb generator gives an opportunity to realize a big progress in multiple-wavelength interferometry. Based on this technology, the third part of this thesis validates a new concept of stabilized multiple-wavelength laser source and proposes a design for its direct application to PRIMET.

Conclusion of Part I

The European Southern Observatory Very Large Telescope Interferometer will soon be equipped with a new instrument, PRIMA, based on dual-feed interferometry. In order to reach the instrument goal of $10\,\mu$as accuracy on astrometric data this technique of observation requires to measure at least at a 8 kHz sampling frequency and with a nanometer level accuracy a differential optical path difference up to 60 mm between two Michelson interferometers with OPDs reaching up to 250 m.

This first part has given an overview of the Very Large Telescope Interferometer and of its instrument the Phase-Referencing Imaging and Microarcsecond Astrometry facility (PRIMA) which form the background of this thesis. The specifications of the key element of PRIMA, its metrology system (called PRIMET), have been recalled. Among all the optical distance measurement methods only single wavelength laser interferometry can meet the high requirements of PRIMET. However in order to reach such a performance extreme care should be applied to the design of the laser source. Indeed for large OPD, i.e large compared to the wavelength, the accuracy of the measurement is mainly limited by the uncertainty on the laser optical frequency. In the case of PRIMET, the required relative frequency accuracy is 10^{-8}.

Although frequency stable interferometers are commercially available, they cannot be used in the framework of PRIMA as they do not meet its specifications. In particular, one has to resort to superheterodyne interferometry to monitor the differential OPD with the desired bandwidth. Due to stringent specifications on the wavelength, power, coherence length and polarization extinction ratio, PRIMET light source is based on a NPRO Nd:YAG laser emitting at $1.319\,\mu$m. Despite the intrinsic stability of such lasers an external absolute frequency stabilization system is required. The first goal of this thesis was to contribute to the development of this light source and to its integration and characterization. Part II focuses on the light source of PRIMET incremental metrology system. The emphasis is put on the integration and test of the laser absolute frequency stabilization system.

Although PRIMA can be operated with an incremental metrology system and reach its goal in term of accuracy [LWS+02], its time efficiency may suffer severely from the time-consuming calibration procedure required because of the limited Non Ambiguity Range (NAR) of single-wavelength interferometry. As an answer to this problem, Part III tackles the problem of extending the NAR of PRIMET by the use of multiple-wavelength laser interferometry. It focuses on the possibility offered by the recent development of optical frequency comb to build a highly stabilized and tunable multiple-wavelength laser source.

References

[Aa04] Robin Arsenault and al. Macao-vlti adaptive optics systems performance. In Domenico Bonaccini, editor, *Advancements in adaptive optics*, volume 5490. SPIE, 2004.

[BW01] Max Born and Emil Wolf. *Principle of optics.* Cambridge University Press, seventh (expanded) edition, August 2001. Electromagnetic theory of propagation, interference and diffraction of light.

[Cre88] K. Creath. *Progress in Optics*, volume XXVI, chapter Phase-measurement interferometry techniques, pages 349–393. Elsevier Science Publishers, Amsterdam, 1988.

[DF00] J. M. De Freitas. Phase nonlinearity extrema in zeeman heterodyne interferometry. *Optical Engineering*, 39(2):572–575, February 2000.

[DLK+00] Françoise Delplancke, Samuel Lévêque, Pierre Kervella, Andreas Glindemann, and Luigi d'Arcio. Phase-referenced imaging and micro-arcsecond astrometry with the vlti. In Pierre J. Lena and Andreas Quirrenbach, editors, *Interferometry in optical astronomy*, volume 4006, pages 365–376. SPIE, 2000.

[DNdM+03] Françoise Delplancke, Jan Nijenhuis, Harry de Man, Luigi Andolfato, Reiner Treichel, Jan Hopman, and Frédéric Derie. Star separator system for the dual-field capability (prima) of the vlti. In Wesley A. Traub, editor, *New frontiers in stellar interferometry*, volume 5491, page 1528. SPIE, 2003.

[DTP88] René Dändliker, R. Thalman, and D. Prongué. Two-wavelength laser interferometry using superheterodyne detection. *Optics Letters*, 13(5):339–341, May 1988.

[ERF00] Simone Esposito, Armando Riccardi, and Bruno Femenía. Differential piston angular anisoplanatism for astronomical optical interferometers. *Astronomy and Astrophysics*, 353:L29–L32, 2000.

[Ga04] Andreas Glindemann and al. Vlti technical advances - present and future. In Wesley A. Traub, editor, *New Frontiers in Stellar Interferometry*, volume 5491. SPIE, 2004.

[HW92] Wenmei Hou and Günter Wilkening. Investigation and compensation of the nonlinearity of heterodyne interferometers. *Precision Engineering*, 14(2):91–98, April 1992.

[HZ94] Wenmei Hou and Xianbin Zhao. Drift of nonlinearity in the heterodyne interferometer. *Precision Engineering*, 16(1):25–35, January 1994.

[Law] Peter Lawson. Optical long baseline interferometry news. http://olbin.jpl.nasa.gov.

[Law00] Peter Lawson. *Principle of long baseline stellar interferometry.* National aeronautics and space aministration, Jet Propulsion Laboratory, California Institute of technology, Pasadena, California, 2000. Course notes from the 1999 Michelson Summer School, held August 15-19, 1999.

[LWS+02] S. Lévêque, R. Wilhelm, Y. Salvadé, O. Scherler, and R. Dändliker. Toward nanometer accuracy laser metrology for phase-referenced interferometry with the vlti. In Wesley A. Traub, editor, *Interferometry for optical astronomy II*, volume 4838, pages 983–994. SPIE, 2002.

[MM87] A. A. Michelson and E. W. Morley. On the relative motion of the earth and the luminuferous ether. *The American Journal of Science*, XXXIV(203):333–345, November 1887.

[MM63] G. Magyar and L. Mandel. Interference fringes produced by superposition of two independent maser light beams. *Nature*, 198:255–256, 1963.

[PDD+03] Francesco Paresce, Françoise Delplancke, Frédéric Derie, Andreas Glindemann, Andrea Richichi, and Massimo Tarenghi. Scientific objectives of eso's prima facility. In Wesley A. Traub, editor, *Interferometry for optical astronomy II*, volume 4838, pages 486–495. SPIE, 2003.

[PRf01] Eso press release 06/01, first light for the vlt interferometer, March 2001. Published by ESO Education & Public Relations Department, http://www.eso.org/outreach/press-rel/pr-2001/pr-06-01.html.

[PRf05] Eso press release 06/01, vlti first fringes with two auxiliary telescopes at paranal, March 2005. Published by ESO Education & Public Relations Department, http://www.eso.org/outreach/press-rel/pr-2005/pr-06-05.html.

[Sci01] Eso press release 23/01, first scientific results with combined light beams from two 8.2-m unit telescopes, November 2001. Published by ESO Education & Public Relations Department, http://www.eso.org/outreach/press-rel/pr-2001/pr-23-01.html.

[SM92] M. Shao and Colavita M. M. Potential of long-baseline infrared interferometry for narrow-angle interferometry. *Astronomy and Astrophysics*, 262:353–358, 1992.

[ST91] Bahaa E. A. Saleh and Carl Malvin Teic. *Fundamental of photonics*. Wiley-Interscience, first edition, August 1991.

[TYN89] Mitsuru Tanaka, Tohru Yamagami, and Kan Nakayama. Linear interpolation of periodic error in heterodyne laser interferometer at subnanometer levels. *IEEE Transactions on instrumentation and measurement*, 34(2):552–554, April 1989.

[WLD99] Chien-ming Wu, John Lawall, and Richard D. Deslattes. Heterodyne interferometer with subatomic periodic nonlinearity. *Applied Optics*, 38(19):4089–4094, July 1999.

[YDC+99] Chunyong Yin, Gaoliang Dai, Zhixia Chao, Yi Xu, and Jie Xu. Determining the residual nonlinearity of a high-precision heterodyne interferometer. *Optical Engineering*, 38(8):1361–1365, August 1999.

Part II

Iodine frequency stabilised Nd:YAG laser for incremental metrology

Forewords

In the previous part, precisely in Section 2.4.2, we have recalled that the accuracy of single-wavelength interferometry is limited by the wavelength accuracy for OPD large compared to the wavelength. As a consequence, PRIMET Nd:YAG laser requires an absolute frequency stabilization system. In this part we tackle the problem of the laser source for the incremental PRIMA metrology system and focus on the frequency stabilization and calibration of the laser.

In *Chapter 4*, we present briefly the basics of laser frequency stabilization and some useful results for the following section of the thesis. Furthermore we recall the principle of the Pound-Drever-Hall method. The preliminary studies we carried out on the second harmonic generation and on the iodine spectroscopy are developed along with their consequences on the set-up build by the Institute of Microtechnology of Neuchâtel (IMT). The set-up as delivered by IMT is described. Finally we explain how we have enhanced the control loop architecture by enabling the simultaneous use of the two frequency actuators of the laser head.

In *Chapter 5*, we describe the tests we have carried out on the stabilized laser and the efforts we have put on the improvement of the stabilization system performance. We compare the frequency stability deduced from the measurement of the closed loop error signal and the one obtained from the beat signal obtained with a self-referenced optical frequency comb generator used as an independent frequency sensor. We have proposed and tested some possible improvements of the stabilization set-up. Finally we present the performance of the absolute frequency stabilization system.

In *Chapter 6*, we study the possibility of calibrating the laser wavelength once PRIMET is installed at the Paranal Observatory. We show that the Nd:YAG laser wavelength cannot be calibrated with the required accuracy by comparison with a reference interferometer available at the observatory.

Outline of Part II

Chapter 4

Contribution to the design of PRIMA Nd:YAG laser absolute frequency stabilization system

In order to fulfill the final 5 nm accuracy on the measurement of the OPD seen by the stellar light, the wavelength of PRIMET laser source must be stabilized over 30 min and known over the PRIMET lifetime with a relative accuracy better than 10^{-8}. Based on the PRIMET specifications the laser chosen to equip PRIMET is a NPRO Nd:YAG laser which satisfies the wavelength, linewidth, polarization and power requirements (as described in Section 3.2). However, it does not reach the required wavelength accuracy although it is by design a stable laser.

This chapter presents the design of the frequency stabilization system and in particular our contribution to it. The stabilization scheme based on the Pound-Drever-Hall method was defined by a feasibility study carried out by the Institute of Microtechnology of Neuchâtel. We have carried out preliminary studies on key components of the system in order to fulfill the requirements of the method with a good power efficiency and a reduced maintenance.

Section 4.1 recalls the basics of laser frequency stabilization and the reason of the choice of the PDH method. The next section, Section 4.2, explains the principle of the PDH technique and presents our work on the second harmonic generation set-up and on the iodine spectrum. The set-up resulting from our preliminary studies and build by IMT is described in Section 5.1.1.

4.1 Overview of laser frequency stabilization

One of the main characteristics of interests of lasers is the monochromaticity of their emission. Nevertheless, in addition to the quantum limit of the linewidth, noise intrudes to enlarge the laser linewidth and change the mean wavelength. The constant need for a better frequency stabilization brought by applications so different as spectroscopy, metrology or detection of gravitational waves has lead to the development of several methods. A review of the main techniques used for laser stabilization is given by Hamilton in [Ham89].

4.1.1 Frequency noise and phase noise in lasers

All the sources of frequency noise in a laser can be classified in two categories:

- fundamental noise: noise inherent to the lasing process, it is due to the spontaneous emission noise;
- technical noise: noise due to the environment or pumping perturbations.

The fundamental limitation of frequency stability is given by the fundamental noise due to the spontaneous emission noise. In the lasing process stimulated emission is the dominant process and is the key to the coherence of the emission. Nevertheless there are always spontaneous emissions giving rise to uncorrelated photons. These photons change slightly the phase of the field as described in Figure 4.1. As the instantaneous frequency is the time derivative of the phase, variations of the phase will lead to variations of the frequency.

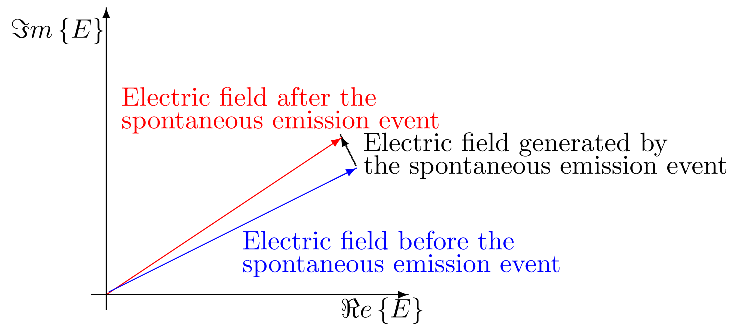

Figure 4.1: Phasor diagram illustrating the phase noise induced by spontaneous emission in the laser gain medium.

Relation between phase noise and frequency noise

The electric field emitted by a single-mode laser can be written as:

$$E(t) = \Re\text{e}\left\{\sqrt{I(t)}\exp\left(i\nu_{ref}t\right)\exp\left(i\phi(t)\right)\right\}, \tag{4.1}$$

where I(t) is the intensity as a function of time, ν_{ref} is a reference frequency and $\phi(t)$ is the phase noise. The intensity noise is ignored here, i.e $I(t) = I$. The instantaneous frequency deviation, $\delta\nu$, from the frequency reference ν_{ref} is:

$$\delta\nu = \frac{1}{2\pi}\phi^{\cdot} = \frac{1}{2\pi}d\phi/dt. \tag{4.2}$$

In an interferometric set-up the phase noise is of importance as it limits the accuracy of the measurement. The quantity:

$$\Delta\phi(t,\tau) = \phi(t) - \phi(t-\tau) \tag{4.3}$$

is particularly interesting as it is the phase noise occurring in a Michelson interferometer of $OPD = c\tau$. One can show that the power spectral density of this quantity, $S_{\Delta\phi(\tau)}(f)$, is related to the power spectral density of the instantaneous frequency deviation, $S_{\phi^{\cdot}}(f)$, by the relation [Pet88]:

$$\begin{aligned} S_{\Delta\phi(\tau)}(f) &= S_{\phi^{\cdot}}(f)\tau^2\left(\frac{\sin\pi f\tau}{\pi f\tau}\right)^2 \\ &= 4\pi^2\tau^2 S_{\delta\nu}(f)\left(\frac{\sin\pi f\tau}{\pi f\tau}\right)^2 \end{aligned} \tag{4.4}$$

However, the measured phase difference is usually averaged over a time T:

$$\Delta\phi(\tau,T,t) = \frac{1}{T}\int_{t-T}^{t}\Delta\phi(\tau,T,t')dt' \tag{4.5}$$

and Equation 4.4 becomes:

$$S_{\Delta\phi(\tau)}(f) = 4\pi^2\tau^2 S_{\delta\nu}(f)\left(\frac{\sin\pi f\tau}{\pi f\tau}\right)^2\left(\frac{\sin\pi fT}{\pi fT}\right)^2. \tag{4.6}$$

Provided the interferometric delay τ is much smaller than the phase integration time T, the previous equation can be simplified into [**?**]:

$$S_{\Delta\phi(\tau)}(f) = 4\pi^2\tau^2 S_{\delta\nu}(f)\left(\frac{\sin\pi fT}{\pi fT}\right)^2. \tag{4.7}$$

Thus it is possible to measure the frequency stability of a laser with an interferometric set-up. Conversely, as the accuracy of an interferometer is deteriorated by its phase noise, it is possible to derive the specifications on the laser frequency stability from the specifications on the accuracy.

4.1.2 Basics of laser frequency stabilization

As any other absolute stabilization system, laser frequency stabilization requires a reference, a sensor and one or several actuators. In the next two sections we give an overview of the state of the art in continuous wave laser frequency stabilization.

Frequency reference and generation of the error signal

PRIMET requires to stabilize the wavelength emitted by a laser on an absolute well-known optical frequency reference. This reference should remain the same throughout the whole life time of PRIMA. Consequently, referencing on a Fabry-Pérot étalon is not possible since the OPL in laser cavity is not constant due to thermal fluctuations and mechanical vibrations. Using a master stabilized laser as a reference does not solve the problem as this master laser will require an absolute reference (this can be avoided by the use of a self-referenced optical frequency comb generator which uses a radio frequency reference instead of an optical frequency reference; however such systems were not available at the time of the feasibility study of PRIMET and thus have not been considered). Atomic or molecular gas transitions provide absolute optical frequency references. He:Ne lasers are usually stabilized using iodine which presents a dense absorption spectrum in the visible. CO_2 lasers can be stabilized on water transitions around $10\,\mu$m. With Nd:YAG lasers, emitting either at $1.064\,\mu$m or $1.319\,\mu$m, the difficulty is to find a gas providing usable absorption lines. Most of the known absorption lines at these wavelength are weak (H_2O, CO_2) or are produced by corrosive or toxic gas (H_2S, HCl) that cannot be used in an astronomical observatory environment, [DCO+02]. Arie has used iodine transitions in the visible after doubling the frequency of the Nd:YAG emission with a non-linear crystal, [ASGB92, ABFB93, AB93].

Once the suitable transition has been found many techniques are available to derive the error signal that will be used in the control loop. The most precise method uses the phenomenon of saturated absorption on Doppler-free absorption lines, [Men01]. However in the case of PRIMET there is not enough optical power after the frequency doubling to apply this technique. It is applied to a Nd:YAG laser in [GHO+04], but the laser output power is 950 mW instead of 100 mW maximum for PRIMA. The side of fringe locking technique, [Ham89], uses a simple set-up but cannot be used to provide an absolute frequency stabilization since the width and the shape of the transition depends on the temperature and pressure of the gas (thus requiring a precise control of these two parameters). The stabilization point has to be located at the centre of the transition. The Pound-Drever-Hall technique, [Bla01], based on the FM-spectroscopy technique developed by Bjorklund, [Bjo80], has been used by Arie to stabilize a Nd:YAG emitting at 1.319 μm, [ABFB93]. The feasibility study of PRIMET laser frequency stabilization, carried out by IMT Neuchâtel, has identified this technique as the best solution.

Correction of the frequency noise

The types of actuators used to apply the correction signal depend on the laser technology. Usually the principle is to change the optical path length in the cavity. At low frequencies the frequency can be tuned by a rotating glass plate located in the cavity. The optical path length in the cavity can also be changed slowly by heating or cooling the cavity to modify its refractive index. Faster corrections can be applied with a piezoelectric actuator which modifies the physical length of the cavity. External elements such as electro-optic or acousto-optic modulators can be used too. Acousto-optic modulators suffer from a low-bandwidth while electro-optic modulators cannot provide a DC correction. Both type of modulators have been used simultaneously by Hall, [HH84].

In the case of PRIMET the NPRO Nd:YAG laser has two voltage driven internal actuators:

- a fast actuator with a small modulation range: a piezoelectric actuator which puts a mechanical strain on the crystal to change the cavity physical size. This actuator has a 1 kHz bandwidth and a ± 20 MHz tuning range;

- a slow actuator with a large tuning range: a system (resistor/Peltier element) which heats/cools the cavity to change the refractive index. This actuator has a 1 Hz bandwidth and a ± 20 GHz tuning range.

4.2 Design of the frequency stabilization system

Based on the result of the feasibility study PRIMET absolute frequency stabilization uses the Pound-Drever-Hall method with a transition of iodine around 659 nm.

4.2.1 Principle of Pound-Drever-Hall laser frequency stabilization

Let's consider a single mode laser emitting at the frequency ν. The laser beam is sent through an electro-optic modulator which introduces a phase modulation of the electric field of amplitude π and frequency f, [ST91]. After the modulation the electric field is expressed by:

$$E(t) = \Re e \left\{ E_0 e^{i2\pi\left(\nu t + \frac{1}{2}\sin(2\pi f t)\right)} \right\}. \tag{4.8}$$

Therefore the instantaneous frequency of the light, ν_{ins}, is given by:

$$\nu_{ins}(t) = \nu + \pi f \cos(2\pi f t). \tag{4.9}$$

The atomic transition is characterized by a frequency dependent absorption. The line shape is denoted $T(\nu)$ and represents the transmission of the gas cell as a function of the optical frequency. The intensity at the output of the gas cell is the product of the input intensity and the transmission factor:

$$I_{out}(\nu_{ins}) = I_{in} T(\nu_{ins}). \tag{4.10}$$

Expanding $T(\nu_{ins})$ in a Taylor serie around the central frequency ν leads to the first order approximation:

$$I_{out}(\nu_{ins}) \approx I_{in}\left(T(\nu) + \frac{d}{d\nu}\left(T(\nu)\right) \pi f \sin(2\pi f t) \right). \tag{4.11}$$

The output intensity is modulated by the frequency modulation with an amplitude proportional to the derivative of the line shape with respect to the optical frequency. An atomic transition is usually described by a Lorentzian lineshape:

$$T(\nu) = 1 - A_{max} \frac{\left(\Delta\nu_{1/2}/2\right)^2}{\left(\nu - \nu_0\right)^2 + \left(\Delta\nu_{1/2}/2\right)^2}, \tag{4.12}$$

where A_{max} is the maximum absorption, ν_0 is the frequency at the centre of the transition and $\Delta\nu_{1/2}$ is the width at half minimum of the transmission. This function and its derivative are plotted in Figure 4.2. The first derivative of $T(\nu)$, $T'(\nu)$, is positive on one side, negative on the other and changes sign at the centre of the transition thus providing a suitable error signal for absolute frequency stabilization. The error signal is generated by detecting synchronously the amplitude of the intensity modulation with a lock-in amplifier working at the phase modulation frequency f. The error

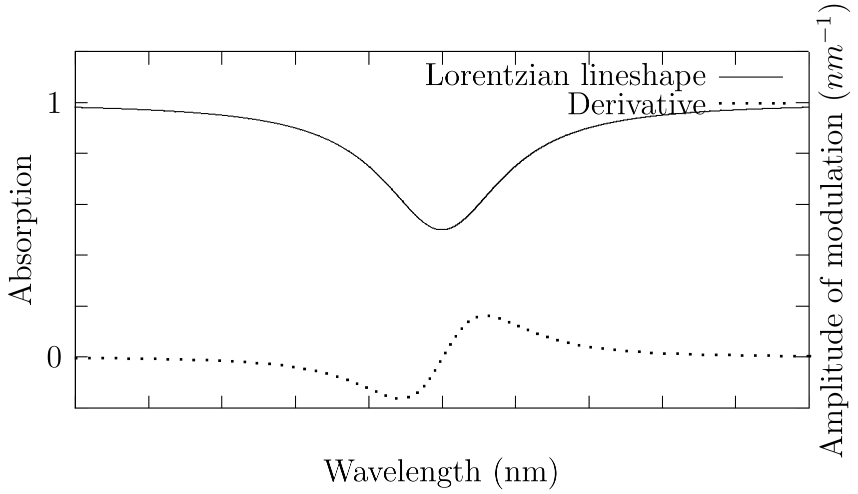

Figure 4.2: Lorentzian lineshape and its derivative (in this example the absorption is 50%).

signal ϵ is then given by:

$$\epsilon(\nu) = G_{amp} S_{detec} \pi f I_{in} T'(\nu), \tag{4.13}$$

where G_{amp} is the gain of the lock-in amplifier and S_{detec} the sensitivity of the detector expressed in V/W. The error signal depends on the line shape of the transition but is positive on one side, negative on the other and changes sign at the centre of the transition. The PDH principle is illustrated in Figure **??**.

4.2.2 Design of the frequency stabilization system

The general design of the frequency stabilization system is presented in Figure 4.4. The power at the output of the laser fiber (SM-PM) is split in two by a fiber coupler with ratio 25%/75%. The part sent to the stabilization system is focused in a non-linear crystal to double the frequency of the light. The light at the output of the crystal is composed of the two frequencies, the laser light of frequency ν and its second harmonic of frequency 2ν. The infrared light remaining from the second harmonic generation is extracted with a dichroic plate. The visible beam is collimated and sent through the electro-optic modulator. The phase modulated, i.e frequency modulated, beam propagates through a I_2 cell in which the frequency modulation is transformed into an intensity modulation due to the frequency dependent absorption coefficient. Finally the beam is focused on an AC coupled detector. The electric signal

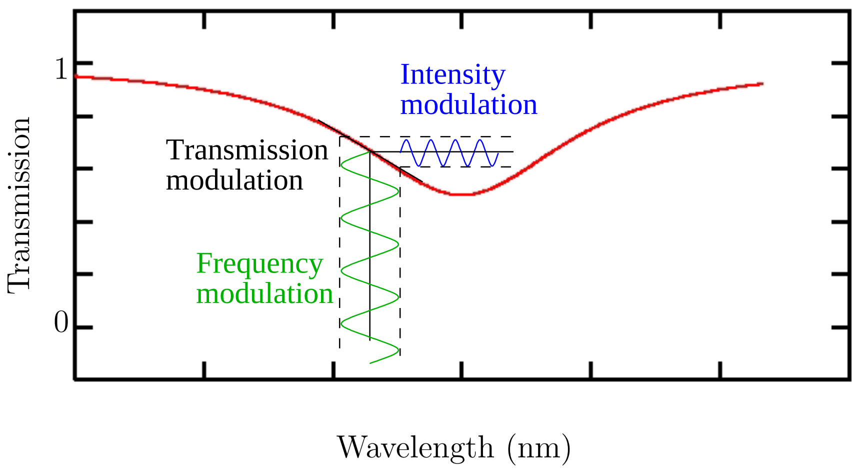

Figure 4.3: Sketch of the principle of the Pound-Drever-Hall stabilization technique. The frequency modulation is transformed into an intensity modulation through the frequency dependent transmission of an atomic transition. The intensity modulation is proportional to the derivative of the transmission with respect to the frequency. Therefore it is zero at the centre of the transition.

is detected synchronously by a lock-in amplifier at the phase modulation frequency. The error signal is fed to the LCU which digitalizes the signal and runs the control loop. The control loop generates two correction signals, one for the piezoelectric actuator and one for the temperature actuator, which are fed to the laser power supply.

4.2.3 Choice of the non-linear crystal

As a consequence of the lack of usable transitions at 1.319 μm the light emitted by the Nd:YAG laser has to be doubled in frequency to 659 nm to use a transition of iodine. Frequency doubling, also known as Second Harmonic Generation (SHG), is a non-linear optical effect of second order. Such an effect appears for large spatial power density in materials with a large non-linear coefficient. Different techniques and different crystals can be used to achieve second harmonic generation at 1.319 μm. We have carried out a preliminary study based on the feasibility study done by IMT in order to design the SHG set-up used in the frequency stabilization system.

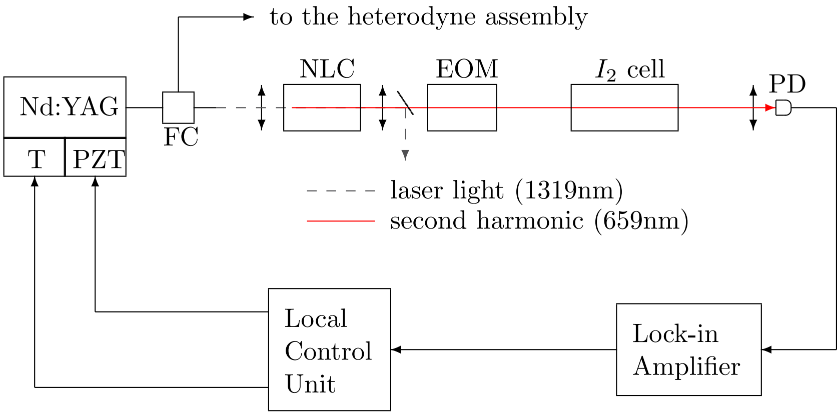

Figure 4.4: Set-up of the frequency stabilization system. PZT: piezoelectric actuator, T: temperature actuator, FC: fiber coupler, NLC: non-linear crystal, EOM: electro-optic modulator, PD: photodiode.

SHG principle

The polarization induced in a medium by an electric field is usually described by a linear expression. Nevertheless it has been shown that by increasing the amplitude of the field non-linear effects appear. One of the second-order non-linear effects is the generation of a polarization oscillating at twice the frequency ν_F of the exciting field. This polarization emits a new wave of frequency $\nu_{SH} = 2\nu_F$ which is spatially superimposed to the fundamental wave. This effect is called Second Harmonic Generation (SHG), [ST91, Men01].

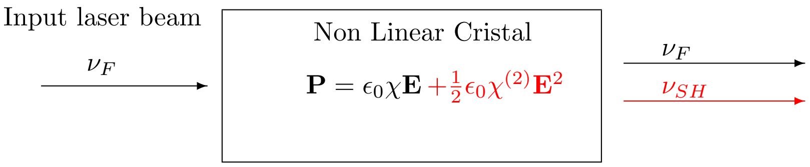

Figure 4.5: Basic principle of Second Harmonic Generation. The incident electric field oscillating at a frequency ν_F induces in the medium a polarization. If the field amplitude is large enough the polarization can oscillate at twice the frequency of the incident wave emitting a new wave at a frequency $\nu_{SH} = 2\nu_F$. This new wave spatially superimposed with the fundamental one is called Second Harmonic (SH).

If one assumes a low conversion rate, the conversion efficiency of the SHG process, η, after a distance z in the non-linear medium is given by [ST91]:

$$\eta(z) = \frac{P_{SH(z)}}{P_F} = \frac{8\pi^2}{n_{SH} n_F^2 \lambda_F^2 c\epsilon_0} \frac{P_F}{A} d_{eff}^2 \left(\frac{\sin\left(\frac{\Delta k z}{2}\right)}{\frac{\Delta k}{2}} \right)^2 , \tag{4.14}$$

with $\Delta k = |k_{SHG} - k_F|$, P_F and P_{SH} the power of the fundamental and Second Harmonic beam respectively, n_F and n_{SH} the refractive indexes at the fundamental and SH wavelength respectively, A the cross sectional area of the beam, d_{eff} a coefficient representing the non-linearity of the crystal (and derived from the second order susceptibility tensor $\chi^{(2)}$).

As a consequence, the conversion efficiency is a function of the phase difference between the fundamental wave and the SH wave. Since the media used for SHG are usually dispersive the phase difference is not zero. Therefore if one looks at the evolution of the SH wave intensity along the propagation axis, one sees it oscillating with a period $\Lambda = 4\pi/\Delta k$ (Figure 4.6). In order to get a significant efficiency one has to maintain the two waves in phase, i.e to create the conditions of phase-matching.

A first phase-matching technique called critical phase-matching, CPM, uses two fundamental waves of orthogonal polarization and the birefringence of the crystal to achieve the phase-matching. However due to the effect of birefringent walk-off in CPM the distance of interaction between the two waves is small which limits the conversion efficiency, [ST91]. Well designed set-up can compensate the birefringent walk-off but they require a careful alignment and a high mechanical stability.

In the second phase-matching technique called quasi phase-matching, QPM, the idea is to compensate periodically the phase mismatch by inverting the orientation of the non-linear medium which shifts the phase of the SH wave by π. If the change of orientation is done when the phase mismatch is an odd multiple of π then the waves are again in phase and the energy keeps being transferred from the fundamental wave to the SH wave, Figure 4.6. The advantage over CPM is that the interaction distance is much longer (centimeters instead of millimeters) and that for some type of crystal it allows to access larger non-linear coefficients of the second order susceptibility tensor $\chi^{(2)}$. Moreover periodically poled structures (crystal in which the polarization vector is periodically inverted) can be confined in a wave-guide which increases the conversion efficiency by increasing the power spatial density.

Tests of different non-linear crystals

SHG with CPM has been tested at IMT with a Potassium Titanyle Phosphate (KTP) crystal. 17 nW of light at 659 nm had been obtained from 60 mW of

Figure 4.6: Growth of the power in the second harmonic beam as a function of the distance of propagation for different phase-matching technique. The plot is calculated for a PPLN crystal. In the three cases the fundamental beam is assumed to have the same geometry and the same power. The significant difference between CPM and QPM in PPLN comes from the difference in the non-linear coefficients used. Λ represents the period over which the power in the SH beam varies because of the phase mismatch. The QPM plot assumes perfect quasi-phase-matching, i.e the period of the polarization poling of the crystal is equal to Λ.

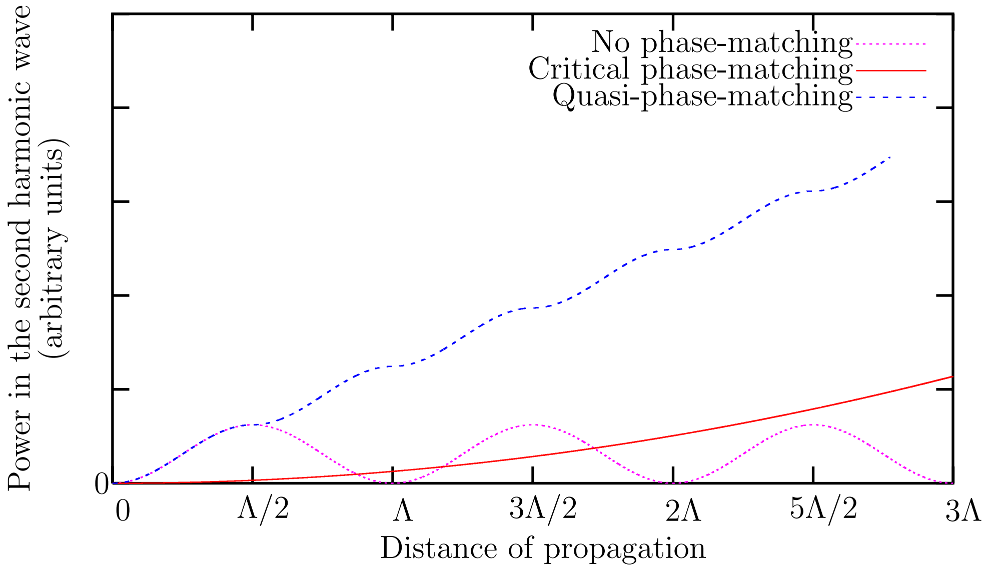

light at 1.319 μm. The efficiency is limited to 3×10^{-7} by the birefringent walk-off which limits the interaction distance to 1.5 mm in that case.

We have carried out tests on QPM with three different periodically poled structures: two bulk crystals of KTP and LN (Lithium Niobate, $LiNbO_3$) and a KTP wave-guide. The tests main objective was to determine the conversion efficiency but also to check that the parameters affecting the conversion efficiency could be easily controlled for each structure.

The 2 cm long KTP wave-guide has been quickly discarded as the injection in the $4 \times 4\,\mu m^2$ wave-guide was extremely difficult and sensitive to mechanical vibrations. No significant results could be obtained and the stability required to inject the light in the wave-guide was judged too high to use such a structure in a robust set-up.

The KTP and LN bulk crystals have been tested with the same set-up presented in Figure 4.7. The laser light was focused by an aspherical lens mounted on a 5 axis stage to allow an easy and precise alignment. The crystal was mounted in a temperature controlled oven.

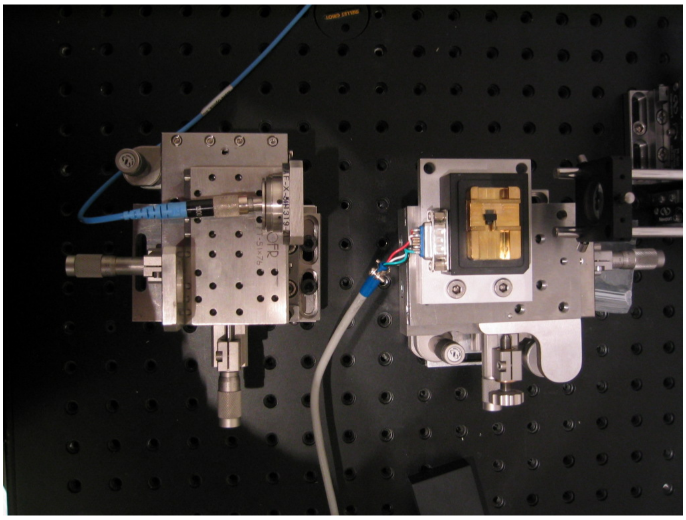

Figure 4.7: Set-up for the second harmonic generation. The light coming from the fibered (SM-PM) Nd:YAG laser is focused with an aspherical lens (focal length 15.4 mm) into the middle of a periodically poled non-linear crystal mounted in a temperature controlled oven. The alignment of the beam is tuned with the 5 axis stage holding the focusing lens.

Quasi-phase-matching uses structures in which the polarization of the material is inverted periodically. Phase-matching is achieved if the OPL seen by the fundamental wave during one period corresponds to a phase shift of π. Three parameters affect this OPL: the geometrical distance between two layers (which depends on the incident angle), the refractive index (which changes with temperature) and the wavelength of the fundamental wave. Consequently these three parameters must be controlled. Furthermore the conversion efficiency depends on the focusing of the beam in the non-linear crystal. The higher the power spatial density is, the higher the conversion efficiency. However, as laser beams are Gaussian and diverging, a compromise has to be found between a large slowly diverging beam and a tight focused but highly diverging beam. The most common focusing configuration is confocal focusing which is achieved when the waist of the beam is in the middle of the crystal and when the length of the crystal is equal to twice the Rayleigh range of the beam. However focusing is more efficient in the Boyd-Kleinmann configuration, [BK68], obtained when:

$$z_R = 5.68 \times L_{crystal}, \tag{4.15}$$

with $L_{crystal}$ the length of the crystal and z_R the Rayleigh range of the Gaussian laser beam. As the Rayleigh range, defined as the distance from the waist for which the radius of the beam is $\sqrt{2}$ times the waist radius, is linked to the radius of the waist w_0 through the equation:

$$z_R = \frac{\pi w_0^2}{\lambda} \tag{4.16}$$

the Equation 4.15 can be rewritten:

$$w_0 = \sqrt{\frac{\lambda}{\pi}\frac{L}{5.68}} \tag{4.17}$$

where the waist of the beam, situated in the middle of the crystal, is given as a function of the wavelength and of the length of the crystal. The experimental results showed that the largest conversion efficiencies were obtained for a focusing close to the Boyd-Kleinmann configuration. We have tested the impact of temperature and of the angle of incidence for both crystals. The experimental results are in good agreement with the theory, [FMJB92]. Experimental results for PPKTP are given as an example in Figure 4.8. In both cases none of the parameters are critical. Furthermore, as the wavelength of the laser light is stabilized the wavelength dependency is not a concern.

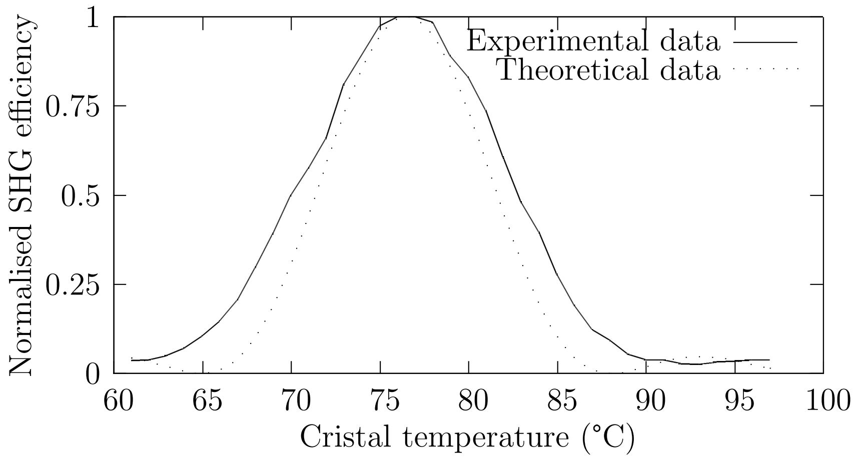

Figure 4.8: Normalised Second Harmonic Generation efficiency for a PPKTP crystal as a function of the crystal temperature.

The conversion efficiency measured with the PPLN crystal is much higher than with the PPKTP crystal. This is mainly due to the fact that in QPM LN presents a much larger non-linear coefficient than KTP ($d_{\text{eff}}=\chi^{(2)}_{333}=13.7\,\text{pm/V}$

for KTP against $d_{eff}=\chi^{(2)}_{333}=44$ pm/V for LN). For 50 mW of infrared input we measured 12 μW of light at 659 nm with the 2 cm PPLN crystal. A similar experiment with a 1 cm PPKTP provided only 4 μW of red light.

4.2.4 Experimental results on iodine spectroscopy and proposition of the specifications for the iodine cell

As the laser does not have an infinite wavelength tuning range a first experiment has been done to check the availability of usable transitions of iodine laying in the emission range of the frequency doubled Nd:YAG laser. Furthermore the experiments carried out with a test iodine cell have been used to establish the specifications of the final cell. We have measured the tuning characteristics of the laser and then the absorption spectrum of iodine.

Experimental determination of the tuning characteristics of the laser

The goal of this first measurement was to determine the tuning range, the tuning conversion rate (both in Hz as a function of the crystal temperature and as a function of the input voltage), the width and the position of the longitudinal mode of the laser emission. The wavelength has been measured with a commercial wave-meter (Burleigh WA-1500) in the visible after frequency doubling. The accuracy of such a system is ±45 MHz.

The centre of the tuning range of the laser is defined by a potentiometer which sets the temperature of the laser cavity (crystal). The wavelength is tuned by feeding the coarse tuning input of the laser power supply with a voltage between -10 V and 10 V. The temperature of the crystal is read on the laser micro-processor based power supply. With the factory settings the laser can be tuned over five longitudinal modes and 33 GHz, Table 4.1 and Figure 4.9.

Table 4.1: Tuning characteristics of the Lightwave NPRO 125 Nd:YAG laser.

Tuning coefficient within a mode	-5.4 GHz/°C, 2.59 GHz/V
Tuning coefficient over several modes	-1.1 GHz/°C, 1.61 GHz/V
Mode width	13.5 GHz
Total tuning range	33 GHz

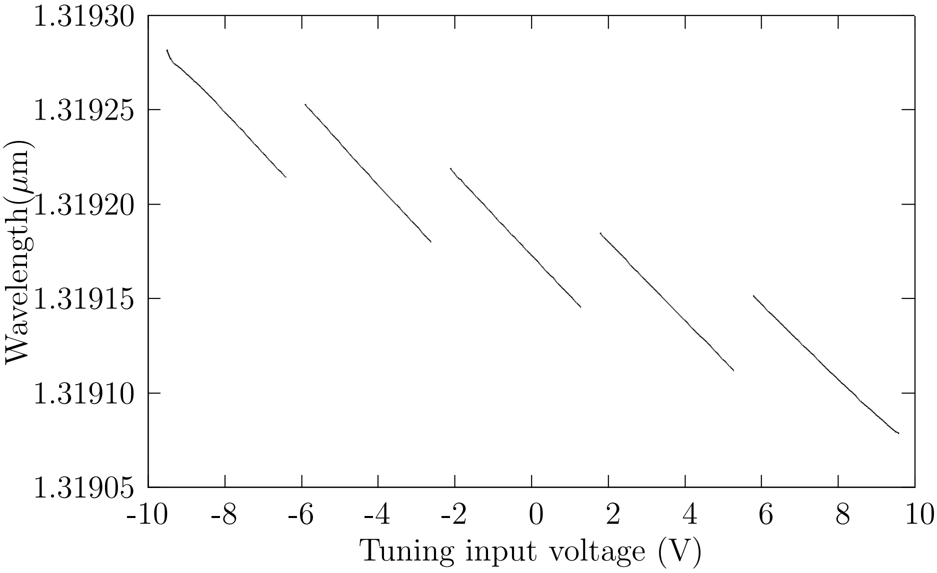

Figure 4.9: Wavelength emitted by the Lightwave NPRO 125 Nd:YAG as a function of the temperature tuning input voltage. The discontinuities are caused by the laser mode-hop during which the laser emission is multimode.

Experimental measurement of the transmission spectrum of iodine around 659.5 nm

The transmission spectrum of iodine has been measured with a test cell over the frequency range of the laser given by the factory settings and over the area used by Arie. The light of the laser was first doubled in frequency. The beam was collimated and sent through a beam splitter. Part of the beam was sent to the wave-meter while the second part was sent through the iodine cell. The intensity at the output of the cell is measured with a photodiode. Unfortunately only one photodiode was available and none could be used before the cell to measure the intensity so as to normalize properly the data. As a consequence our measurements were dependent on the intensity variation due to the laser or to the SHG. Nevertheless absorption lines were clearly visible in the data.

The tests on the test cell have also shown that the window of the cell should be optimized to maximize the transmission. Consequently the iodine cell for PRIMET has windows at the Brewster angle. PRIMET iodine cell is also equipped with a cold finger which allows to get the desired pressure at a temperature lower than the one required by the test cell. The transition line denoted P(49)6-6 in the Iodine atlas [GVC82] has been identified as being the best candidate for the frequency stabilization.

The transmission spectrum of iodine has been measured more precisely with the final cell and two photodiodes in order to get rid of the intensity fluctuations. The set-up used for the measurement is shown in Figure 4.10. In this experiment the laser wavelength is tuned by applying a slowly varying voltage to the temperature tuning input of the laser power supply. The transmission spectrum is presented in Figure 4.11.

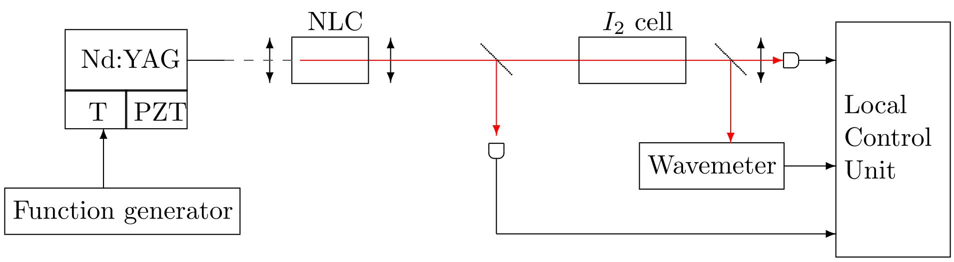

Figure 4.10: Iodine spectroscopy set-up

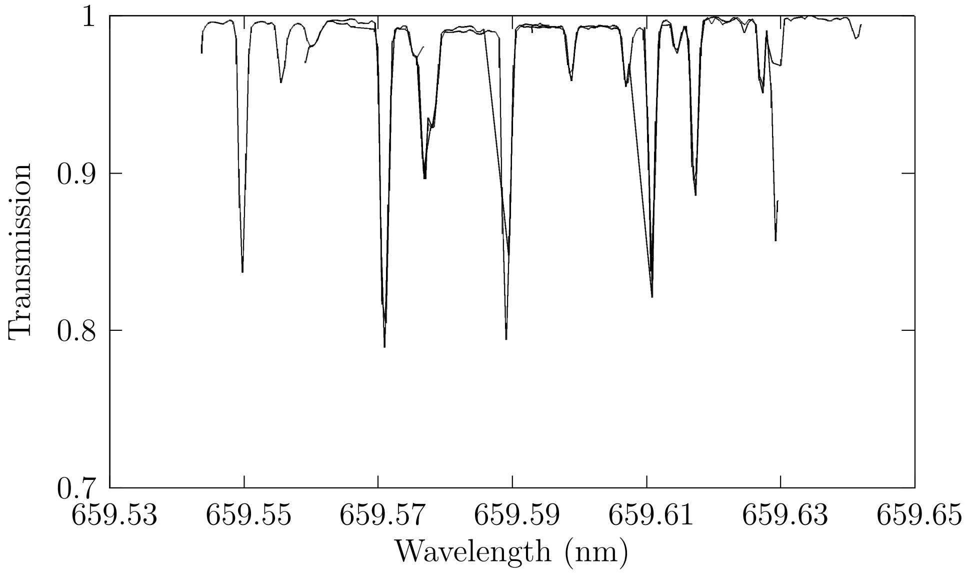

Figure 4.11: Iodine transmission spectrum around 659.5 nm obtained with PRIMET iodine cell (cold finger temperature 60 °C). The different curves correspond to different longitudinal modes of the laser. Outliers appear close to the mode-hops where the laser is no longer mono-mode. The absorption line at 659.5880 nm is denoted P(49)6-6 and has been chosen for the stabilization as it is deep and does not have close neighbours.

Experimental characterization of the transition P(49)6-6

In the transmission spectrum presented in Figure 4.11 the transition P(49)6-6 is the most interesting as it is deep, narrow and as it has no close neighbours which reduces the risks of locking the laser on another transition. P(49)6-6 has been scanned more precisely at different cell temperatures, Figure 4.12.

Figure 4.12: Iodine spectroscopy results (the wavelength resolution given by the wave-meter is 0.1 pm and the accuracy is ±0.1 pm). Left: profile of the absorption line P(49)6-6 of iodine for three different cold finger temperatures (50 °C, 60 °C and 70 °C). As the increase of the temperature increases the pressure in the cell, it deepens and broadens the absorption line. Right: comparison of the experimental data to two models of profile for the transition measured with a cold finger temperature of 70 °C. The best model is Gaussian centered on ν_0=659.5885 nm with a FWHM $\Delta\nu$=864 MHz and a maximum absorption A_{max}=0.35

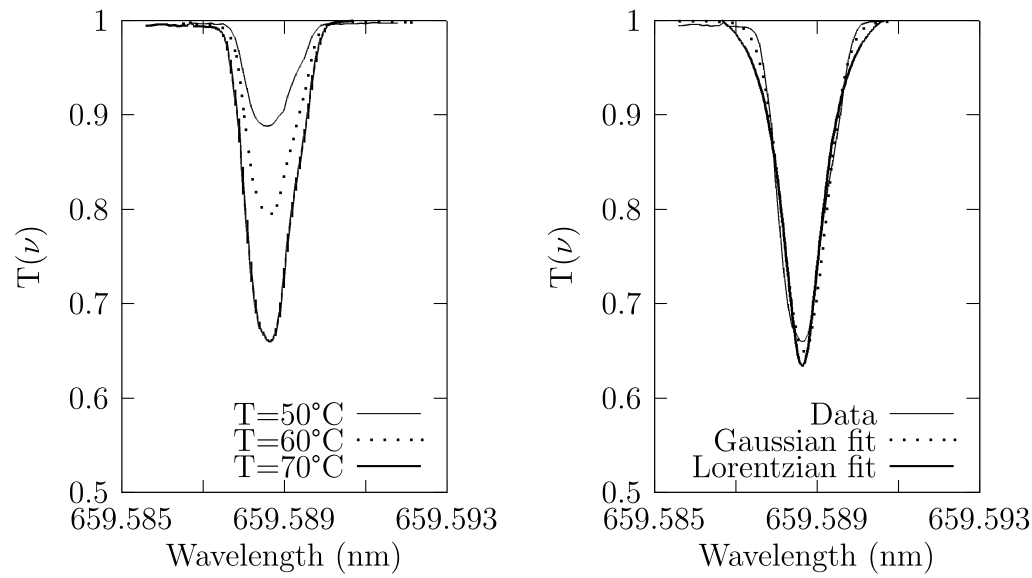

As explained in Section 4.2.1 the error signal generated by the Pound-Drever-Hall method is proportional to the first derivative of the absorption line profile. Absorption lines present usually a Lorentzian profile or a Gaussian profile if they are broadened by the Doppler effect due to the pressure, Table 4.2. Of special interest is the slope of the error signal for wavelength close to the centre wavelength as it is the working regime of the system. The steeper the slope is, the faster and the more accurate the system is.

The data are best fitted by a Gaussian profile. For the three test temperatures the characteristics obtained after fitting the data are given in Table

Table 4.2: Transmission models of a transition and corresponding error signals. T(ν) is the absorption profile, $\epsilon(\nu)$ is the error signal and $\epsilon_0(\nu)$ is the error signal close to the centre of the transition.

	Gaussian	Lorentzian
T(ν)	$T_0 - A_{max} \exp\left(-\frac{(\nu-\nu_0)^2}{2\sigma^2}\right)$ T_0 transmission of the cell A_{max} maximum absorption ν_0 centre frequency $\sigma = \Delta\nu/2\sqrt{2\ln 2}$, $\Delta\nu$ the line-width (FWHM)	$T_0 - A_{max} \frac{(\Delta\nu/2)^2}{(\nu-\nu_0)^2+(\Delta\nu/2)^2}$ T_0 transmission of the cell A_{max} maximum absorption ν_0 centre frequency $\Delta\nu$ the line-width (FWHM)
$\epsilon(\nu)$	$\frac{P_{in}\pi\nu_{FM}S_{VP}A_{max}(\nu-\nu_0)}{\sigma^2} \exp\left(-\frac{(\nu-\nu_0)^2}{2\sigma^2}\right)$ P_{in} incident power ν_{FM} modulation frequency S_{VP} detector sensitivity	$2A_{max}\left(\nu-\nu_0\right) \frac{P_{in}\pi\nu_{FM}S_{VP}(\Delta\nu/2)^2}{\left((\nu-\nu_0)^2+(\Delta\nu/2)^2\right)^2}$ P_{in} incident power $\pi\nu_{FM}$ modulation frequency S_{VP} detector sensitivity
$\epsilon_0(\nu)$	$\frac{P_{in}\pi\nu_{FM}S_{VP}A_{max}}{\sigma^2}\left(\nu-\nu_0\right)$ P_{in} incident power ν_{FM} modulation frequency S_{VP} detector sensitivity	$\frac{8A_{max}P_{in}\pi\nu_{FM}S_{VP}}{\Delta\nu^2}\left(\nu-\nu_0\right)$ P_{in} incident power ν_{FM} modulation frequency S_{VP} detector sensitivity

4.3. The slope of the error signal close to the centre wavelength, which is proportional to A_{max}/σ^2 for a Gaussian like transition, increases with the temperature of the cold finger. Consequently the stabilization is operated with the cold finger at 70 °C. A higher temperature would increase the error signal but may reduce the lifetime of the iodine cell. During these tests the wavelength has been measured with a commercial wave-meter which indicated 659.58855 nm. This does not correspond to the centre wavelength of P(49)6-6 measured previously with another wave-meter or given in the literature, [ABFB93, GVC82]. Additional measurements done with a self-referenced optical frequency comb generator at the Max Planck Institute for Quantum Optics (see Section 5.2.5) confirmed that the centre wavelength of P(49)6-6 is ν_0=659.5880 nm.

Table 4.3: Characteristics of P(49)6-6 for three different temperatures of the cold finger (the transition is assumed to have a Gaussian profile).

Cold finger temperature (°C)	A_{max} (%)	σ (MHz)	A_{max}/σ^2 (Hz^{-2})
50	11.58	352	9.34×10^{-9}
60	21.16	362	1.6×10^{-8}
70	34.97	367	2.59×10^{-8}

4.2.5 Proposition of an upgrade of the control loop

As delivered by IMT the system operated only the fast actuator. Due to its limited range, ± 20 MHz, and to the slow drift of the laser frequency, the loop could be kept closed only for a few tens of minutes. This is not compatible with PRIMA which requires 30 minutes continuous observation. Moreover the loop should be kept closed over a full night to minimize the technical downtown and increase the efficiency of the instrument. Therefore we have implemented an upgrade of the control loop which uses the temperature actuator to desaturate the piezo. With its large operating range, ± 20 GHz, the temperature actuator allows theoretically to keep the loop closed indefinitely.

The specific of the control loop comes from the characteristics of the two actuators that can be used to correct for the frequency noise of the laser. Piezo tuning provides a fast correction (bandwidth around 1 kHz) with a high resolution (600 Hz) over a limited range. Temperature tuning offers a broad range of correction with a poor resolution (around 400 kHz, set by the voltage source resolution) and a small bandwidth (1 Hz).

The difficulty is to implement a loop using these two actuators in spite of their much different scalings. The design of the loop is given in Figure 4.13.

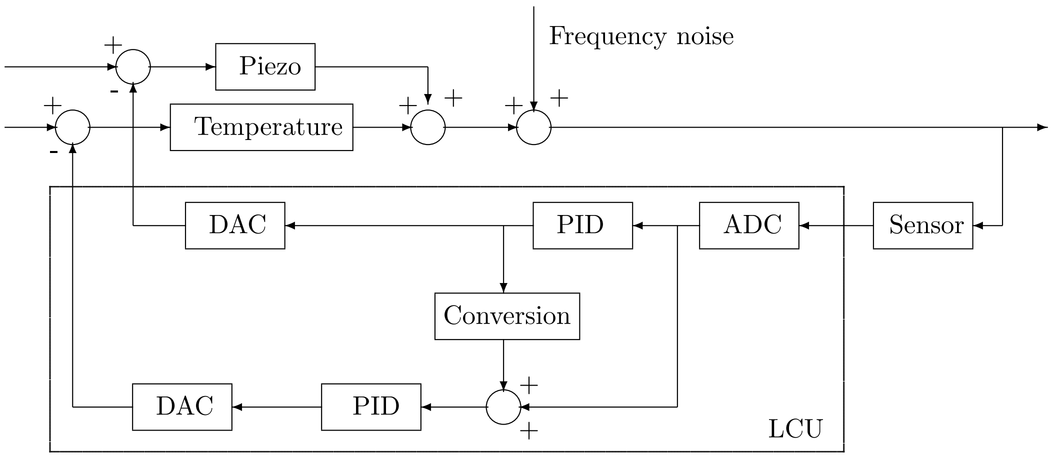

Figure 4.13: Control loop architecture. The block Sensor includes all the hardware required for the generation of the error signal with the Pound-Drever-Hall method.

The signal fed to the piezo actuator is generated by a PID corrector. This signal is converted into its equivalent frequency shift and is then added to the error signal seen by the PID used by the temperature actuator. This is done so that the temperature actuator which has a large range of correction desaturates the piezo actuator. The PID parameters are calculated separately using the Ziegler-Nichols method. Such an architecture for a control loop is usually not advised since there is the possibility that the two loops compete against each other. However in this case the dynamics of the two loops are so different that the correction of the piezo has a limited effect on the temperature loop.

The control loop is implemented digitally using TAC which is an ESO standard library for control. In this configuration the loop remains closed for hours. Over one year of regular tests and operation no failure have been observed proving the efficiency of the system.

Chapter 5

Experimental characterization of the performance of the stabilized Nd:YAG laser

In order to perform accurate measurements over several years, the PRIMET laser is frequency stabilized on a transition of iodine using the Pound-Drever-Hall method described in the previous chapter. IMT has delivered to ESO the set-up of the laser frequency stabilization system. However the system was not fully functional and characterized.

My work has been to characterize the system and optimize it when possible. The difficulty of frequency stabilization of lasers emitting around 1.3 microns is the absence of references as explained in the previous chapter. Consequently, we have first tried to characterize the performance of the system from the error signal of the control loop. However such a characterization is flawed as the sensor measuring the performance is the one used in the control loop. That's why we have proposed to use an independent sensor and have taken the opportunity offered to ESO by the Max Planck Institute of Quantum Optics (Garching bei München, Germany) to use their self-referenced optical frequency comb generator.

This chapter presents the characterization of the PRIMET stabilized laser and how the system has been improved. In the first section the system set-up is presented along with the performance as measured from the control loop residual error signal. Then, in Section 5.2, a self-referenced frequency comb generator is used to measure the frequency stability of the system and calibrate its wavelength.

5.1 Experimental measurement of the residual error signal in closed loop

5.1.1 Set-up

The system has been installed on a $75\times 90\,\mathrm{cm}^2$ breadboard on an optical table in the ESO laboratory. The optical set-up and its associated electronics are presented in Figure 5.1.

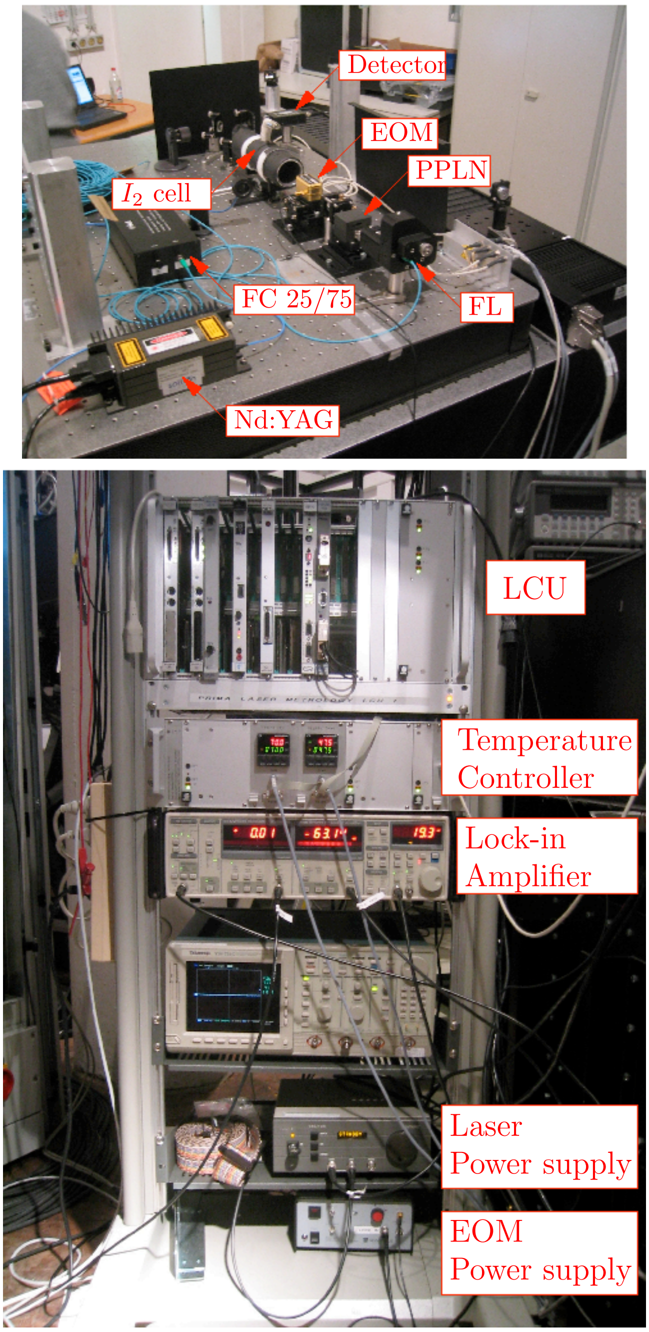

Figure 5.1: Setup of PRIMET absolute laser stabilization system. Top: optical setup. FL: Focusing Lens; FC: Fiber Coupler; PPLN: Periodically Poled Lithium Niobate; EOM: Electro-Optic Modulator. Bottom: control electronics. LCU: Local Control Unit.

5.1.2 Experimental calibration of the error signal

The error signal generated by the Pound-Drever-Hall method is a function of several parameters. Thus it has to be calibrated if one wants to use it as an indicator of the stability of the system. According to the Gaussian model of the transition obtained in Section 4.2.4 the slope of the error signal close to the centre of the transition is given by:

$$\epsilon_0 = 8 \ln 2 \frac{P_{in} \nu_{FM} S_{VP} A_{max}}{\Delta\nu^2} \tag{5.1}$$

with P_{in} the power in the input beam at 659 nm, ν_{FM} the phase modulation frequency, S_{VP} the sensitivity of the detector, A_{max} the maximum absorption of the transition and $\Delta\nu$ the width at half minimum of the transition. A_{max} and $\Delta\nu$ have been measured to be 0.35 and 864 MHz for a cold finger temperature of 70 °C. We measured the sensitivity of the Si AC coupled photodiode (bandwidth 36 MHz) to be 0.49 V/μW at 659.5 nm. The phase modulation frequency is 25 MHz. Assuming the power of the input beam is 12 μW the slope of the error signal close to the centre of the frequency should be approximately 1.2 V/GHz.

The transition as been scanned several time by applying a triangular signal to the temperature tuning input of the laser controller. The error signal has been recorded along with the tuning signal. From the tuning signal it is possible to deduce the frequency shift using the conversion factor measured with the wavemeter and summarized in Table 4.1. In Figure 5.2 the error signal is plotted as a function of the frequency shift for several successive scans of P(49)6-6. The temperature modulation of the laser cavity used to tune the frequency presents an hysteresis clearly visible on the plot. The variations of amplitude are due to intensity fluctuations, Residual Amplitude Modulation (RAM) and electronic cross-talk on the detector cables. The asymmetry of the absorption profile, barely noticeable in Figure 4.12, is here clearly visible.

The average slope of the error signal in the range ±10 MHz around the centre of the transition, working range when the loop is closed, is approximately 350 mV/GHz. The discrepancy with the theoretical value may be explained by an amplitude of the phase modulation smaller than π.

5.1.3 Results of the stability tests based on the error signal

A voltage offset was fed to the temperature tuning input to preset the laser frequency close to the centre of the transition. The error signal was measured

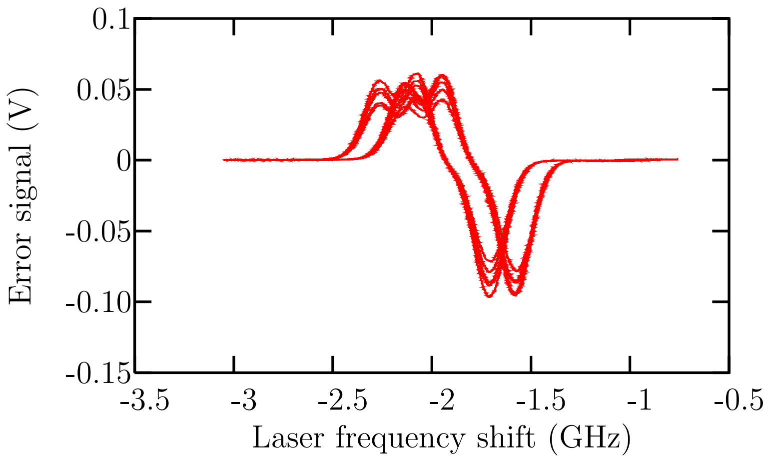

Figure 5.2: Error signal as a function of the frequency shift for several successive scans of P(49)6-6. The presence of two groups of scans is due to the hysteresis of the frequency tuning process. The variations of amplitude are due to intensity fluctuations, Residual Amplitude Modulation (RAM) and electronic cross-talk on the detector cables. The asymmetry of the absorption profile is clearly visible.

in open loop at the output of the lock-in amplifier using the LCU and a TAC interface. A closed loop measurement has also been done.

The results of both measurements are plotted in Figure 5.3. The conversion coefficient calculated in the previous section is used to estimate the frequency error from the error signal measured by the LCU.

The measurements show a significant reduction of the frequency noise. Over half an hour the standard deviation is estimated to 72 kHz. However these measurements can only be considered as a rough indicator as they are based on the same detector than the one used by the control loop. Detection noise appears in the sensor and is uncorrelated with the frequency noise. It is introduced and amplified in the control loop, see Figure 5.4. The actuators driven by the control loop transform the detection in frequency noise which compensates for the error signal due to detection noise. Therefore the error signal may appear stable while the loop is creating noise in the system. As a consequence an external detector has to be used to measure the performances of the stabilization system independently.

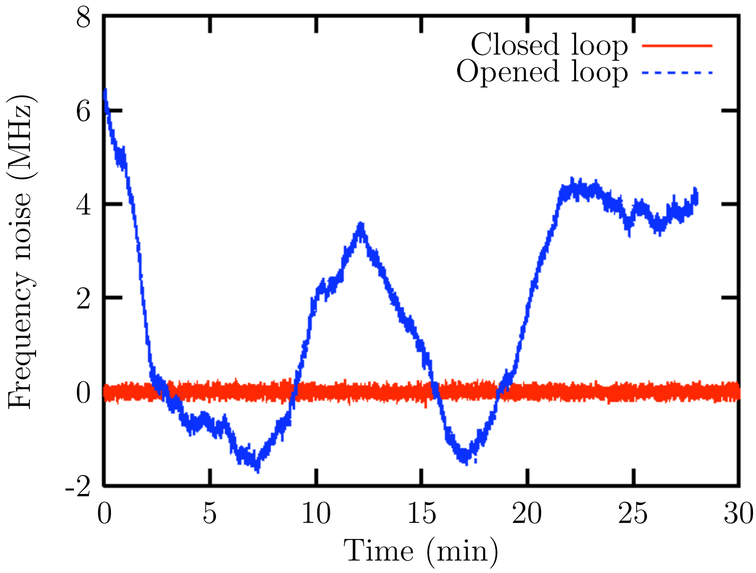

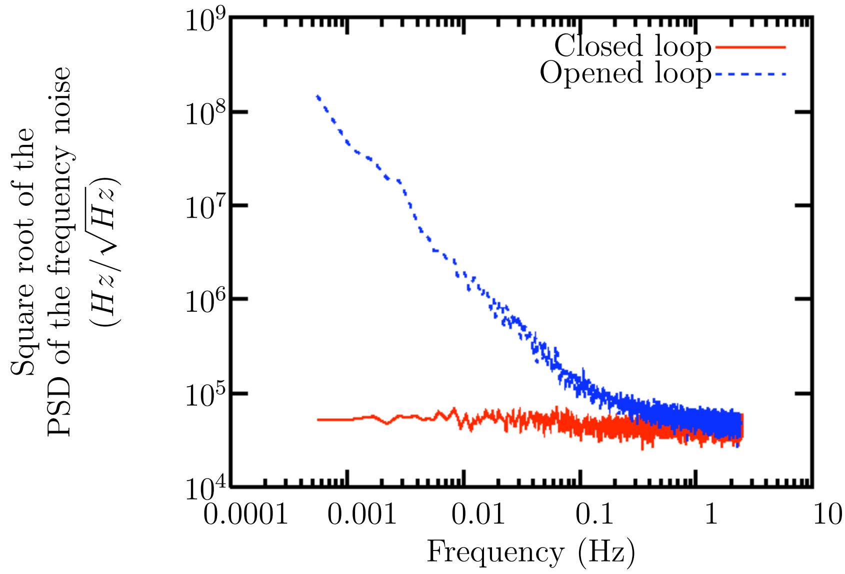

Figure 5.3: Estimated frequency noise in opened loop and closed loop. The frequency noise is estimated from the error signal using the conversion coefficient equal to 350 mV/GHz. Top: frequency noise as a function of time. Bottom: square root of the power spectral density of the frequency noise.

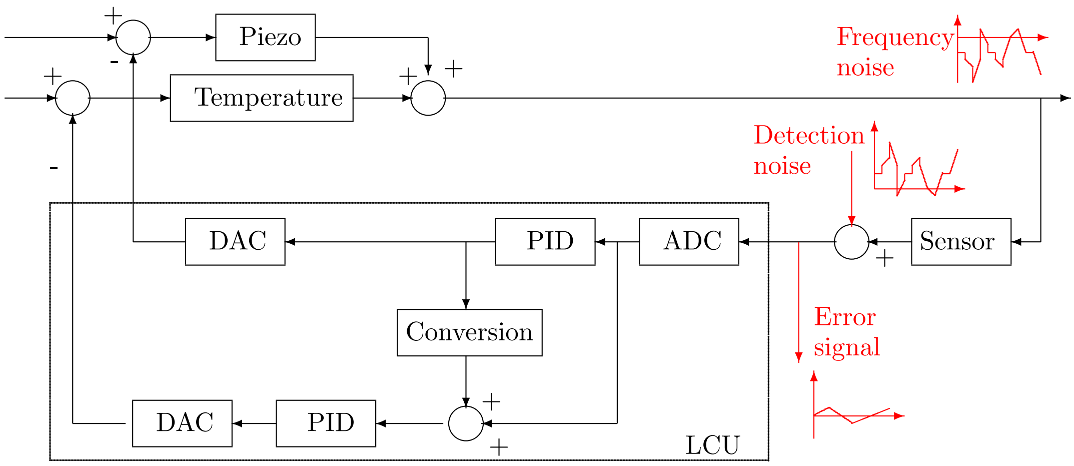

Figure 5.4: Detection noise in the control loop.

5.2 Results of the stability test carried out with an independent frequency sensor

The difficulty of frequency stabilization at 1.319 μm lies in the measurement of the frequency since few references are available. The stability of a laser is usually measured by beat frequency with an identical laser. Both lasers are assumed to have an equivalent contribution to the frequency noise of the beat signal. However, as it was not foreseen to build a second stabilized laser for cost reasons this could not be done. No single mode continuous wave stabilized laser, which could have served as a reference, are commercially available at this wavelength. However Optical Frequency Comb Generators (OFCG) can be stabilized at another wavelength and provide a reference at 1.319 μm due to their broad spectrum. Moreover self-referenced OFCG do not require a reference at optical frequencies since they are stabilized on a radio frequency. The Max Planck Institute for Quantum Optics is developing such optical frequency combs and they have offered to us the opportunity to test and calibrate the stabilized laser by comparison with one of their fibered self-referenced optical frequency comb generators.

5.2.1 Spectrum delivered by an optical frequency comb

An optical frequency comb delivers a discrete spectrum made of equally spaced modes in the frequency domain. Different techniques can be used to emit such a comb as described in [Lui01]. In this section we will define a few quantities that describes the comb. A comb has two degrees of freedom as shown in Figure 5.5.:

- the dilatation of the space between the modes of the comb
- the translation of the whole comb toward lower or larger frequencies.

The frequency between two adjacent modes of the comb is called the repetition rate, f_{rep}, as it is the inverse of the time between two pulses emitted by the comb. The translation of the whole comb is described by the quantity called the offset frequency, f_0, which is the distance between the modes of the comb and their closest harmonics of the repetition rate.

Consequently if one considers that the comb is infinite and defines the closest mode to the zero frequency as being the mode number 0, the frequency f_n of the n^{th} mode is given by:

$$f_n = f_0 + n \times f_{rep}, \tag{5.2}$$

where f_0 is the offset frequency and f_{rep} the repetition frequency.

If one considers now the beat frequency f_{beat} measured between the comb and the Nd:YAG laser it is possible to deduce the frequency f of the Nd:YAG laser provided three parameters are known: the offset frequency, the repetition frequency and the number of the mode with which the beat signal is obtained:

$$f = f_n + f_{beat} = f_0 + n \times f_{rep} + f_{beat} \tag{5.3}$$

Unfortunately only absolute values of the offset frequency and beat frequency are measurable. Nevertheless one can determine the sign of these quantities if the Nd:YAG laser is stable enough. Indeed if one increases the repetition frequency of the comb one sees the absolute value of the beat frequency increasing if the beat frequency is negative and decreasing if it is positive. Knowing the sign of the beat frequency one can deduce the sign of the offset frequency. Let's consider the case when the beat frequency is negative and measure the variation of the beat frequency when the absolute value of the offset frequency is increased. If the absolute value of the repetition frequency increases it means that the comb is translated toward the high frequencies, i.e the offset frequency is positive. In the opposite case it means the comb is translated toward the low frequencies and the repetition rate is negative. The same reasoning can be applied to the case where the beat frequency is positive.

The number of the mode is determined with a wave-meter which has an accuracy better than 50 MHz which is the half of the repetition rate.

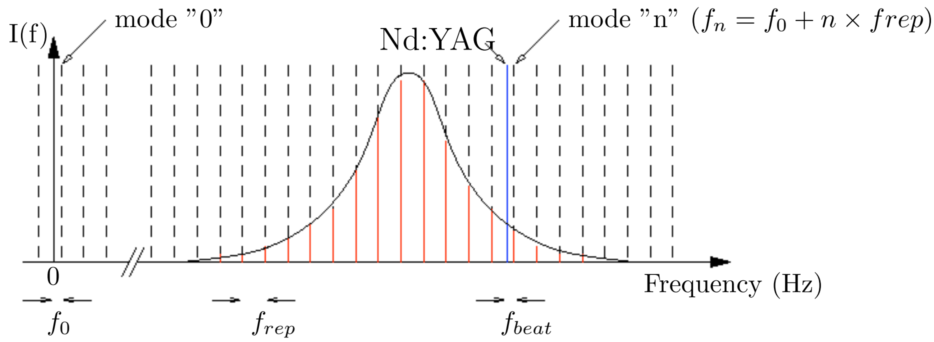

Figure 5.5: Sketch of the comb spectrum.

5.2.2 Set-up

The frequency comb of the MPQ was stabilized on a cesium clock ensuring a relative frequency accuracy better than 10^{-12}. The comb provides modes spaced by 100 MHz over the range 1050-2100 nm.

The PRIMET laser stabilization system was transferred to the Max Planck laboratory to perform the tests, Figure 5.6. The frequency stability of the Nd:YAG laser is measured by monitoring the frequency of the beat signal obtained between the Nd:YAG and one mode of the comb. This is assumed to be perfectly stable. The optics for the interface of the two lasers and the controlling electronics were already installed by the MPQ. At the comb output a part of its spectrum (around 15 nm over the full 1000 nm spectrum) is selected using a grating and injected into a single mode fiber. A fiber coupler is used to mix the light of the Nd:YAG with the light of the comb. The comb fiber is equipped with a polarization controller and a variable attenuator to maximize the signal to noise ratio of the beat signal. The beat signal is detected with a high sensitivity avalanche detector. Its output is amplified and band-pass filtered around the beat frequency to maximize the SNR. Around 10 mW of laser light from the Nd:YAG laser were required to get a 30 dB SNR. A counter is used to measure the frequency of the beat signal. Data are transferred to a computer via a RS-232 connexion and recorded. In addition to the beat signal and the time stamps, the data contain the repetition rate of the comb and its offset frequency (these quantities are defined in more details in Section 5.2.1) both of them are measured by a counter (HP 53131A). A schematic of the set-up is given in Figure 5.6.

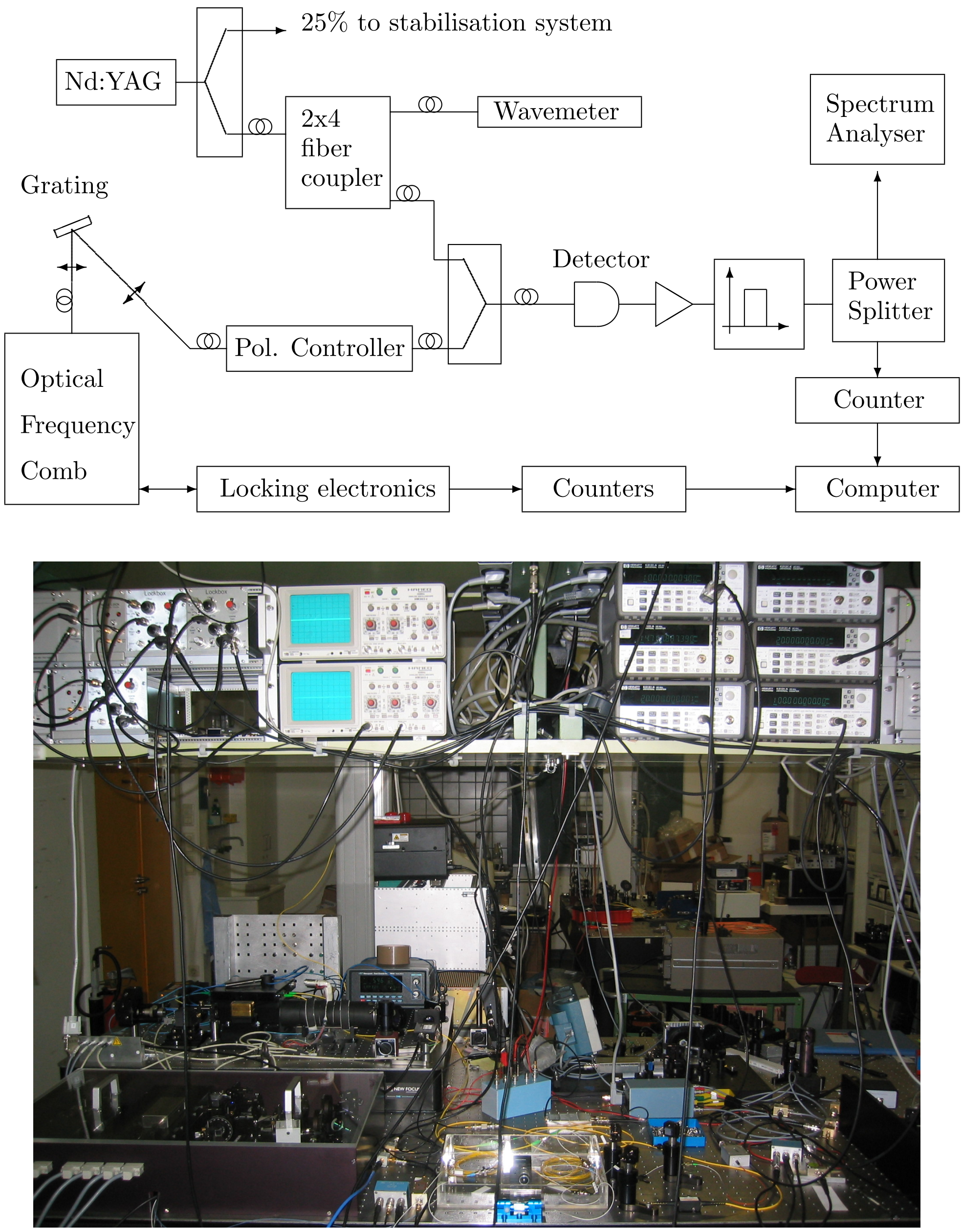

Figure 5.6: Set-up for the measurement of the Nd:YAG frequency stability by comparison with a mode of a self-referenced optical frequency comb generator. Top: Sketch of the set-up. Bottom: Picture of the set-up. The comb is at the bottom left in the black box. PRIMET laser is on the breadboard just behind it. On top are the counters and the locking electronics.

5.2.3 Results of the frequency stability measurements

A beat frequency measurement is shown in Figure 5.7. The counter delivered contiguous samples averaged over 0.1 s. The power spectral density of the frequency noise is compared to the one estimated from the loop residual signal in Figure 5.7. These measurements show the presence of detection noise in the stabilization loop. Indeed, the performances measured with the frequency comb are worse than the one deduced from the error signal. For the data set plotted in Figure 5.7 the standard deviation is 224 kHz and the peak-to-valley frequency noise is 1.45 MHz. This is to be compared to a standard deviation of 72 kHz using the error signal (see Section 5.1.3).

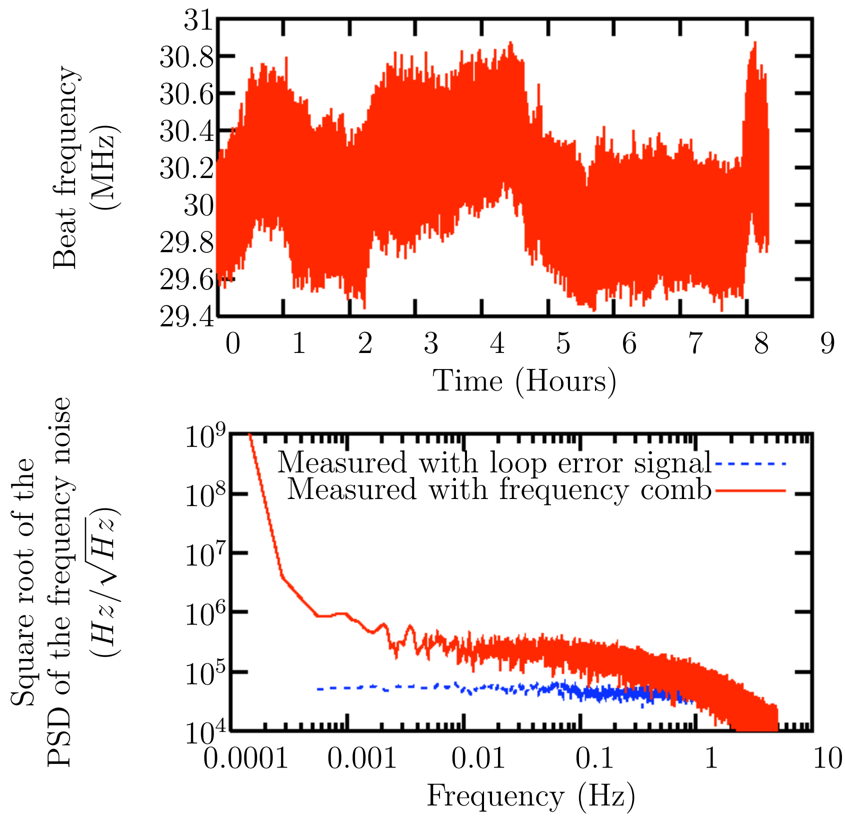

Figure 5.7: Top: beat frequency between the stabilized Nd:YAG laser and one mode of the frequency comb. Bottom: square root of the power spectral density of the error signal for the laser operated free-running or in closed loop.

5.2.4 Results of the experimental estimation of the detection noise

As it has been shown in the previous section the performance of the laser stabilization system is decreased by detection noise. We have measured this detection noise by locking the Nd:YAG laser on the frequency comb at the frequency of the centre of the transition. The Nd:YAG is stabilized with a phase-lock-loop on a mode of the optical frequency comb close to the centre of the transition P(49)6-6. An offset is applied to the error signal in order to tune the wavelength of the Nd:YAG so that its frequency is at the centre of the transition, i.e so that the error signal derived with the PDH method is zero. The stability of the Nd:YAG laser with respect to the comb is measured with a counter from the beat signal. It is better than 1 Hz peak-to-peak. Therefore it is limited by the accuracy of the reference clock which is used by the counter. The absolute frequency of the Nd:YAG laser is stable at least at the kHz level.

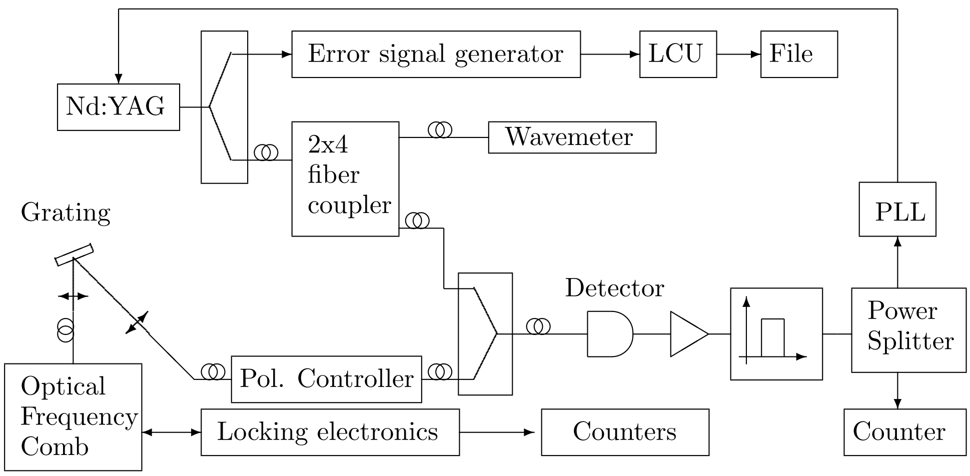

Figure 5.8: Setup for the estimation of the detection noise of the frequency sensor. The Nd:YAG laser is stabilized to the optical frequency comb with a phase-lock loop and the piezo actuator. The locking frequency is at the centre of the transition used for the iodine stabilization. The error signal seen by the Nd:YAG control loop is recorded.

As the the laser is perfectly stable at the centre of the transition the error signal should be constant and equal to zero. However we have measured a non zero varying error signal corresponding to the detection noise, see Figure

5.9. For the control loop this error corresponds to a frequency shift to be corrected. This noise is injected in the laser frequency and creates a real frequency noise. The signal is plotted in Figure 5.9 and the right axis shows which frequency shift would create such an equivalent level of frequency noise. The detection noise corresponds to a frequency noise of standard deviation 135 kHz which cannot be neglected compared to the 224 kHZ standard deviation measured previously for the laser frequency stability. Methods to reduce this noise are presented in Section 5.3.

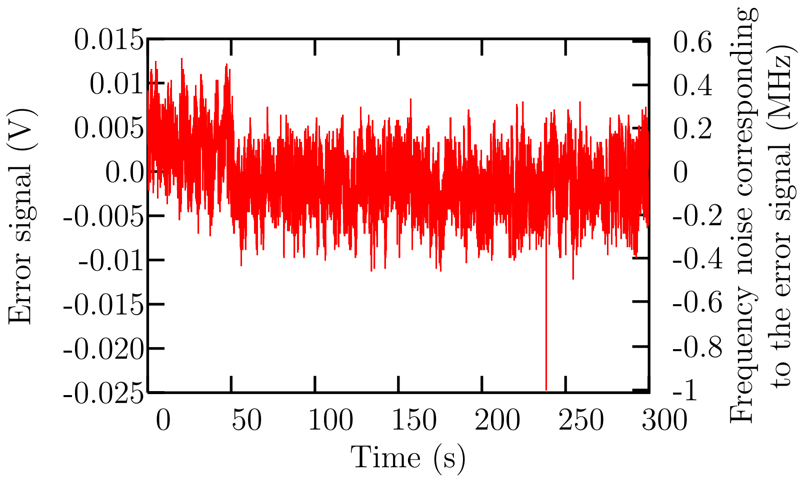

Figure 5.9: Detection noise measured by the lock-in amplifier with the Nd:YAG laser locked on the frequency comb in the middle of the P(49)6-6 transition. This error signal should be zero as the Nd:YAG locked to the comb is stable at the kilohertz level. When the loop is closed on the iodine transition, this detection signal is seen by the controller as a frequency noise and is injected in the loop.

5.2.5 Results of the experimental calibration of the laser wavelength

The PRIMET laser frequency must calibrated with an accuracy better than 10^{-8}. The laser frequency has been measured by means of an optical frequency comb. The number of the mode with which the beat signal was observed has been determined with a wave-meter. The sign of the beat frequency and of the offset frequency have been determined as described in Section 5.2.1. The average frequencies of every measurement file have been computed and are plotted in Figure 5.10. We obtained an average laser frequency of 227,257,330,623,020 Hz with a standard deviation of 94 kHz. The wavelength is 1.319,176 μm. This wavelength corresponds to a second harmonic wavelength of 659.5880 nm in good agreement with other measurements made of P(49)6-6, [ABFB93, GVC82]. The repeatability of the wavelength is better than 100 kHz over one week as shown in Figure 5.10.

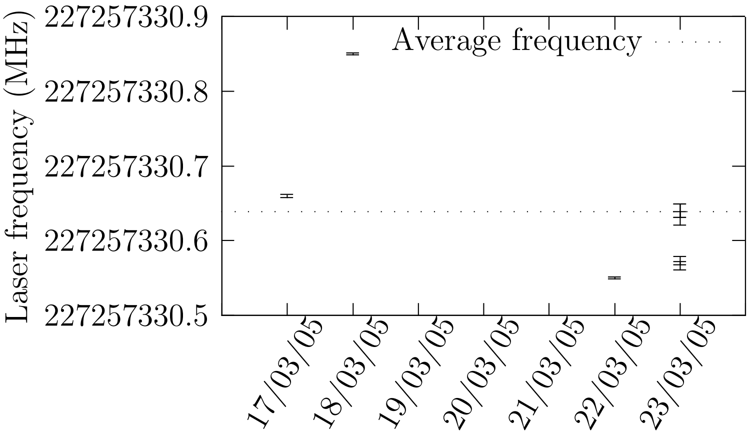

Figure 5.10: Average locking frequency for several measurement files obtained in March 2005. The frequency is measured with an optical frequency comb generator from the Max Planck institute for Quantum Optics. The repeatability of the wavelength is better than 100 kHz over one week.

5.3 Propositions for the reduction of the detection noise

The sources of detection noise have been investigated and two sources have been found, namely electronic cross-talk between the EOM and the detector and Residual Amplitude Modulation in the EOM. As the lock-in amplifier applies a narrow band-pass filter (bandwidth 120 Hz) around the reference frequency, most of the detection noise has no consequence on the loop stability. However any source of noise around 25 MHz will add frequency noise to the laser output.

5.3.1 Detection and reduction of the electronic cross-talk

A first source of detection noise has been identified using a power spectrum analyzer at the output of the photodiode. We noticed that the signal at the output of the photodiode presented a strong component at 25 MHz even in the absence of light. This signal is due to Electro-Magnetic Compatibility problem between the EOM driver signal and the photodiode. The wire transmitting the phase modulation signal to the EOM acts like an antenna. Its signal was picked up by the photodiode or its power or bias cables. This source of noise could be reduced to the noise level of the detector, see Figure 5.3.1, by a careful wiring of the whole set-up.

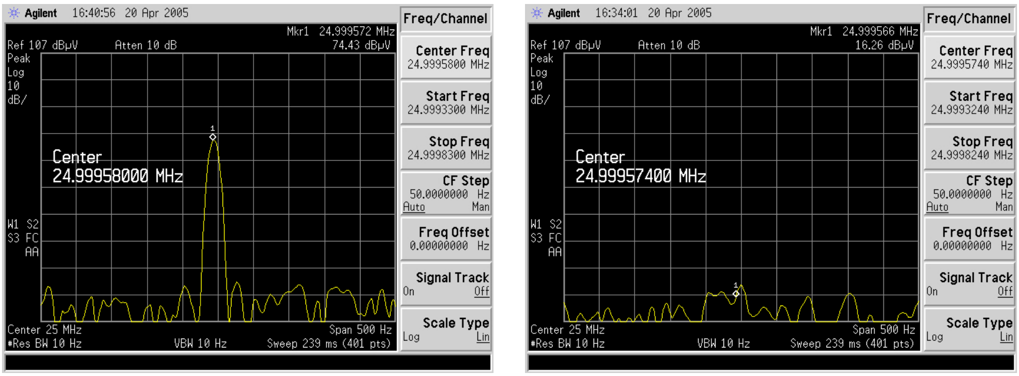

Figure 5.11: Reduction of the RAM obtained by a careful wiring of the set-up. Left: RAM level due to Electro-Magnetic Compatibility problems between the EOM and the photodiode. Right: RAM level after a careful wiring of the system.

5.3.2 Measurement of the Residual Amplitude Modulation and conclusion on its reduction

Detection noise can be caused optically if there is an intensity noise in the bandwidth of the lock-in amplifier which is 25 MHz ±60 Hz. This intensity noise is created by the EOM and is generally called Residual Amplitude Modulation (RAM). It has at least two different origins.

Part of the RAM is created by a polarization mismatch between the incoming polarization state and the axis of the crystal. In the EOM the refractive index is modulated by the electric field only along one axis of the crystal. Thus only the light linearly polarized along this axis is phase modulated, whereas the perpendicular polarization component remains unchanged. If the output beam goes through any polarizing optics, interference are created between the two components. This generates an intensity modulation at the phase modulation frequency. In the set-up the EOM is followed by the iodine cell whose windows are at the Brewster Angle 4.4. However in the set-up the light is linearly polarized before the EOM by the SHG process 4.2.3. The insertion of a half-wave plate before the EOM does not decrease significantly the detection noise. Therefore this phenomenon is not the source of RAM in the set-up.

On the other hand RAM can be introduced by a cavity effect in the EOM. This is described in [WGB85]. The RAM is a function of the cavity optical length. A pure offset of the error signal caused by this cavity effect would not be a problem for PRIMET, provided the wavelength is calibrated. However, this cavity effect is temperature dependent and the temperature fluctuations generate a slow drift of the RAM level which makes any calibration useless. As a consequence a temperature stabilization set-up has been designed and implemented for the EOM in order to asses the importance of the temperature fluctuations on the RAM level. The EOM is mounted in a custom made aluminum box with two small apertures for the input and output beams. A pt-100 sensor is is fixed with thermal glue to the EOM while heating bands are applied on top and at the bottom of the box. No actuators are used to cool the box. The sensor is read by a temperature controller which uses a PID corrector to deliver a feedback voltage between 0-10 V. This voltage is amplified and applied to the heating bands. Due to the resolution of the controller the stability is limited to $\pm$ 0.1 °C.

The RAM has been measured for a step command applied to the temperature of the EOM. The result is plotted in Figure 5.12. One can see that the RAM oscillates with the variations of the temperature. The period of the RAM oscillation is approximately 0.2 °C. The amplitude is equivalent to an error signal caused by a frequency drift of 840 kHz. Therefore the temperature stabilization of the EOM should be better than 0.2 K to reduce the RAM. Such an upgrade of the system would increase its complexity and provide only little improvement. Therefore it has not been implemented.

The sources of detection noise and their magnitude are recalled in Table 5.1. The electric cross-talk could be reduced to the detector noise level. The polarization induced RAM can be neglected. Detection noise is mostly produced by the RAM created in the EOM cavity and is limited to 840 kHz standard deviation when the temperature of the EOM is stabilized to $\pm$ 0.1 °. The sum of the frequency variations induced by detection noise remains below the specifications (2.26 MHz standard deviation).

Origin of noise	Equivalent frequency noise (standard deviation (kHz))	Comments
Electric cross-talk	114 kHz	Reduced to the detector noise level
RAM (polarization)	-	can be neglected compared to RAM cavity
RAM (cavity)	400 kHz/K	840 kHz, EOM temperature stabilized to ± 0.1K
Detector + Lock-in + acquisition board	50 kHz	

Table 5.1: Summary of the sources of detection noise.

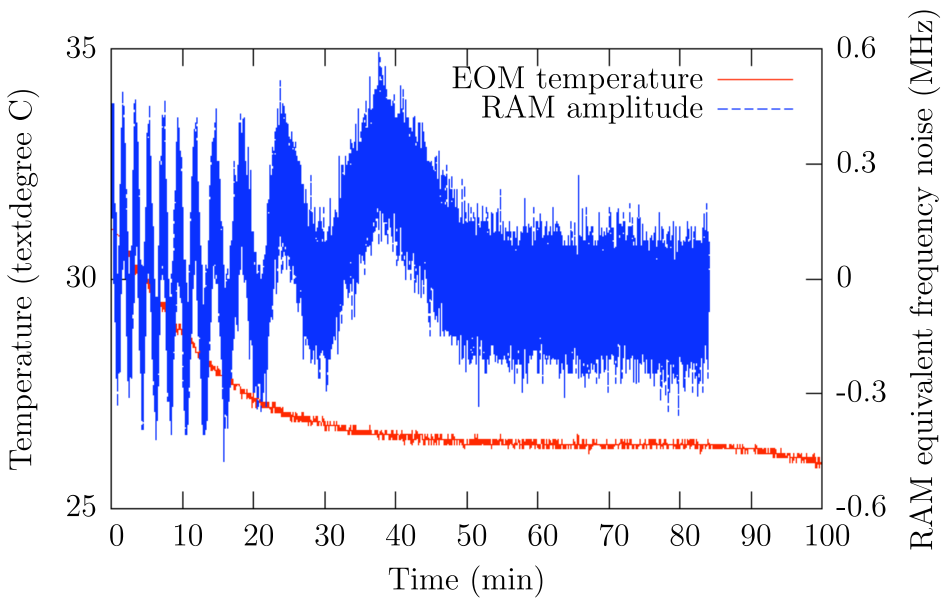

Figure 5.12: EOM temperature (°C) and RAM equivalent frequency noise (MHz) as a function of time (min).

5.4 Conclusion on the impact of the stabilization performance on PRIMET

The specifications of PRIMET is 5 nm accuracy with a 8 kHz bandwidth over a maximal stellar OPD of Δ L = 60 mm. It is given by the 30 minutes observation of two stars with maximal separation (1 arcmin) with a maximum baseline of 200 m. To keep a security margin the maximum error of PRIMET due to the frequency calibration and stability is set to 3.6 nm. For a normal distribution this corresponds to a standard deviation $\sigma_{\Delta L}$=0.6 mm. The relative accuracy of the system is then:

$$\epsilon_R = \frac{\sigma_{\Delta L}}{\Delta L} = 10^{-8}. \tag{5.4}$$

In order to achieve such a performance the laser optical frequency accuracy should be the same according to the Equation 2.49:

$$\frac{\sigma_\nu}{\nu} = \frac{\sigma_\lambda}{\lambda} = \epsilon_R = 10^{-8}. \tag{5.5}$$

As the optical frequency of the laser is approximately $\nu = 227\,\mathrm{THz}$ the maximum standard deviation of the laser over the bandwidth 0.5 mHz - 8 kHz is:

$$\sigma_\nu < 2.27\,\mathrm{MHz}. \tag{5.6}$$

The measurements we have carried out with the frequency comb gave us access to a maximum bandwidth of 10 Hz limited by the acquisition electronics. However the spectral density of the frequency noise of the NPRO Nd:YAG had been estimated earlier by Salvadé during the preliminary study at IMT [SS02] or by Dubovitsky [DSLG98]. They have both measured the beat frequency between two identical free running lasers. They have observed a 1/f noise for frequencies below 10 kHz. Thus it is possible to infer the part of the closed loop power spectral density that we could not measure in order to integrate the standard deviation over the whole bandwidth 0.5 mHz - 8 kHz.

We have considered two cases. The first case, first model in Figure 5.13, assumes that above 10 Hz the closed loop PSD behaves like the opened loop PSD and the noise decreases with a 1/f law. The second case, more conservative, assumes that the correction carried out by the piezo actuator may introduce a white frequency noise from 10 Hz to 1 kHz (bandwidth of the actuator). The standard deviation of the laser frequency over the bandwidth 0.5 mHz - 8 kHz is respectively 155 kHz and 1.870 MHz for the first and second model. The laser stabilization system is within the specifications.

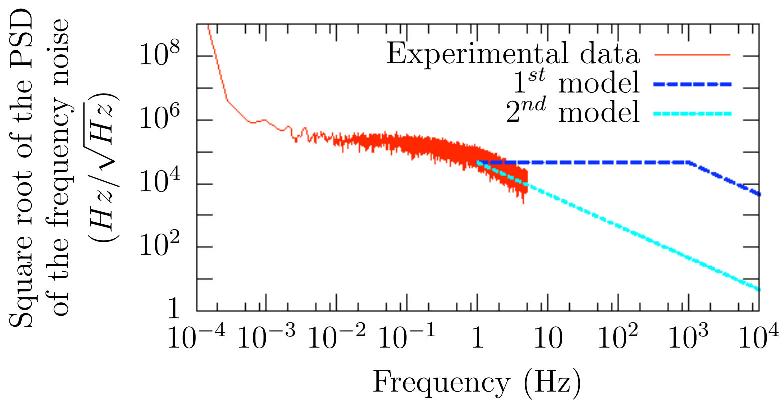

Figure 5.13: Models of the PSD of the frequency noise used for the estimation of the standard deviation over the bandwidth 0.5 mHz - 8 kHz.

Chapter 6

Proposition of a procedure for the calibration of PRIMET laser wavelength

PRIMA objectives require stable measurements over several year. Although a molecular transition provides an absolute frequency reference the stabilization set-up may not be stable on a long time scale (few months). The sensitivity of the set-up to RAM, created either by electro-magnetic compatibility, misalignment or temperature drift, is a good example of possible long term instability of the locking frequency. Even if rather unlikely, a slow contamination of the iodine cell remains possible. Therefore a mean to calibrate the wavelength of the stabilized laser, at least once after its integration at the observatory or on a periodical basis , has been investigated.

As in the stabilization process the difficulty is to find a frequency reference for the laser. The Paranal observatory is operating many iodine stabilized He:Ne laser for the interferometer delay lines metrology. Once calibrated these commercial laser heads provide a wavelength calibrated to the 10^{-8} accuracy. However the wavelength of such a laser is too far away from the doubled Nd:YAG to be monitored directly by heterodyne beating. Nevertheless it may be possible to achieve a calibration of the Nd:YAG by comparison with the He:Ne laser by measuring simultaneously a same optical path.

6.1 Proposed calibration procedure

6.1.1 Principle

The principle is to measure the same distance with two different optical wavelengths. If one wavelength is calibrated it is possible to deduce the value of the second one as follows. Let's consider a Michelson operated with two different wavelengths λ_{Ref} and λ_{Met}. One assumes that both wavelengths travel exactly along the same optical path. If one denotes L the distance difference between the two arms of the interferometer and ϕ_{Ref} and ϕ_{Met} the phases of the interferometric signals obtained respectively with λ_{Ref} and λ_{Met}, then:

$$\left\{ \begin{array}{lcl} L & = & \frac{\phi_{\text{Ref}}}{2\pi}\frac{\lambda_{\text{Ref}}}{2n_{\text{Ref}}} \\ L & = & \frac{\phi_{\text{Met}}}{2\pi}\frac{\lambda_{\text{Met}}}{2n_{\text{Met}}} \end{array} \right. .$$

Thus λ_{Met} can be deduced from λ_{Ref} from the equation:

$$\lambda_{\text{Met}} = \frac{\phi_{\text{Ref}}}{\phi_{\text{Met}}}\frac{n_{\text{Met}}}{n_{\text{Ref}}}\lambda_{\text{Ref}}. \tag{6.1}$$

6.1.2 Experimental requirements

Even if the calibration procedure seems simple its application requires some precautions. Indeed the method is based on the measurement of exactly the same optical path L. The distance measured with the two interferometers, L_{Ref} and L_{Met}, will be slightly different. The relative error between the two optical paths measured has to be smaller than the relative accuracy desired for the calibration. In order to reach an accuracy as high as 10^{-8} several sources of error have to be minimized.

Cosine error One has to make sure that the two wavelength travel exactly the same optical path. The beams emitted by the two lasers have to be superimposed over a distance large enough so that the so called cosine error is reduced to the required level. Indeed if the laser beam to be calibrated is tilted by an angle α with respect to the reference beam the wavelength is calibrated with a relative error ϵ:

$$\epsilon = \frac{cos(\alpha)}{1 - cos(\alpha)} \tag{6.2}$$

Measurements synchroneity The optical path difference is varying in time because of the atmospheric turbulence and because of the vibrations in the interferometer. As a consequence the measurements done with the two wavelengths have to be done simultaneously. The required level of synchroneity between the two measurements depends on the spectrum of the OPD variations.

Refractive index of air Depending on the difference between the reference wavelength and the wavelength to be measured the dispersion has to be taken into account. At a level of accuracy as high as 10^{-8} the environmental condition such as the temperature and the pressure may have to be monitored and used in the computation of the refractive index. The Edlen [Edl66] or Owens [Owe67] equations may be used to calculate the refractive index of air.

Minimum OPD to be measured The phase measured by the interferometer to be calibrated has an error due to the phase-meter or to the polarization cross-talk. If one wants to derive the wavelength with a given accuracy α one has to make sure that the phase error is below this level, i.e that:

$$\frac{\delta OPD_{phase}}{OPD} < \alpha = \frac{\delta\lambda}{\lambda}. \tag{6.3}$$

Stability of the frequency shift (in heterodyne interferometry) In heterodyne frequency the frequency should be taken into account. The stability of the frequency shifting can usually be neglected. It is typically 10^{-6} applied to the frequency shift which is typically tens of MHz. Therefore the error on the optical wavelength would be of the order of 10^{-14}.

Error source	Uncertainty on result	Set-up
Accuracy of the reference wavelength	$\delta\lambda/\lambda$	2×10^{-8}
Cosine error (α)	$\frac{\cos(\alpha)}{1-\cos(\alpha)}$	0.5×10^{-8}
Interferometer phase error ($\delta\phi$)	$\frac{\delta\phi}{2\pi}\frac{\lambda}{OPD}$	10^{-8}
Dispersion (Δn)	$n_{Ref} - n_{Met}$	10^{-8}
Frequency shift stability ($\delta\Delta\nu$)	$\frac{\delta\Delta\nu}{\nu}$	10^{-14}

Table 6.1: Summary of the error sources in the wavelength calibration set-up.

6.2 Experimental set-up for the calibration of PRIMET laser wavelength with a commercial interferometer

The wavelength of the stabilized Nd:YAG laser is compared to the wavelength of an iodine stabilized dual wavelength He:Ne laser part of a commercial HP/Agilent interferometer. The laser head (HP5519A) has a calibrated wavelength, $\lambda_{\mathrm{HP}} = 632.9913720\,\mathrm{nm} \pm 0.02\,\mathrm{ppm}$ stable at the level $\pm 0.02\,\mathrm{ppm}$ over its lifetime and $\pm 0.002\,\mathrm{ppm}$ over one hour. The interferometer uses heterodyne detection with the two frequencies generated by Zeeman effect and separated by 2.4M Hz. The reference signal is generated in the laser head while the probe signal is detected by a detector (Agilent E1709A). The phase measurement is done by a HP 10897 board located in an LCU.

The Nd:YAG interferometer light source is the iodine stabilized Nd:YAG laser. A pair of heterodyne frequencies is generated with two acousto-optic modulators operated at -40 MHz and -39.45 MHz. These two frequencies are mixed in a single beam with orthogonal linear polarization states with a polarizing beam splitter. The beam is then superimposed to the Agilent interferometer beam with a dichroic plate (reflecting the visible and transmitting the infrared) and launched in the Michelson interferometer. The Nd:YAG reference signal is obtained from the leakage of the polarizing beam splitter used for the combination of the heterodyne frequencies. After a round trip in the interferometer the two heterodyne frequencies are made to beat with each other using a linear polarizer and the light is sent to the PRIMET phase-meter (see Section 3.2.6) through a multimode fiber.

The Michelson interferometer uses a non polarizing beam splitter and a Glan-Thompson polarizer in each of its arm to reduce the polarization cross-talk. The corner cube of one arm of the interferometer is mounted on a motorized translation stage with maximum stroke 90 cm. Preliminary tests have shown that an accuracy better than 13 nm can be expected from the interferometer with this set-up. Therefore the relative error due to the phase error is limited to 7×10^{-9}. The Nd:YAG interferometer and the Agilent interferometers are triggered simultaneously at 1 kHz. The beams of the two interferometers are superimposed over 10 m with an accuracy of 1 mm to reduce the cosine error to 5×10^{-9}, i.e 35 cm. The refractive index of air is computed for the standard environmental conditions for the two wavelengths.

Taking into account the possible errors listed in Table 6.1 the result of the calibration should have an uncertainty of approximately $4{\times}10^{-8}$.

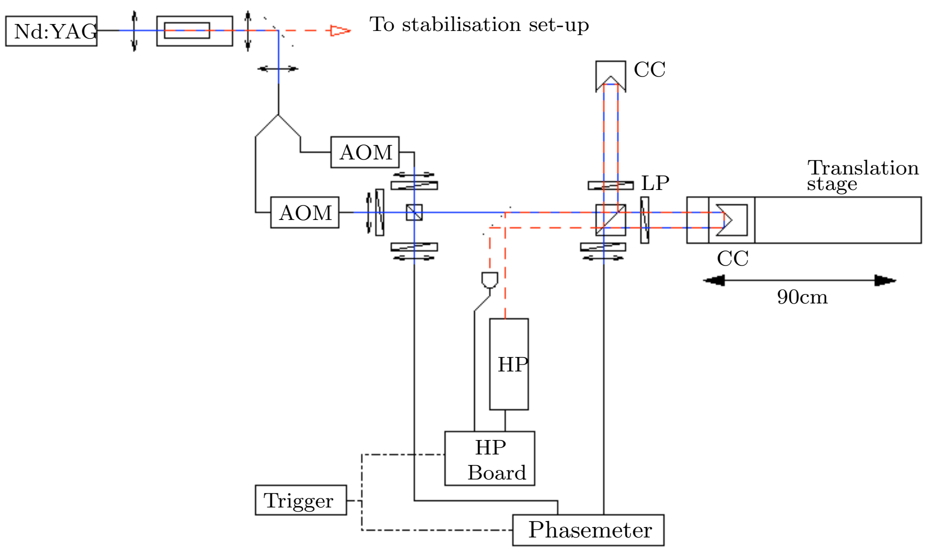

Figure 6.1: Schematic of the set-up for the calibration of PRIMET laser wavelength by comparison with a commercial HP/Agilent interferometer.

6.3 Experimental results

Data are acquired while the corner cube mounted on the translation stage is scanned several time along the full stroke (90 cm). Raw phases delivered by the phase-meter have to be unwrapped as the capacity of the fringe counter designed for PRIMET is limited to 2^{19} fringes. From these data the phase of the Nd:YAG interferometer is plotted as a function of the phase of the reference interferometer. A linear fit is applied to the data set to get the ratio $\phi_{\mathrm{Met}}/\phi_{\mathrm{Ref}}$. An example of data along with the residuals of the fit is shown in Figure 6.2. The error with respect to the wavelength measured with the self-referenced comb (taking into account the shift due to the AOM) is 0.35 pm, i.e 61 MHz. The relative error is 2.6×10^{-7}. The measurement has been repeated several time to assess the its repeatability and the stability of the whole calibration system. 8 calibrations carried out successively over 12 days exhibit a standard deviation of 4×10^{-7} (92 MHz). The calibration procedure is not repeatable enough to be useful. The instability may be cause by mechanical drifts in the set-up or by a drift in the reference wavelength by a quantity larger than the specifications. The temperature variations are too low to explain these results. Indeed according to the Edlen equation a difference of one degree Celsius results in a change at the 10^{-8} level of the dispersion.

The calibration of the Nd:YAG wavelength by comparison with a reference HP/Agilent interferometer is not accurate and repeatable at the 10^{-8} level. A systematic error may have come from a bad calibration of the Nd:YAG laser and could have been removed. Nevertheless the instability of the system, caused by mechanical drifts or by the instability of the reference laser frequency, prevents to reach the specifications. As we have seen that the system will require a wavelength calibration after its integration in Paranal other alternatives have been studied. The possibility to use a self-referenced optical frequency comb at the observatory is investigated. It may also be possible to use the two-wavelength frequency comb referenced light source as a reference as explained in Part III.

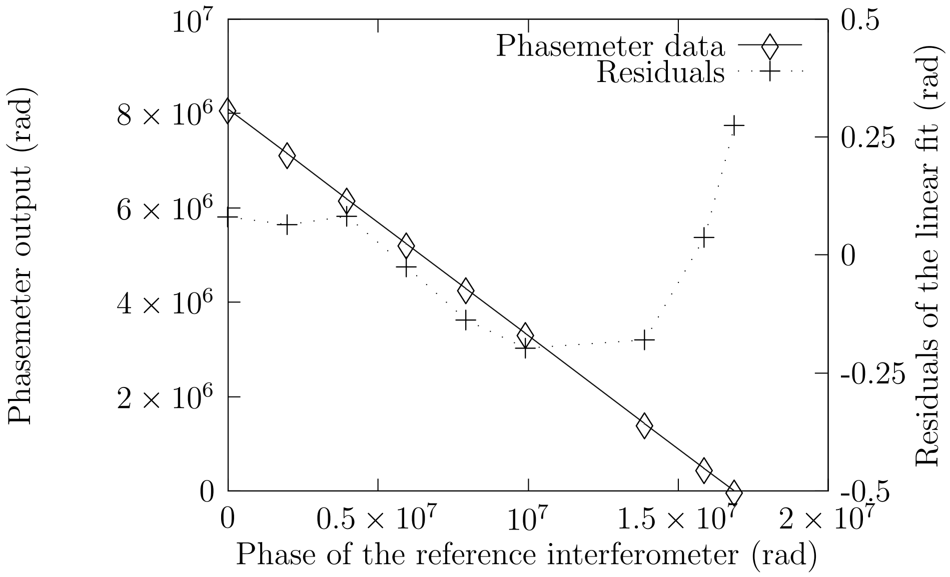

Figure 6.2: Results of the Nd:YAG calibration with respect to a calibrated HP/Agilent commercial interferometer. For different positions along the translation stage the phase of both interferometers is averaged. The phase read at the output of the phase-meter is plotted as a function of the reference interferometer phase. The corresponding linear fit and its residuals are plotted. The slope of the linear fit is the ratio between the wavelength of the two lasers. From these data the Nd:YAG wavelength is calculated to be $1.31917654\,\mu m$.

Conclusion of Part II

For distances large compared to an optical wavelength the relative accuracy of laser interferometry is equal to the relative accuracy of the optical frequency. In order to reach the specifications PRIMET laser optical frequency must be calibrated and stabilized at the 10^{-8} level, i.e 2.27 MHz. This second part has presented our contribution to the development, integration and testing of the absolute frequency stabilization of this laser.

The PRIMET laser is frequency doubled and stabilized using the Pound-Drever-Hall method on a transition of iodine. We have tested two non-linear bulk crystals and a non-linear waveguide for the second harmonic generation. We have shown that PPLN is the most suitable. In the set-up it is used to generate approximately $12\,\mu$W of light at 659 nm from 50 mW of infrared light. We have studied the iodine spectrum in the tuning range of the laser and pointed out the transition P(49)6-6 as the best candidate for the frequency reference. Based on these measurements we have designed the iodine cell used in the stabilization set-up. These results have been used by IMT to finalize the design and built the stabilization system. After delivery of the system (not fully functional) we have tested and enhanced its performance. Moreover we have calibrated the error signal. Therefore it can be used to estimate the frequency noise of the laser. We have improved the system delivered by IMT by implementing a feedback loop that controls both actuators of the laser head. This allows to keep an accurate correction over long periods of time whereas previous systems were limited by the limited range of the fast actuator.

In order to characterize the system with the best accuracy possible we have used a self-referenced optical frequency comb generator at the Max Planck Institute for Quantum Optics (Garching bei München). Based on these results we have proved that the system performance is deteriorated by detection noise caused by electro-magnetic compatibility issues and residual amplitude modulation in the electro-optic modulator. We have reduced the electric cross-talk and limited the RAM by stabilizing the temperature of the EOM. With its actual temperature stabilization, the noise introduced by the RAM is limited to 800 kHz standard deviation. The power spectral density of the closed loop laser frequency has been measured with a 10 Hz bandwidth. We have calculated the standard deviation over the full PRIMET bandwidth, 0.5 mHz - 8 kHz by extending the PSD with theoretical models. The worst case model yields a standard deviation of σ=1.87 MHz. Thus the specifications are met. We have calibrated the wavelength with the frequency comb with an accuracy of 10^{-12} and measured a repeatability of the optical frequency better than 100 kHz over one week.

As our measurements have shown the sensitivity of the system with respect to its environment (electric cross-talk, residual amplitude modulation variations due temperature fluctuations) we have investigated the possibility to calibrate the system at the Paranal observatory. We have shown that the calibration with a reference interferometer, available at the observatory, is limited to an accuracy of 10^{-7}. Therefore the laser will have to be calibrated at the observatory with a self-referenced frequency comb. The two-wavelength interferometer proposed in Part III may also be used to calibrate the Nd:YAG.

References

[AB93] Ady Arie and Robert L. Byer. Frequency stabilization of the 1064-nm nd:yag laser to doppler-broadened lines of iodine. *Applied Optics*, 32(36):7382–7386, December 1993.

[ABFB93] A. Arie, M. L. Bortz, M. M. Fejer, and R. L. Byer. Iodine spectroscopy and absolute frequency stabilization with the second harmonic of the 1319-nm nd:yag laser. *Optics Letters*, 18(20):1757–1759, October 1993.

[ASGB92] Ady Arie, Stephan Schiller, Erik K. Gustafson, and Robert L. Byer. Absolute frequency stabilization of diode-laser-pumped nd:yag lasers to hyperfine transitions in molecular iodine. *Optics Letters*, 17(17):1204–1206, September 1992.

[Bjo80] Gary C. Bjorklund. Frequency-modulation spectroscopy: a new method for measuring weak absorptions and dispersions. *Optics Letters*, 5(1):15–17, January 1980.

[BK68] G. D. Boyd and D. A. Kleinman. Parametric interactions of focused gaussian light beams. *Journal of applied physics*, 39(8):3597–3639, July 1968.

[Bla01] Eric D. Black. An introduction to pound-drever-hall laser frequency stabilization. *American Journal of Physics*, 69(1):79–87, January 2001.

[DCO+02] T. Dennis, E. A. Curtis, C. W. Oates, L. Hollberg, and S. L. Gilbert. Wavelength references for 1300-nm wavelength division multiplexing. *Journal of lightwave technology*, 20(5):804–810, May 2002.

[DSLG98] Serge Dubovitsky, David J. Seidel, Duncan Liu, and Roman C. Gutierrez. Metrology sources for high-resolution heterodyne interferometer laser gauges. In Robert D. Reasenberg, editor, *As-*

tronomical interferometry, volume 3350, pages 973–984. SPIE, 1998.

[Edl66] B. Edlen. The refractive index of air. *Metrologia*, 2:71–80, 1966.

[FMJB92] Martin M. Fejer, G. A. Magel, Dieter H. Jundt, and Robert L. Byer. Quasi-phase-matched second harmonic generation: Tuning and tolerances. *IEEE Journal of Quantum Electronics*, 28(11):2631, November 1992.

[GHO+04] Ruixiang Guo, Feng-Lei Hong, Atsushi Onae, Zhi-Yi Bi, Hirokazu Matsumoto, and Nakagawa Ken'ichi. Frequency stabilization of a 1319-nm nd:yag laser by saturation spectroscopy of molecular iodine. *Optics Letters*, 29(15):1733–1735, August 2004.

[GVC82] S. Gerstenkorn, J. Verges, and J. Chevillard. *Atlas du spectre d'absorption de la molécule d'iode*. 1982.

[Ham89] M. W. Hamilton. An introduction to stabilized lasers. *Contemporary Physics*, 30(1):21–33, 1989.

[HH84] J. L. Hall and T. W. Hänsch. External dye-laser frequency stabilizer. *Optics Letters*, 9(11):502–504, November 1984.

[Lui01] Andre N. Luiten, editor. *Frequency measurement and control: advanced techniques and future trends*, chapter Generation and metrological application of optical frequency combs, page 295. Topics in applied physics. Springer Berlin / Heidelberg, 2001.

[Men01] Ralf Menzel. *Photonics*. Advanced Texts in Physics. Springer, first edition, Mars 2001. Linear and Nonlinear Interactions of Lasr Light and Matter.

[Owe67] J. C. Owens. Optical refractive index of air. *Applied Optics*, 6:51–59, 1967.

[Pet88] K. Petermann. *Laser diode modulation and noise*, chapter 7. Advance in optoelectronics. Kluver Academic Publishers in cooperation with KTK Scientific Publishers, 1988.

[SS02] Yves Salvadé and Olivier Scherler. Feasibility stury for the frequency stabilzation of the prima metrology laser. Technical Report VLT-TRE-IMT-15731-2868, Institut de Microtechnologie de Neuchâtel, July 2002.

[ST91] Bahaa E. A. Saleh and Carl Malvin Teic. *Fundamental of photonics*. Wiley-Interscience, first edition, August 1991.

[WGB85] Edward A. Whittaker, Manfred Gehrtz, and Gary C. Bjorklund. Residual amplitude modulation in laser electro-optic phase modulation. *Journal of the Optical Society of America B*, 2(8):1320–1326, August 1985.

Part III

Development of frequency-comb stabilised laser sources for absolute laser metrology

Forewords

As seen in Section 2.1.2 single-wavelength interferometry suffers from a limited Non Ambiguity Range (NAR) of $\lambda/2$. It is defined by the maximum OPD measurable without requiring phase unwrapping. Because of this limitation, PRIMET must be calibrated before every measurement. The calibration decreases the time efficiency of PRIMA and requires the addition of complex subsystems to PRIMET. The NAR can be enlarged without loosing the accuracy of the system by the use of multiple-wavelength interferometry. This technique requires the stabilization of at least two wavelengths with respect to each other. We propose a new concept of a stabilized multiple-wavelength laser source for absolute metrology. We have used an optical frequency comb as a reference grid to stabilize two lasers with respect to each other over large frequency ranges.

In *Chapter 7*, we give a brief state of the art of optical methods for distance measurements. We show that multiple-wavelength interferometry is the only technique that fulfills PRIMET requirements. The principle of multiple-wavelength metrology is described. A state of the art of two-wavelength laser sources is given to highlight the benefits provided by the new concept. The algorithm applied to process the multiple-wavelength data is recalled and is used to build an error budget for a multiple-wavelength interferometer.

In *Chapter 8*, we present the prototype of the frequency comb stabilized light source and the first results obtained on the wavelength stability, wavelength calibration and on the system accuracy.

In *Chapter 9*, we use the results obtained with the prototype to propose a design of an absolute PRIMA Metrology system.

Outline of Part III

Chapter 7

Multiple-wavelength laser interferometry

An upgrade of PRIMET to absolute metrology had been scheduled at the beginning of PRIMA. At the time of the design of PRIMA no practical solution had been identified for an absolute PRIMET. A short summary of the different laser ranging techniques is given. Then, multiple-wavelength interferometry, the only method capable of matching the PRIMET requirements, is presented theoretically. A state of the art is given. The algorithm used to link two-wavelength measurements to single wavelength measurements is recalled. Finally, the sources of error of the technique are described.

7.1 Absolute and large NAR laser ranging methods

Many optical techniques have been invented to suppress the limitation of the NAR (defined in Section 2.1.2) and achieve a so called "absolute metrology". *An absolute metrology system does not have a NAR or has a NAR larger than the maximum distance to be measured.* A review of common laser ranging system is given in [ABL+01]. Many articles about multiple-wavelength laser interferometry are compiled in [BL95]. Most of these techniques have already been studied in the framework of ground based or even spatial interferometers, [WCSC02].

Optical triangulation is a technique use commonly in the industry. A laser beam is focused on the object of interest which reflects it back on a lens focusing the beam on a linear CCD sensor. The position of the spot on the CCD is linked to the distance between the laser and the object. The technique is limited by the speckle noise [DHH94].

The "time-of-flight" technique based on the measurement of the time required for a light pulse to travel back and forth to the target object has no ambiguity range. The measured distance is limited by the width of the pulse, which defines the minimum measurable distance, and by the power of the laser and the reflectivity of the target which define the maximum distance. The accuracy is set by the accuracy of the clock. This technique is used for long distance measurements, hundreds of meters to several kilometers. The resolution is limited by the electronics to 10 ps which corresponds to 3 mm.

The continuous wave intensity modulation technique is an incoherent equivalent of the single wavelength metrology system. The intensity of the light source is modulated at a radio frequency f_{mod} provided by a local oscillator. After retroreflection on the target a photodiode collects a part of the laser beam and the phase of the signal is compared to the phase of the local oscillator. The equation giving the OPD is similar to the single-wavelength interferometry equation but the wavelength is no more optical and is given by the modulation frequency $\lambda = c/f_{mod}$. As the modulation frequency is much smaller than an optical frequency the wavelength and the corresponding NAR is much larger (a few meters for a few megahertz). The Green Bank radio telescope uses many range finders based on this technology to measure the shape of the telescope dish. Errors of less than 50 μm over 120 m single way OPD are obtained with a 1.5 GHz modulation frequency, i.e a 20 cm wavelength, [PPB92].

Sweeping-wavelength metrology takes advantage of the frequency tunability of some lasers (laser diode, external cavity laser diode). In this technique a Michelson interferometer is illuminated with a time varying wavelength. At the output of the interferometer a detector measures the beat frequency created by the waves coming from the two arms of the interferometer. The beat frequency is proportional to the OPD. The accuracy of the measurement depends on the accuracy of the wavelength scanning and on the accuracy of the beat frequency measurement, [B.02]. This technique has also been applied to synthetic wavelength (Section 7.2) generated with two different wavelengths [BF98, KS02].

None of these technologies has reached the accuracy of single-wavelength metrology and could replace the PRIMA Metrology system. Consequently the single-wavelength metrology system has to be upgraded with a system running in parallel and providing the fringe order of the single-wavelength signal. However, to measure the single-wavelength fringe order without error, the accuracy of the OPD measurement should be better than $\lambda/2$, i.e 659 nm. None of the previously described technologies can reach such an accuracy. Only multiple-wavelength interferometry provides the required accuracy and at the same time offers an enlarged NAR.

7.2 Principle of two-wavelength laser metrology

The ambiguity in a single-wavelength interferometry measurement can be removed provided the fringe order of the interferometric signal can be determined. Benoit has proposed a technique based on the simultaneous use of several wavelengths. This technique, called *the excess fraction method (or the method of coincidence)*, has been used by Michelson to define the meter étalon as a function of wavelengths emitted by a cadmium discharge lamp, [Mic93] available in [Har91]. N wavelengths, $\lambda_k (k \in [1, \mathrm{N}])$, illuminate a Michelson interferometer. Each of them creates an interferometric signal of wrapped phase $\phi_k(OPD)(k \in [1, \mathrm{N}])$ and period $\lambda_k(k \in [1, \mathrm{N}])$. Nevertheless, the set of phase measurements $(\phi_1(\mathrm{OPD}), \phi_2(\mathrm{OPD}), \ldots, \phi_N(\mathrm{OPD}))$ has a period larger than an optical wavelength [LE01]. Therefore it can be used to extend the NAR of the single wavelength measurements. For a given ϕ_1 known modulo 2π, the phase sets corresponding to the different fringe orders of λ_1 are computed and compared to the measured phase set. The closest to the measurements defines the fringe orders of the interferometric signal at λ_1. This method is still used for some applications such as segmented mirror phasing, [LE00, LE01, SDM02].

However when only two wavelengths are used this technique has been replaced by the so called *synthetic wavelength method* introduced by Wyant, [Wya71]. This technique uses a faster algorithm to get the fringe order of one of the two wavelengths. In this technique a beam composed of two wavelengths is sent into a Michelson interferometer. An interferometric signal is generated for each wavelength. The phases of the two signals are

$$\phi_1 = 2\pi \frac{OPD_{\lambda_1}}{\lambda_1} \tag{7.1}$$

$$\phi_2 = 2\pi \frac{OPD_{\lambda_2}}{\lambda_2}. \tag{7.2}$$

Assuming the wavelengths are close enough, the dispersion can be neglected and $OPD_{\lambda_1} = OPD_{\lambda_2}$ (the effect of dispersion is described more precisely in Section 7.5.3). The phase difference, Φ, of the two signals is then given by

$$\Phi = \phi_1 - \phi_2 = 2\pi \frac{OPD}{\Lambda} \tag{7.3}$$

where Λ *is called the "synthetic" wavelength* and is equal to

$$\Lambda = \frac{\lambda_1 \lambda_2}{|\lambda_2 - \lambda_1|} = \frac{c}{|\nu_1 - \nu_2|}. \tag{7.4}$$

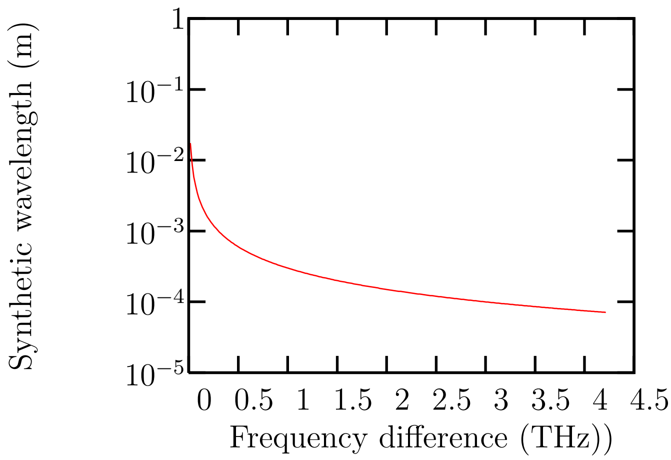

Figure 7.1: Synthetic wavelength as a function of the frequency separation between the two optical frequencies.

Consequently the phase difference of the two interferometric signals is a function of a "synthetic" wavelength and *the NAR is* $\Lambda/2$. Provided the two optical wavelengths are taken close enough the synthetic wavelength is much longer than an optical wavelength and so is the NAR, Figure 7.1. Nevertheless, if the phase of the synthetic wavelength is measured with the same accuracy, $\delta\phi$, as the phase of the optical wavelength, the error on the OPD, δOPD, is increased by the same factor as the NAR:

$$\begin{aligned} \mathrm{NAR}_\Lambda &= \frac{\Lambda}{\lambda}\mathrm{NAR}_\lambda & (7.5) \\ \delta\mathrm{OPD}_\Lambda &= \frac{\Lambda}{\lambda}\delta\mathrm{OPD}_\lambda. & (7.6) \end{aligned}$$

As a consequence, two-wavelength interferometry increases the NAR but at the cost of a reduced accuracy. Therefore, two-wavelength interferometry cannot be used alone for PRIMET. Nevertheless, provided it is accurate enough, it may be used in parallel to single-wavelength interferometry to determine the fringe order of the single-wavelength signal. The NAR can be enlarged even more by the use of a chain of increasing synthetic wavelengths. It is given by the largest synthetic wavelength while the final accuracy is given by the accuracy of the single-wavelength interferometer.

7.3 State of the art of multiple-wavelength interferometry

7.3.1 Laser sources

Many sources have been used for multiple-wavelength interferometry. The first sources were mercury or cadmium discharge lamps. CO_2 lasers have been the first lasers used for multiple-wavelength interferometry as they can generate a wide range of synthetic wavelengths (from tens of microns to several meters) and as they can be switched from one to another [BO79, GBR81, Mat84, Wal87, GC97]. He-Xe and He-Ne have also been used as dual longitudinal mode laser to provide synthetic wavelengths: $80\,\mu$m [Mat81], $55.5\,\mu$m [SFIT91], 280 mm [CCL02, ZZL99]. Two multimode laser diodes have been used by de Groot who had selected three wavelengths among the combined spectrum of the diodes to get two synthetic wavelengths of $720\,\mu$m and $20\,\mu$m [dG91].

An alternative to multimode lasers is single mode lasers stabilized independently, with respect to each other or on a common reference. Yokoyama has used two stabilized He-Ne lasers at 633 nm and 612 nm to generate a synthetic wavelength of $18.4\,\mu$m [YOI$^+$99]. Mahal and Arie have worked with two Nd:YAG lasers stabilized on sub-Doppler transitions of $^{127}I_2$ and $^{133}Cs_2$. The dense spectra of both molecular absorbers allow to select a synthetic wavelength over a wide range (between 8.5 mm and more than 1 m [MA96]). A master and slave configuration, where one laser is stabilized with respect to the other with a PLL, has been used with two Nd:YAG lasers generating a tunable synthetic wavelength over the range 0.1 m - 1 m, [GMD94]. The minimum size of the synthetic wavelength is limited in that case by the bandwidth of the detector measuring the beat signal used by the PLL and by the limited tuning range of the lasers. Fabry-Pérot étalons have been used as frequency reference combs to stabilize two Nd:YAG lasers (synthetic wavelength 26.1 mm) [DSLG98] or two laser diodes (synthetic wavelength $15\,\mu$m) [dGK91]. Zimmermann et al have developed a stabilized three-wavelength source using laser diodes stabilized on a same Fabry-Pérot étalon. This source was used to generate two synthetic wavelengths of 4.00 mm and 4.04 mm to create a larger synthetic wavelength of 400 mm [ZSD96, DSZ98]. The stability of the synthetic wavelength in this method is limited to 10^{-5} by the thermal fluctuations and mechanical vibrations of the Fabry-Pérot étalon.

Lay proposed another approach and generated synthetic wavelengths from a single mode laser by using the sidebands created by phase modulation, [LDP$^+$03]. The stability of the synthetic wavelengths is given by the stability of the local oscillator used by the EOM. The minimum size of the synthetic wavelength is limited by the bandwidth of the phase modulator, i.e a few tens of megahertz's corresponding to synthetic wavelength of a few millimeters.

7.3.2 Synthetic phase measurement

As in single-wavelength interferometry the two methods of phase measurement are phase-stepping and heterodyne detection. However, these methods have to be adapted to accommodate the simultaneous use of several wavelengths. Contrast measurements [MA96, GC97] have also been tested but the results exhibit a lower accuracy than the two other methods.

In multiple-wavelength interferometry, phase-stepping requires to separate spatially the different wavelengths to measure each fractional order. This can be done with interference filters [dGK91], polarizers [MA96] or gratings [dG91]. The measurements can be done simultaneously provided the phase steps are known precisely for each optical wavelength. *The phase accuracy on the synthetic wavelength measurement can reach 0.5 % ($2\pi/200$).*

Heterodyne detection applied to multiple-wavelength is called superheterodyne detection and was introduced by Dändliker [DTP88]. Like in heterodyne detection a frequency offset is generated between the reference and the measurement waves. In two-wavelength superheterodyne interferometry the frequency offsets is different for each optical wavelength. As the two wavelengths are not spatially separated the detected interference signal is the incoherent superposition of the two beating signals. The signals are processed as explained in Section 3.1.1. The phasemetre measures the phase difference of the two optical wavelength signals, i.e the phase of the synthetic wavelength signal. *Phase accuracy close to $2\pi/800$ can be achieved.* The technology for the phasemeter is similar to the one used in single-wavelength superheterodyne interferometry and the error introduced by the phasemeter should be comparable. However, in the case of two-wavelength interferometry the cross-talk phase error of each interferometric signal adds up. It results in a periodic phase error of amplitude the sum of the single-wavelength signal phase error (Section 2.4.1) and of period Λ.

Yokoyama et al [YOI$^+$99] have improved the method by separating electrically the single wavelength signal which is fed to another digital phasemeter . With the phases of the synthetic and optical wavelength the system has the accuracy of single-wavelength interferometry and the NAR of two wavelength interferometry.

7.4 Linking single-wavelength and multiple-wavelength measurements

The algorithm described in the following paragraph is used to link the two-wavelength measurement to the single-wavelength measurement, i.e to determine the fringe order of the single-wavelength signal. However, for the algorithm to be applicable, the two-wavelength measurements must be accurate enough. The required accuracy is derived hereafter.

7.4.1 Algorithm to retrieve the single-wavelength fringe order

Let's assume the interferometer is operated along an OPD range smaller than the NAR of the two-wavelength interferometer, i.e:

$$-\frac{\Lambda}{2} < \mathrm{OPD} < \frac{\Lambda}{2}. \tag{7.7}$$

The phase of the synthetic wavelength signal is in the range $[-\pi;\pi]$ and the fringe order of the signal (as defined in Section 2.1.2 Equation 2.18) is always $M_\Lambda = 0$. Consequently, one has:

$$\mathrm{OPD} = \frac{\Phi}{2\pi}\Lambda, \Phi \in [-\pi;\pi]. \tag{7.8}$$

The same OPD measured with a single optical wavelength λ is given by

$$\mathrm{OPD} = (M_\lambda + f(m_\lambda))\,\lambda \tag{7.9}$$

where M_λ is the fringe order and $f(m_\lambda)$ the fractional part. Therefore the single wavelength fringe order can be computed from the multiple-wavelength phase as follows:

$$M_\lambda = \mathrm{round}\left(\frac{\Phi}{2\pi}\frac{\Lambda}{\lambda} - \frac{\phi_\lambda}{2\pi}\right) \tag{7.10}$$

$$= \mathrm{round}\left(\frac{\mathrm{OPD}_\Lambda}{\lambda} - \frac{\phi_\lambda}{2\pi}\right) \tag{7.11}$$

where round() is the function that returns the closest integer to its argument.

7.4.2 Maximum error on the synthetic wavelength measurement

If one takes into account the possible error in the optical and synthetic wavelength measurements the previous equation becomes:

$$M_\lambda = \mathrm{round}\left(\frac{\mathrm{OPD}_\Lambda + \delta\mathrm{OPD}_\Lambda}{\lambda} - \frac{\phi_\lambda + \delta\phi_\lambda}{2\pi}\right) \tag{7.12}$$

where $\delta\mathrm{OPD}_\Lambda$ is the error in the synthetic wavelength measurement and $\delta\phi_\lambda$ the error in the phase measurement of the single wavelength interferometric signal. The single wavelength fringe order is correct provided that:

$$\left|\frac{\delta\mathrm{OPD}_\Lambda}{\lambda} - \frac{\delta\phi}{2\pi}\right| < \frac{1}{2}. \tag{7.13}$$

As the second term of the sum can be neglected one can deduce a limit on the accuracy of the synthetic wavelength system

$$|\delta\mathrm{OPD}_\Lambda| < \frac{\lambda}{2}. \tag{7.14}$$

One may want to use a chain of several synthetic wavelengths to enlarge even more the NAR of the system. In the case of two synthetic wavelengths $\Lambda_2 > \Lambda_1$, it is easy to derive that the maximum error on the Λ_2 wavelength is

$$|\delta\mathrm{OPD}_{\Lambda_2}| < \frac{\Lambda_1}{2}. \tag{7.15}$$

As the errors are proportional to the wavelength of the measurement, the wavelength should be small enough to yield the required accuracy. Therefore the expansion of the NAR between to element of the wavelength chain is limited. For instance if the phase accuracy is $2\pi/200$ the NAR cannot be enlarged by more than a factor 100 between two elements of the wavelength chain.

7.5 Sources of error in multiple-wavelength interferometry

The relation between the phase of the two-wavelength interferometric signal and the OPD is identical to the one tying a single wavelength interferometric signal to the OPD:

$$\mathrm{OPD} = \frac{\Phi_{unwrapped}}{2\pi}\Lambda. \tag{7.16}$$

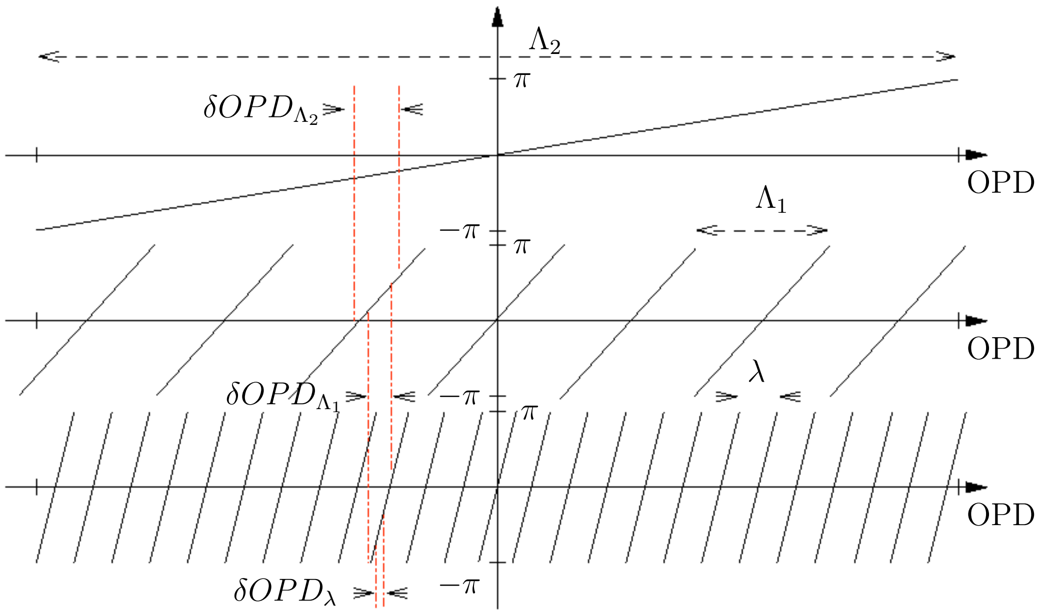

Figure 7.2: Schematic of a 2 synthetic wavelengths chain leading to an optical wavelength measurement. δOPD$_{\Lambda_2}$, δOPD$_{\Lambda_1}$ and δOPD$_\lambda$are the error on the OPD measured respectively with Λ_2, Λ_1 and λ. These measurements have NAR equal to their wavelength and must fulfill an accuracy better than half of the next smaller wavelength of the chain.

Consequently, the sources of error are the same: the phase error and the wavelength uncertainty error:

$$\begin{aligned} \mathrm{OPD}_{measured} &= \frac{\Phi + \delta\Phi}{2\pi}\frac{\lambda + \delta\Lambda}{2} \\ &= \mathrm{OPD} + \frac{\Phi}{2\pi}\delta\Lambda + \frac{\delta\Phi}{2\pi}\Lambda + \frac{\delta\Phi}{2\pi}\frac{\delta\Lambda}{2}. \end{aligned} \quad (7.17)$$

7.5.1 Phase error

In phase stepping two-wavelength interferometry the phase of the signal is the difference of the phases measured separately. Therefore the maximum phase error is the sum of the individual maximum phase errors.

In superheterodyne two-wavelength interferometry two different kinds of phase errors have to be considered. The error due to the phasemeter on the synthetic wavelength phase is similar to the one obtained with superheterodyne single-wavelength interferometry since the phasemeter architecture is almost the same (see Section **??** and Section 9.1.1).

In addition both optical signals will suffer from cross-talk phase error. Assuming the cross-talk relative amplitude, ρ, is the same for both wavelengths and using Equation 2.44, one obtains for the two-wavelength phase error:

$$\begin{aligned}\eta_{2\lambda} &= \eta_{\lambda_1} - \eta_{\lambda_2} \\ &= 2\rho\left(\sin(\phi_1) - \sin(\phi_2)\right) \\ &= 4\rho\sin(\frac{\Phi}{2})\cos(\frac{\phi_1+\phi_2}{2}).\end{aligned} \tag{7.18}$$

The amplitude of the two-wavelength cross-talk phase error is twice the single wavelength error and is applied to the synthetic wavelength:

$$\delta\mathrm{OPD}_{\mathrm{cross-talk}} = \frac{4\rho}{2\pi}\Lambda. \tag{7.19}$$

7.5.2 Synthetic wavelength calibration and stability

As in single wavelength interferometery the error due to the uncertainty on the synthetic wavelength in two-wavelength interferometry is proportional to the OPD:

$$\delta\mathrm{OPD}_{\Lambda} = \mathrm{OPD}\frac{\delta\Lambda}{\Lambda}. \tag{7.20}$$

In order to achieve an absolute OPD measurement with a relative accuracy δOPD/OPD, the optical wavelength must be stable and calibrated with the same relative accuracy whereas the synthetic wavelength must be stable and calibrated at a $\lambda/(2\mathrm{OPD})$ to possibly resolve the optical wavelength. As the accuracy expected from single wavelength measurement is usually at least $\lambda/200$, the calibration and the stability of the synthetic wavelength is relaxed by a factor 100 compared to the optical wavelength. Moreover the two optical frequencies do not need to be absolutely stabilized as the synthetic wavelength depends only on their difference.

7.5.3 Dispersion and effective synthetic wavelength

All the previous results have been derived neglecting the dispersion. By taking into account the dispersion, the phase difference between the two single-wavelength interferometric signals becomes:

$$\Phi = \frac{4\pi L}{c}n_1\left((\nu_1-\nu_2) + \frac{n_1-n_2}{n_1}\nu_2\right) = \frac{4\pi n_1 L}{\Lambda_{\mathrm{eff}}} \tag{7.21}$$

where the synthetic wavelength is replaced by the "effective synthetic wavelength":

$$\Lambda_{\text{eff}} = \frac{c}{\Delta\nu + \frac{\Delta n}{n_1}\nu_2} = \frac{\Lambda}{1 + \frac{\Delta n}{\Delta\nu}\frac{\nu_2}{n_1}}, \tag{7.22}$$

with $\Delta\nu = \nu_1 - \nu_2$, $\Delta n = n_1 - n_2$ and Λ the vacuum synthetic wavelength.

The refractive index of air is a function of the optical frequency and its value, $n(\nu)$, can be approximated with the Edlen equation for instance. Expanding $n(\nu)$ in a Taylor serie around the central frequency ν_2 leads to the first order approximation:

$$\Delta n = \left.\frac{dn}{d\nu}\right|_{\nu_2} \Delta\nu \tag{7.23}$$

which is plotted in Figure 7.3. One can see that the effect of dispersion is much more significant in the visible than the in the infrared. The frequency difference corresponding to the synthetic wavelength in the air, $\Delta\nu_{\text{eff}}$, is given by:

$$\Delta\nu_{\text{eff}} = \Delta\nu \left(1 + \left.\frac{dn}{d\nu}\right|_{\nu_2} \frac{\nu_2}{n_1}\right). \tag{7.24}$$

Therefore, for $\nu_2 = c/\lambda_2$, the corrective term to apply to the frequency difference is always 2.3×10^{-6} the frequency difference.

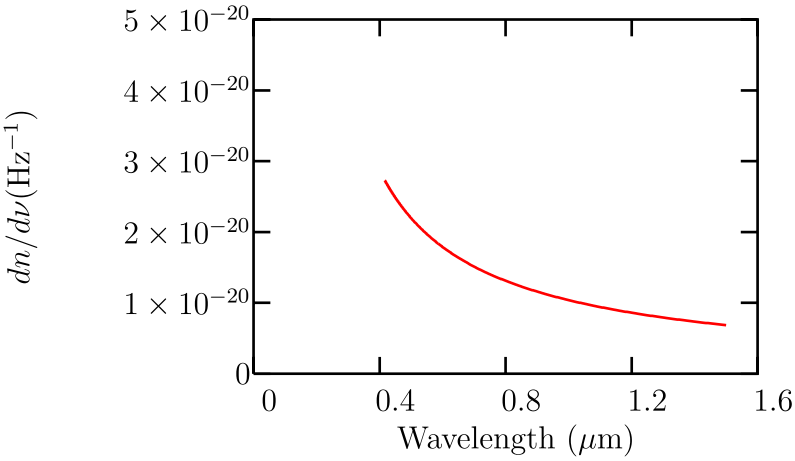

Figure 7.3: Derivative of the refractive index with respect to the optical frequency plotted as a function of the wavelength (calculated from the Edlen equation for dry, CO_2 free air under Standard Conditions (P = 1013.25 mb, T = 288.16 K)). The dispersion is more important at short wavelengths.

Chapter 8

Development and experimental proof of principle of a frequency-comb referenced multiple-wavelength laser source for interferometry

In Chapter 7 we have recalled the principle of two-wavelength interferometry and its possible extension to multiple-wavelength interferometry. The study of the error sources in two-wavelength interferometry shows that the error due to the uncertainty on the synthetic wavelength is proportional to the OPD. Therefore long OPD measurements require a calibrated and stabilized two-wavelength light source, i.e the two optical wavelengths must be stabilized with respect to each other.

Many concepts of two-wavelength laser source are reported in Section 7.3.1. The drawback of most of these sources is the limitation of the range of the synthetic wavelength created by the minimum and maximum frequency separation between the two optical wavelengths. Indeed, the minimum frequency separation sets the size of the maximum synthetic wavelength, i.e the largest NAR that can be achieved with the source. The maximum frequency separation is equally important as it defines the smallest synthetic wavelength. If the smallest synthetic wavelength is too large, it is not possible to resolve an optical wavelength and bridge the two-wavelength measurements with the single wavelength measurements. For instance, if one considers a typical phase accuracy $\delta\phi = 2\pi/200$ and an optical wavelength of $1\,\mu$m the first synthetic wavelength cannot be larger than $200\,\mu$m to resolve the optical wavelength. Such a synthetic wavelength is generated by two optical frequencies separated by at least 2 THz. Stabilization of the lasers sources on a common Fabry-Pérot resonator overcomes this problem. However the stability of the synthetic wavelength is limited to 10^{-5} without the use of a laser stabilized resonator. Independent stabilization on atomic transitions may be possible provided two transitions with the right separation can be found within the tuning range of the two laser sources. The stability can be very high (10^{-12} for saturated absorption technique on Doppler free transitions) but the choice of synthetic wavelength is limited.

We propose a new concept of stabilized two-wavelength source based on the use of an optical frequency comb. Indeed such commercially available combs generate a dense grid of tens of thousands of modes, equally separated by tens of megahertz and spread over several terahertz. Used as a frequency reference such comb opens the possibility of generating synthetic wavelengths from a few micrometers to several meters.

In this chapter we will present the general concept of the frequency comb referenced two-wavelength laser source. From this concept we have developed a prototype described in Section 8.2. We present the result of the stability of the synthetic wavelength in vacuum and its calibration in the air. We described the experiments comparing a two-wavelength interferometer fed by the prototype to a commercial interferometer.

8.1 Principle of operation

Optical frequency combs, generated passively or actively, have become a powerful tool in frequency metrology. This type of lasers is now commonly used in the in the field of optical frequency metrology, and has been drastically simplified by the development of optical frequency combs based on fibered Kerr-lens mode-locked femtosecond lasers. The idea developed in this thesis is to transfer the high frequency accuracy to high distance accuracy through multiple-wavelength interferometry.

8.1.1 Frequency combs

Frequency comb generators are laser sources that emit a discrete, comb like, spectrum. The quantities defining the frequency comb have already been described in 5.2.1. The sketch summarizing the definition of these quantities is reproduced in Figure 8.1. Optical frequency comb generators are said to be passive or active depending on the technology.

Passive frequency combs use the phase modulation of a single-mode continuous wave laser by an electro-optic modulator to create sidebands at the

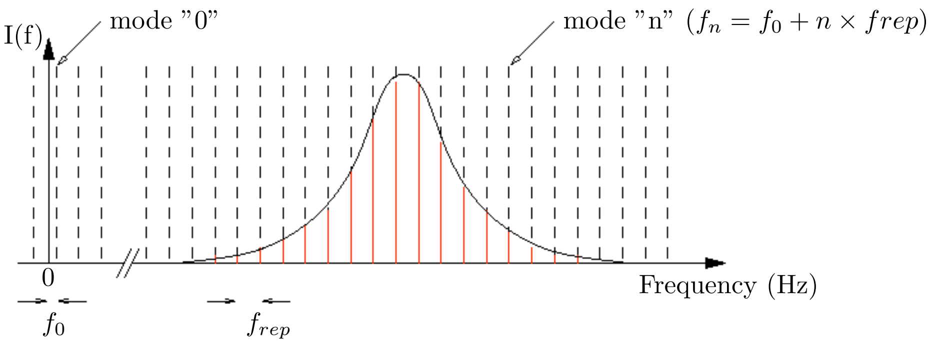

Figure 8.1: Sketch of the optical frequency comb generator spectrum. f_0 is the offset frequency and f_{rep} is the repetition frequency.

modulation frequency. The efficiency of the generation of sidebands can be improved by putting the phase modulator inside a cavity whose free spectral range is equal to a multiple of the modulation frequency [Lui01]. A simplified sketch of a passive frequency comb is shown in 8.1.1. The power of the comb is given by the input laser. The span of the laser is a function of the phase modulation efficiency and of the laser power. Passive frequency combs are commercially available of the shelves at 1.5 μm. They offer a span of a few THz (typically 10 THz) with a repetition rate of a few GHz. The stability of the repetition rate is given by the stability of the phase modulating signal (10^{-11}). The offset frequency drifts with the frequency of the input continuous wave laser.

Active frequency combs are based on mode-locked lasers. Mode locking is usually achieved by means of the Kerr lens non-linear effect in the cavity. In the visible the gain medium is titanium doped sapphire while in the infrared erbium doped fibers are used. The repetition rate is typically of the order of tens to hundreds of MHz and can be stabilized to a radio frequency reference by mean of a phase lock loop. Therefore its accuracy can be as high as the accuracy of the reference signal. The span is limited by the gain curve of the laser medium and can reach several tens of MHz. The offset frequency is due to the difference between the group and phase delay in the cavity. It can be stabilized by locking one mode of the comb by mean of a PLL to a single mode frequency stabilized laser. A powerful mean of stabilizing the offset frequency is the so called self-referencing techniques [Lui01]. This technique requires an octave large frequency comb. The high frequency side of the comb is made to beat with the frequency doubled low frequency side of the comb. The resulting beat signal has the frequency f_0. The stabilization is achieved by mean of a PLL on a reference radio frequency signal. The

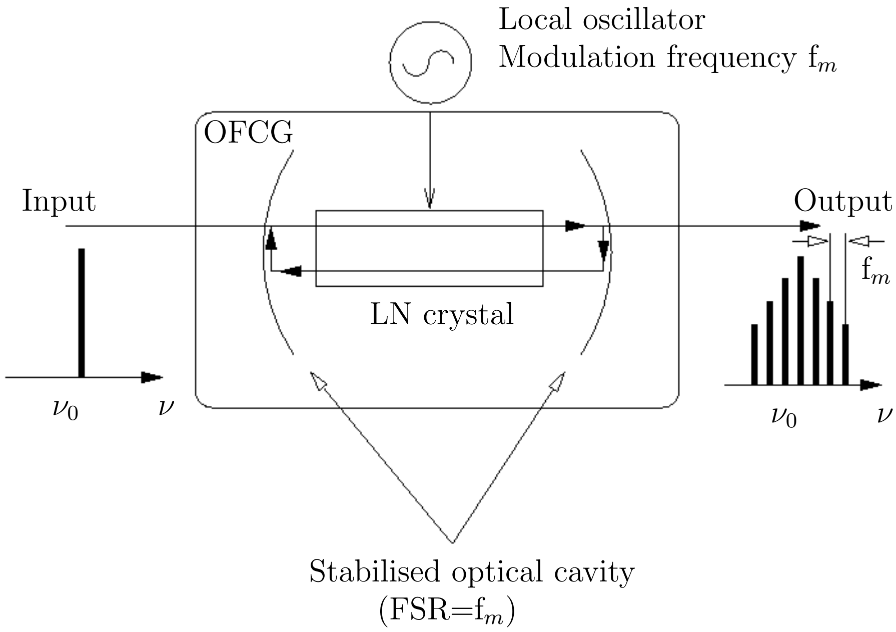

Figure 8.2: Sketch of a passive frequency comb.

	Passive Comb Optocomb	Active comb Menlo Systems
Span	6 THz	tens of THz
Repetition rate	6.25 GHz	100 MHz
Repetition rate accuracy	10^{-11}	$\leq$ reference $\leq 10^{-13}$

Table 8.1: Characteristics of a passive and an active optical frequency comb generated modified to emit at 1.3 microns.

accuracy is given by the reference signal and can therefore reach level as high as 10^{-13}.

The characteristics of a passive and an active optical frequency comb, both modified to work at 1.3 μm, are compared in Table 8.1.1. The active frequency comb has a larger span and smaller repetition rate which provides much more flexibility in the choice of the frequency difference between the two lasers that will be stabilized. As a consequence the two-wavelength laser source can be tuned on a wider range and with a higher resolution. Considering that the prices are equivalent and that ESO has already collaborated with Menlo Systems we have chosen to use an active frequency comb.

8.2 Experiment

8.2.1 Goal of the prototype

As explained previously, optical frequency comb generators may enhance the accuracy and stability of synthetic wavelengths used in two-wavelength interferometry. In the framework of the study of the upgrade of PRIMET towards absolute metrology, we have proposed and developed a prototype of two-wavelength laser source based on the general concept previously described. The goal is to show that the prototype can be used in a two-wavelength interferometer to resolve the optical wavelength, λ=1.319 μm, of PRIMET Nd:YAG laser.

The demonstrator should comply with PRIMET specifications in terms of accuracy, range of measurement, coherence length and sampling frequency. Moreover one of the two wavelength emitted by the source should be the wavelength of the Nd:YAG laser.

8.2.2 Frequency comb

The frequency comb is generated by a custom made Kerr-lens mode-locked fiber laser TC-1500 from Menlo Systems. The spectrum is enlarged by self-phase modulation in a photonic crystal fiber, [IKO98]. The repetition rate and the offset frequency can be modulated by a piezo fiber stretcher which modifies the length of the cavity and by the power of the pump laser. The frequency comb and its control electronics is presented in Figure 8.3. As the iodine stabilization system was already developed for the incremental metrology the frequency comb is not self-referenced and will be stabilized by locking one of its mode on the Nd:YAG.

8.2.3 Single mode lasers

The source uses two single mode lasers. The first single mode laser is the Nd:YAG used for the incremental metrology, see Part II. Due to the required linewidth the choice of the second single mode laser is limited to solid state laser or external cavity laser diode (ECLD).

Solid state lasers offer high power but have a very limited frequency tuning range (typically ten to twenty gigahertz) which limits the choice of synthetic wavelength. Nd:YLF laser emit at 1.313 μm which would generate with the Nd:YAG a 288 μm synthetic wavelength. Nd:YVO_4, emitting at 1.342 μm, would provide a 77 μm synthetic wavelength.

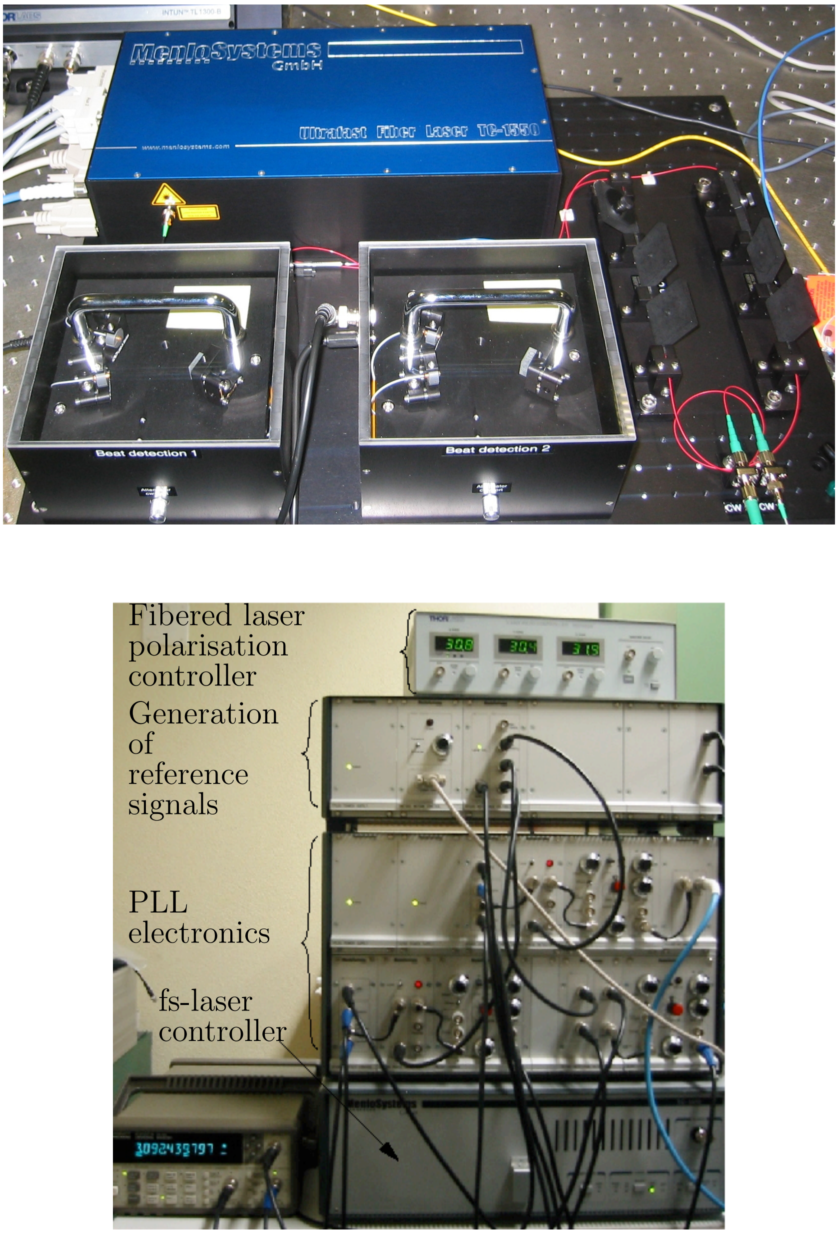

Figure 8.3: Optical frequency comb generator. Top: Housing of the optical frequency comb generator. The two black boxes contain the beat detection units. The two polarization controllers on the right are used to match the polarization of the comb with the polarization of the single mode lasers. Bottom: electronics for the comb and the stabilization of the lasers.

Contrary to solid state lasers, ECLDs offer very large wavelength tuning range. Therefore they can take benefit of the large span of the comb. Indeed one ECLD can be used to generate one synthetic wavelength and then be locked to another mode of the comb to generate a smaller synthetic wavelength. Consequently with only one ECLD and the Nd:YAG it is possible to generate a chain of synthetic wavelength capable of calibrating the interferometer. The ECLD used in the set-up is a Intun 1300 adapted from 1.5 μm to 1.3 μm. In theory it provides more than 20 mW over a 110 nm tuning range centered on 1.32 μm. The linewidth is less than 150 kHz. We had specified a continuous tuning range of 20 nm from 1300 nm to 1320 nm. Unfortunately the laser is not single mode at high power. Tests have shown that to remain single mode over this tuning range the laser cannot emit more than 10 to 15 mW. Moreover the laser frequency is extremely sensitive to vibrations and acoustic noise. In the set-up the laser had to be mechanically isolated from the optical bench to avoid the vibrations created by the experimental set-up.

8.2.4 Experimental set-up and results of the measurements of the prototype performance

The tunable two-wavelength source (Figure 8.4) consists of a Nd:YAG laser at λ_1=1.319 μm (Lightwave Model 125), of an External Cavity Laser Diode (ECLD, Thorlabs INTUN 1300) at λ_2=1.3 μm and finally of a mode-locked fiber laser (Menlo Systems TC-1500). A master clock, synchronized to the carrier frequency of the HBG signal[1] [BDS06], delivers a 10 MHz signal with relative accuracy 10^{-11}. This signal is used by the TC-1500 to generate two signals with the same relative accuracy at 100 MHz and 20 MHz, respectively.

The repetition rate f_{rep} is measured internally by a fast photodiode and phase-locked to the 100 MHz signal by changing the pump power of the mode-locked fiber laser. For each single mode laser, the beat signal f_b with the closest mode of the frequency comb is detected and phase-locked to the 20 MHz signal. In this way, the frequency comb is stabilized on the Nd:YAG frequency by means of a negative feedback to the frequency offset (as defined in Figure 8.2.4) using a fiber-stretching piezo actuator. The phase-locking of the ECLD to the comb is achieved by feeding the laser diode injection current.

[1] The HBG longwave transmitter in Prangins (Switzerland) diffuses at 75 kHz the official time signals synchronized to Universal Time Coordinated. In addition to second pulses, coded information giving the time of day and the date are also sent. The precise carrier frequency of 75 kHz, synchronized by an atomic clock, and the time markers, can be used for the verification of frequency standards and time control purposes. The carrier frequency is maintained within 2×10^{-12} at 75 kHz

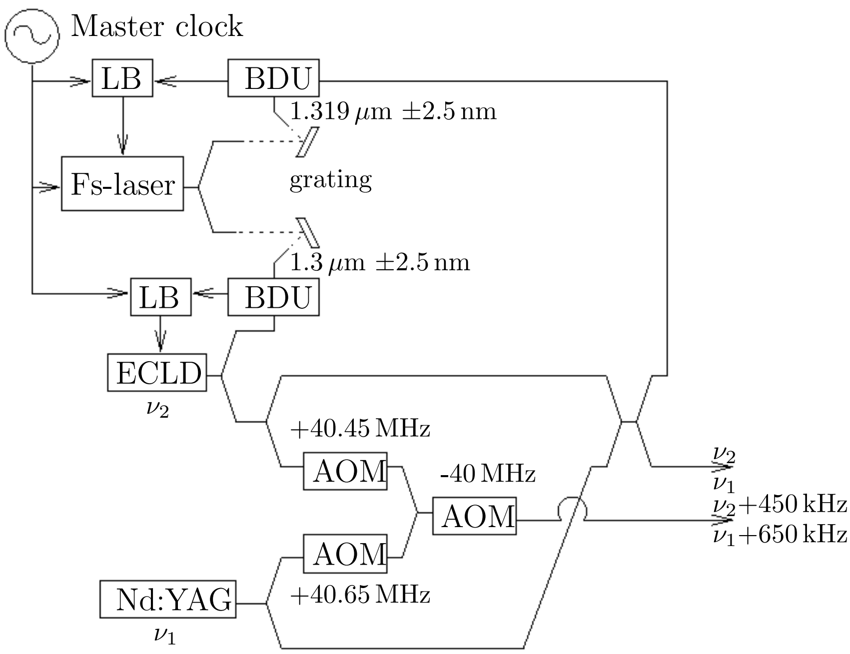

Figure 8.4: Two-wavelength source prototype set-up. LB: Lock-Box (Menlo systems) contains the phase detector and the PI corrector; BDU: Beat Detection Unit (Menlo Systems) consists of a fibered variable attenuator and of a fast photodiode and associated electronics; AOM: Acousto Optical Modulator.

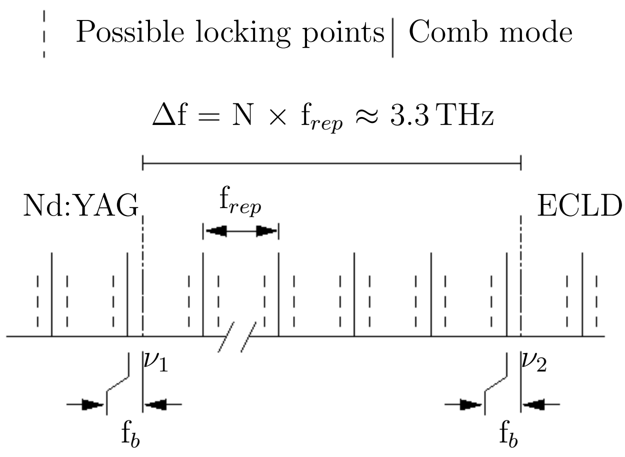

Figure 8.5: Sketch of the prototype source spectrum.

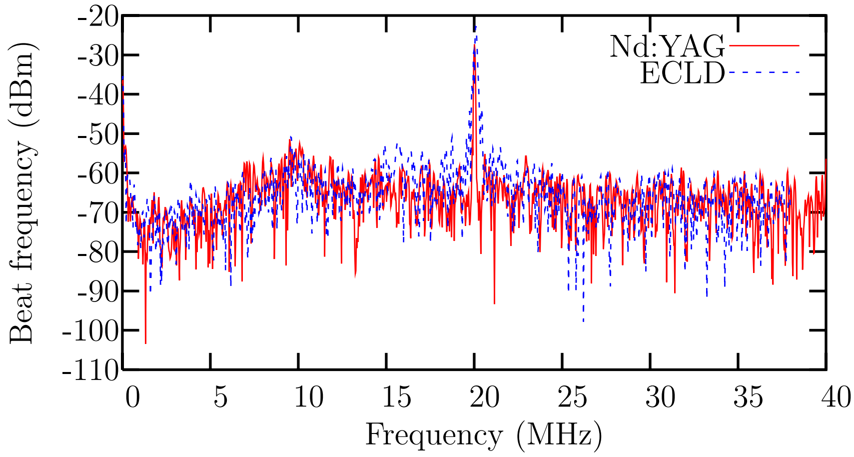

Figure 8.6: Spectrum of the beat signal between one mode of the comb and the Nd:YAG and one mode of the comb and the ECLD.

Signal	Stability (Peak-to-valley)	Relative stability
Repetition rate	1 mHz	10^{-11}
Beat signal Nd:YAG/comb	10 mHz	0.5×10^{-10}
Beat signal ECLD/comb	1 Hz	0.5×10^{-7}
ν_{ECLD}-$\nu_{\mathrm{Nd:YAG}}$	$\approx$ 35 Hz	10^{-11}

Figure 8.7: Summary of the stability of the three stabilization loops of the prototype.

Figure 8.6 shows an example of the spectrum of the beat signal obtained with the Nd:YAG and one mode of the comb and with the ECLD and another mode of the comb. The remaining beat frequency fluctuations of the Nd:YAG laser and the ECLD with their closest frequency comb mode were measured with a frequency counter (HP53131A). The beat frequency were averaged over 1 s. We measured stabilities of 0.01 Hz and 1 Hz Peak-to-Valley for the Nd:YAG laser and the ECLD, respectively. This difference in behavior can be explained by the extreme sensitivity of the ECLD to vibrations and acoustic noise as well as by the 1/f frequency noise of diode lasers [SD00]. The repetition rate of the comb is monitored in the same way and exhibits a stability of 1 mHz Peak-to-Valley. Table 8.7 summarizes the stability of the three stabilization loops and the resulting stability of the frequency difference between the Nd:YAG and the ECLD. The relative stability of the frequency difference between the two lasers is 10^{-11}. *Consequently the relative stability of the synthetic wavelength in vacuum is* 10^{-11}.

8.3 Experimental calibration of the synthetic wavelength and validation of the accuracy of the system

In order to check the accuracy of the synthetic wavelength we made a calibration of the synthetic wavelength by comparison with a commercial HP/Agilent laser interferometer (HP5529A, resolution of 10 nm, accuracy of ± 0.002 ppm). The calibration principle is the same as used in Section 6. The set-up is modified to use the two-wavelength light source described in Figure 8.8. Figure 8.9 shows the optical set-up used for the calibration of the synthetic wavelength.

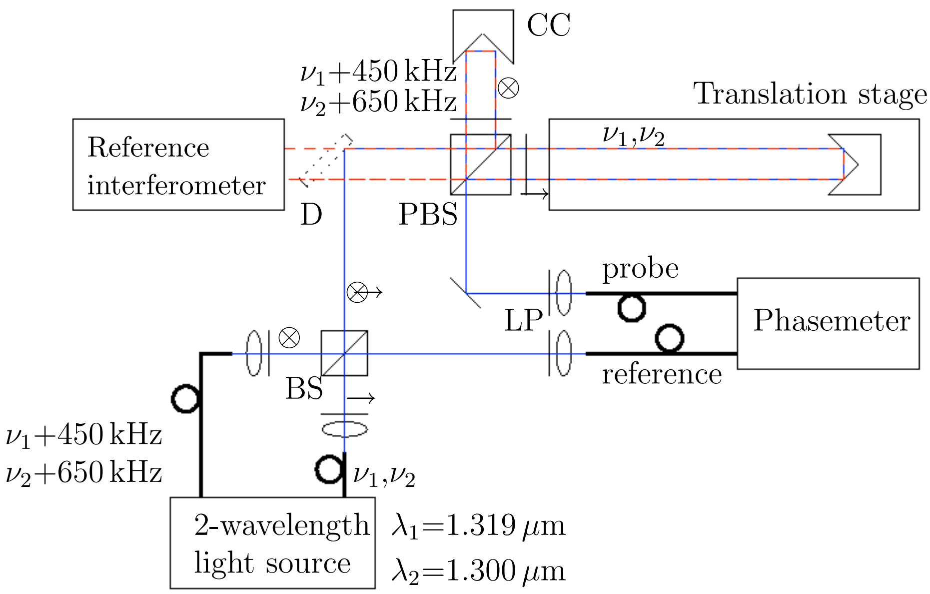

Figure 8.8: Set-up for the calibration of the synthetic wavelength by comparison with a commercial interferometer (HP/Agilent 5529A).

The laser beams of the two interferometers are superimposed with an accuracy of ± 3 mm over 6 m reducing the cosine error to 0.13 ppm . The corner cube of the target arm is mounted on a motorized translation stage with a 90 cm stroke. The translation stage was moved in steps of 50 mm. After each step, the phase $\Phi = \phi_1 - \phi_2$ and the optical path difference at 633 nm are measured by means of the digital phasemeter and the HP interferometer, respectively. The optical path difference $n_1 L$ at 1.3 μm is calculated by taking the air dispersion into account. The integration time of the phasemeter was 2 ms. Results are shown in Figure 8.10.

The linear regression gives a slope $\alpha = \Phi(L)/n_1 L$ of 139.541582 rad/mm with a standard deviation of 11 μrad/mm yielding a synthetic wavelength in air of Λ=90.054666 μm. The residual errors are lower than 22 mrad, corresponding to a phase accuracy better than $2\pi/285$. *Therefore the distance accuracy is about 160 nm, and the inequality 7.14 is satisfied. Thus it is possible to estimate the number of optical wavelengths within the optical path difference and to use interferometric measurements at λ to reach nm accuracy.*

From Equation 7.22 one can see that the frequency difference is:

$$\Delta\nu = \frac{c}{4\pi}\alpha - \frac{\Delta n}{n_1}\nu_2. \tag{8.1}$$

The correction term is estimated from the updated Edlen equations [BD93]. For $\lambda_1 = 1319$ nm and $\lambda_2 = 1300$ nm, one found a correction of about 5.77 MHz. The uncertainty of $\Delta\nu$ is mainly limited by the experimental standard deviation of α, and the cosine error. Therefore the estimation of the frequency difference is $\Delta\nu$= (3.32899949$\pm$0.00000067) THz at a confidence level of 95 %. *The relative accuracy of this calibration is better than 0.2 ppm.* Within this uncertainty range, we see that the *frequency difference corresponds to 33,290 modes.*

We have proposed and tested experimentally a new concept of two-wavelength laser source based on the use of a femtosecond pulsed laser. It uses the optical frequency comb to stabilize the frequency of two lasers with respect to each other over a wide range of frequency intervals. The stability of the frequency difference is given by the frequency reference used to stabilize the repetition rate of the femtosecond laser. Therefore the prototype can provide synthetic wavelengths from tens of microns to one meter with a relative accuracy of 10^{-11} in vacuum. Therefore it can be used to generate a chain of synthetic wavelength to make a distance measurement with a NAR of up to 0.5 m with a nanometer accuracy. As a consequence it is the perfect tool for an upgrade of PRIMET towards absolute distance measurements.

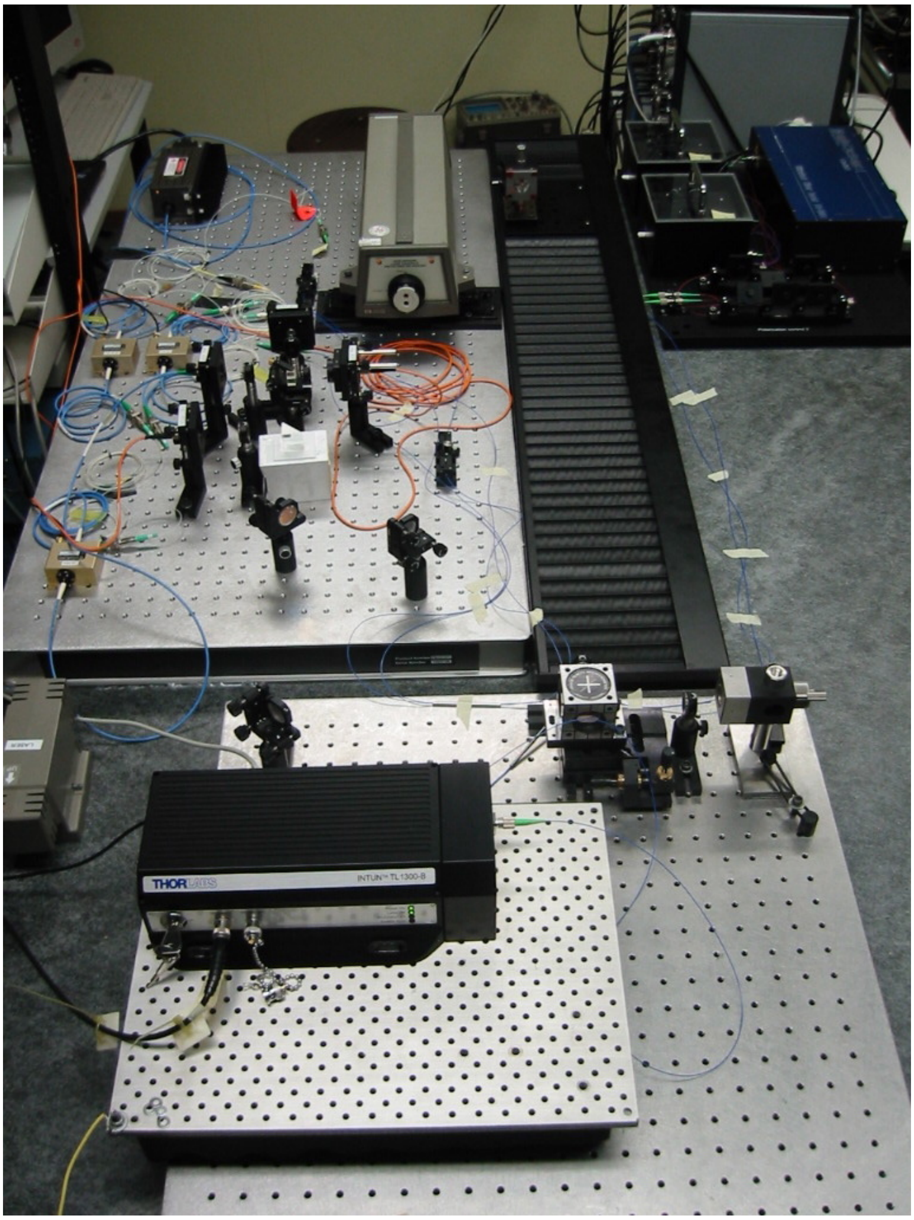

Figure 8.9: Picture of the set-up used for the calibration of the synthetic wavelength by comparison with a commercial laser interferometer. On the top-left breadboard are the Nd:YAG, the HP interferometer laser head, the three Acousto-optic modulators and the launching optics. On the breadboard at the bottom, the ECLD is mounted on an steel plate on top of a foam block used to damp the vibrations. The beam splitter and the reference corner cube are on the same breadboard. The second corner cube is mounted on the translation stage at the centre. The black breadboard at the top-right corner of the table is the optical frequency comb generator.

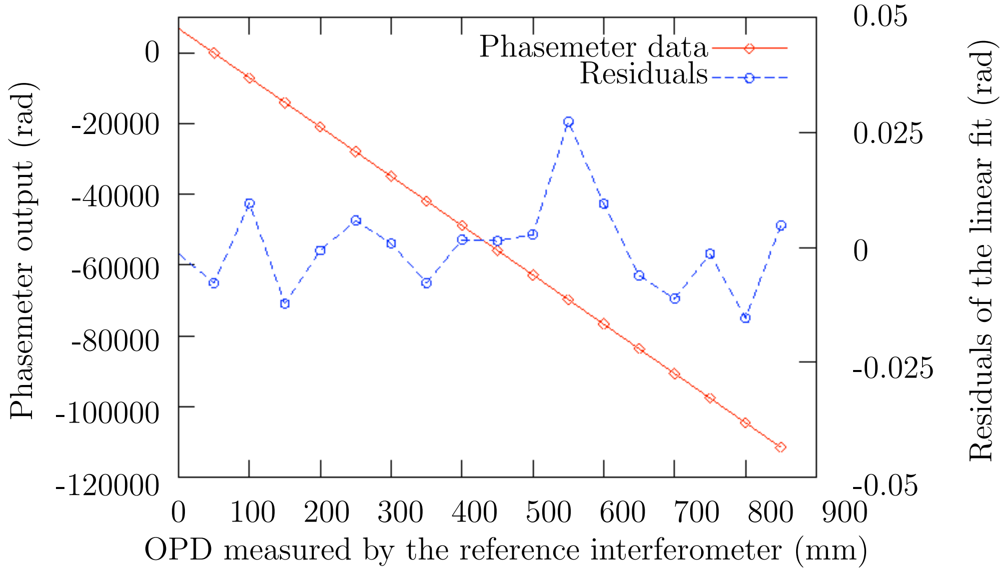

Figure 8.10: Calibration of the synthetic wavelength by comparison with a commercial interferometer.

Chapter 9

Proposition of a frequency comb referenced two wavelength laser source for a PRIMA absolute metrology system

We have proposed in the previous chapter a new concept of two-wavelength laser source. We have tested a prototype of such a source and demonstrated its capability to generate a chain of synthetic wavelength from a few tens of microns to one meter with high accuracy. In this chapter, we use the knowledge acquired from the two-wavelength source prototype to propose an upgrade of the PRIMA Metrology System. As an upgrade the new system should use as much as possible the hardware already available.

In the first part of this chapter, we propose an upgrade of the prototype laser source which permits two-wavelength differential OPD measurements. Then, based on the results obtained in the previous chapter, we estimate a possible wavelength chain for the calibration of the PRIMET. We propose a second approach for the interferometer calibration which requires smaller scans of the ECLD frequency.

9.1 Proposition of a two-wavelength laser source for absolute measurements of differential OPD

The upgrade of PRIMET needs to measure directly the difference of OPD of two different interferometers with a synthetic wavelength. With single-wavelength interferometry the differential OPD between two interferometers can be directly monitored by the use of superheterodyne interferometry. This technique uses the beat signal of two heterodyne signals obtained in two different interferometers as explained in Section 3.1.1. In two-wavelength interferometry the superheterodyne technique uses two different wavelengths in a same interferometer to measure the phase of the synthetic wavelength. The incremental PRIMET uses two heterodyne frequencies, one for each interferometer. The two wavelength PRIMET must use a different heterodyne frequency per wavelength and per interferometer. Consequently, 4 heterodyne pairs must be generated by the laser source instead of 2 currently provided by the prototype. Moreover, the current superheterodyne phasemeter measures only the phase difference between two heterodyne signals. It will have to be modified to measure the phase of the synthetic wavelength linked to the differential OPD. Indeed this phase is obtained from the phase difference of 4 different heterodyne signals. Finally both the source and the phasemeter must remain compatible with the use of single wavelength interferometry.

9.1.1 Generation of four heterodyne frequencies and signal processing

Two possible schemes can be used to generate the four heterodyne frequencies and process the signals. We describe here the one requiring two additional AOM, the replacement of the actual photodetectors by faster ones and the use of an additional phasemeter. A sketch of such a source is given in Figure 9.1.

With this source the four heterodyne frequencies are:

- f_{11}=40.65 MHz and f_{12}=40 MHz which propagate in the reference interferometer;
- f_{21}=40.45 MHz and f_{22}=40 MHz which propagate in the science interferometer.

Signal processing for the two-wavelength measurement The measurement of the synthetic wavelength phase requires to replace the detec-

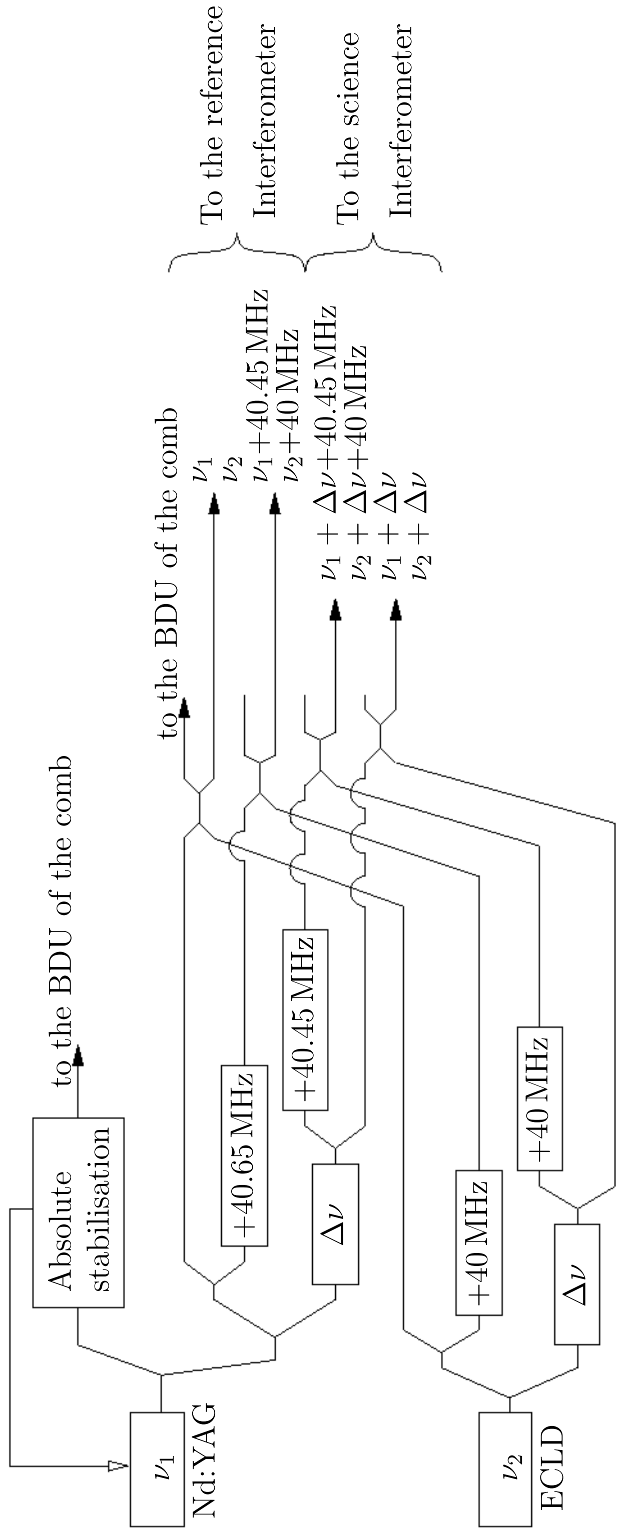

Figure 9.1: Upgrade of the two-wavelength prototype to a two-wavelength laser source compatible with the measurement of differential OPD.

tion stage of the actual phasemeter by a new one. New photodiodes with a bandwidth larger than 41 MHz are used. At the output of the reference interferometer, the signal detected is:

$$I_{ref} = A_{0,\mathrm{ref}} + A_{1,\mathrm{ref}} \cos\left(2\pi f_{11} t + \phi_{11}\right) + A_{2,\mathrm{ref}} \cos\left(2\pi f_{12} t + \phi_{12}\right) \tag{9.1}$$

where the coefficients $A_{0,\mathrm{ref}}$, $A_{1,\mathrm{ref}}$ and $A_{2,\mathrm{ref}}$ depend on the amplitude of the different waves and where the phases are

$$\phi_{11} = \frac{2\pi}{c}\nu_1 \mathrm{OPD_{ref}} \tag{9.2}$$

$$\phi_{12} = \frac{2\pi}{c}\nu_2 \mathrm{OPD_{ref}}. \tag{9.3}$$

This signal is then self-multiplied and band-pass filtered around f_{11}-f_{12}=650 kHz. The same processing is applied to the science interferometer except that the signal is filtered around f_{21}-f_{22}=450 kHz. One has then two signals S_{ref} and S_{sc} for the reference and science interferometer respectively:

$$S_{ref} \propto \cos\left(2\pi \left(f_{11} - f_{12}\right) t + \phi_{ref}\right) \tag{9.4}$$

$$S_{sc} \propto \cos\left(2\pi \left(f_{21} - f_{22}\right) t + \phi_{sc}\right) \tag{9.5}$$

where the phases are given by:

$$\phi_{ref} = 2\pi \frac{OPD_{\mathrm{ref}}}{\Lambda} \tag{9.6}$$

$$\phi_{sc} = 2\pi \frac{OPD_{\mathrm{sc}}}{\Lambda}. \tag{9.7}$$

These electric signals are equivalent to the ones used in the phasemetre of the incremental PRIMET (described in Section 3.2.6). However the phase of these signals depends on the synthetic wavelength and not on the optical wavelength anymore. One can feed these signals to the electrical input of the phasemetre to get the phase of the synthetic wavelength signal. This phase contains the information on the differential OPD between the reference and science interferometer:

$$\Phi_\Lambda = 2\pi \frac{\mathrm{OPD_{ref}} - \mathrm{OPD_{sc}}}{\Lambda}. \tag{9.8}$$

Signal processing for the single wavelength measurement At the output of the detector the signals are multiplied by the signal of a local oscillator to generate the two signals:

$$S_{\mathrm{ref},\lambda} \propto \cos\left(2\pi \left(f_{11} - f_{LO}\right) t + \phi_{\mathrm{ref},\lambda_1 - \phi_{\mathrm{LO}}}\right) \tag{9.9}$$

$$S_{\mathrm{sc},\lambda} \propto \cos\left(2\pi \left(f_{21} - f_{LO}\right) t + \phi_{\mathrm{sc},\lambda_1 - \phi_{\mathrm{LO}}}\right) \tag{9.10}$$

$$\tag{9.11}$$

where f_{LO}=40 MHz is the frequency of the local oscillator. In this case again, the signals are similar to the one at the output of the detector board of the phasemeter used for the incremental metrology. Therefore, a second phasemetre, identical to the first one, measures the differential OPD of the two interferometers as a function of the optical wavelength $\lambda_{Nd:YAG}$=1.319 μm.

9.2 Derivation of an error budget and a corresponding possible wavelength chains

The two-wavelength source prototype has shown that it was possible to calibrate the synthetic wavelength with an accuracy better than 0.2 ppm. Considering the maximum differential OPD given by the specifications (summarized in Table 1.1), $\Delta\mathrm{OPD}_{\mathrm{max}}$=120 mm, the maximum error due to the uncertainty on the synthetic wavelength is:

$$\delta\Delta\mathrm{OPD}_{\Lambda} = \frac{\delta\Lambda}{\Lambda}\Delta\mathrm{OPD}_{\mathrm{max}} = 24\,\mathrm{nm}. \tag{9.12}$$

The prototype has exhibited a phase error of $2\pi/285$. However, this accounts for one interferometer only and not for a differential OPD measurement. We can safely assume that the error on the differential OPD is about twice this value, i.e $\delta\Phi \approx 2\pi/140$. In order to resolve the optical wavelength, $\lambda_{\mathrm{Nd:YAG}}$=1.319 μm, the maximum total error should be less than:

$$\delta\mathrm{OPD} = \frac{\delta\Lambda}{\Lambda}\Delta\mathrm{OPD}_{\mathrm{max}} + \frac{\delta\Phi}{2\pi}\Lambda \leq \frac{\lambda_{\mathrm{Nd:YAG}}}{2}. \tag{9.13}$$

Therefore the first synthetic wavelength must be smaller than 75.5 μm to possibly resolve the optical wavelength. One can now apply recursively the same calculation to get increasing synthetic wavelengths until we reach the desired NAR=OPD_{max}=120 mm. The result is the wavelength chain summarized in Table 9.1.

	Wavelength	$\Delta\nu = \lvert\nu_{\mathrm{Nd:YAG}} - \nu_{\mathrm{ECLD}}\rvert$	λ_{ECLD}
$\lambda_{\mathrm{Nd:YAG}}$	1.319 μm	-	-
Λ_1	75.5 μm	3.97 THz	1.296 μm
Λ_2	5.27 mm	56.9 GHz	1.318,67 μm
Λ_3	0.369 m	812 MHz	1.318,995 μm

Table 9.1: Possible wavelength chain for PRIMET calibration.

Table 9.1 assumes that the synthetic wavelength is always generated by the Nd:YAG and the ECLD. In that case, the ECLD frequency has to be tuned over 3.9 THz between the measurement at Λ_2 and the measurement at Λ_1. Another approach which requires shorter frequency scans can be used as explained below.

Let's assume that the calibration of the interferometer begins with the ECLD at the optical frequency $\nu_{\mathrm{ECLD}} = \nu_{\mathrm{Nd:YAG}} + 3.97\,\mathrm{THz} + 56.9\,\mathrm{GHz} + 812\,\mathrm{MHz}$ yielding a synthetic wavelength Λ_3'. The phase of the interferometric signal obtained with Λ_3' is measured at the time t_1. Then the frequency of the ECLD is scanned to $\nu_{\mathrm{ECLD}} = \nu_{\mathrm{Nd:YAG}} + 3.97\,THz + 56.9\,GHz$ which generates a new synthetic wavelength Λ_2' with the Nd:YAG. The phase is measured at the instant t_2 and the phase difference with the measurement done with Λ_3' is calculated:

$$\begin{aligned} \phi_{\Lambda_3}(t_2) &= \phi_{\Lambda_2'}(t_2) - \phi_{\Lambda_3'}(t_1) && (9.14) \\ &= 2\pi\frac{\mathrm{OPD}(t_2)}{\Lambda_3} - 2\pi\frac{OPD(t_2) - OPD(t_1)}{\Lambda_3'}. && (9.15) \end{aligned}$$

The phase difference is almost the phase of the interferometric signal that would have been obtained at the instant t_2 with a synthetic wavelength $\Lambda_3 = \frac{\Lambda_1 \times \Lambda_2}{|\Lambda_1 - \Lambda_2|}$. A corrective term is added because of the OPD variation between the two phase measurements. The variation of OPD can be measured by the incremental metrology system and corrected for. Thus the OPD at time t_2 is known as a function of the synthetic wavelength Λ_3=0.369 m.

For the next step the frequency of the ECLD is tuned to $\nu_{\mathrm{ECLD}} = \nu_{\mathrm{Nd:YAG}} + 3.97\,\mathrm{THz}$. The synthetic wavelength generated by the Nd:YAG and the ECLD is now Λ_1. Using the same procedure as before the OPD is computed with the wavelength $\Lambda_2 = \frac{\Lambda_2' \times \Lambda_1}{|\Lambda_2' - \Lambda_1|}$=5.27 mm. Finally, from that point, the OPD is given in real time by the two wavelengths $\lambda_{\mathrm{Nd:YAG}}$=1.319 μm and Λ_1=75.5μm. The Table 9.2 summarizes the new wavelength chain. One can see that frequency of the ECLD has to be tuned over 60 GHz (0.3 nm) instead of 4 THz (23 nm). This reduces the time required for the calibration and decreases the requirements on the ECLD.

	Wavelength	Obtained by	λ_{ECLD}
$\lambda_{\mathrm{Nd:YAG}}$	1.319 μm	-	-
Λ_1	75.5 μm	$\Lambda_1 = \frac{\lambda_{\mathrm{Nd:YAG}} \times \lambda_{\mathrm{ECLD}}}{|\lambda_{\mathrm{Nd:YAG}} - \lambda_{\mathrm{ECLD}}|}$	1.296,361 μm
Λ_2	5.27 mm	$\Lambda_2 = \frac{\Lambda_1 \times \Lambda_2'}{|\Lambda_1 - \Lambda_2'|}$, $\Lambda_2' = \frac{\lambda_{\mathrm{Nd:YAG}} \times \lambda_{\mathrm{ECLD}}}{|\lambda_{\mathrm{Nd:YAG}} - \lambda_{\mathrm{ECLD}}|}$	1.296,042 μm
Λ_3	0.369 m	$\Lambda_3 = \frac{\Lambda_2 \times \Lambda_3'}{|\Lambda_2 - \Lambda_3'|}$, $\Lambda_3' = \frac{\lambda_{\mathrm{Nd:YAG}} \times \lambda_{\mathrm{ECLD}}}{|\lambda_{\mathrm{Nd:YAG}} - \lambda_{\mathrm{ECLD}}|}$	1.296,037 μm

Table 9.2: Wavelength chain for PRIMET calibration with synthetic wavelengths obtained from synthetic wavelengths.

9.3 Next steps in the development of PRIMET upgrade

The measurements obtained with the two-wavelength laser source prototype have demonstrated the capacity to resolve one optical wavelength. Moreover, it has allowed to quantify the accuracy of a two-wavelength superheterodyne interferometer and to calculate the wavelength chain that would permit the absolute calibration of PRIMET with nanometer accuracy. However there are still issues to cover before proposing a final design for the upgrade of PRIMET. Some of the key points to be studied are presented here.

Replacement of the ECLD The ECLD used in the prototype is the source of a few problems. The main one is this the limited power at its output. The ECLD is not single-mode for power larger than 15 mW. Moreover the power has to be significantly decreased to allow a continuous single-mode frequency tuning over the desired range. The second wavelength chain proposed in the previous section relaxes the specifications on the ECLD and it may be possible to operate it in these conditions. Nevertheless, 20 mW is not enough to operate PRIMET with four heterodyne frequencies along the whole VLTI.

A solution may be to include in the source Semiconductor Optical Amplifiers (SOA) which have already been used in the context of two-wavelength interferometry, [Sal99]. SOA exist at 1.3 μm. They present typically gain of 20 dB and saturate around 10 mW. Therefore, introduced just before the injection in the interferometer they would provide enough power. The ripple of the gain has to be measured precisely to check if it is compatible with the frequency tuning of the ECLD.

Although Ytterbium doped fibered amplifier at 1.3 μm are available and have higher saturation , they are too expensive.

The development of new high power DFB lasers at 1.3 μm may be an alternative to the ECLD and to the SOAs.

Automatic calibration of the frequency difference The frequency difference between the two lasers used in the two-wavelength source can be determined with a commercial wave-meter of accuracy 50MHz. However, to simplify the frequency scans a procedure counting the number of modes of the frequency comb is under study.

Upgrade of the phasemetre As explained in Section 9.1.1, the phasemeter has to be upgraded to permit the simultaneous measurement at an optical wavelength and at the synthetic wavelength. The actual phasemetre and the spare part will be used. The replacement of the photodiodes is already under study. The modification of the PRIMA LCU to read two phasemeters simultaneously is done. Tests are scheduled.

Conclusion of Part III

The incremental PRIMET requires a time consuming calibration procedure. This can be avoided if the fringe order of the interferometric signal can be determined without ambiguity over the whole measurement range. This may be achieved by the use of two-wavelength interferometry. This third part of the thesis addresses the upgrade of the incremental PRIMET to an absolute PRIMET through the use of two-wavelength interferometry. It insists on the development of a new concept of two-wavelength light source which offers unprecedented tunability and accuracy.

Two-wavelength interferometry allows to measure distance with a great flexibility in terms of range of accuracy. It replaces the optical wavelength of single-wavelength interferometry by a so called synthetic wavelength obtained from two optical wavelengths. This synthetic wavelength is typically in the range $100\,\mu$m - 1 m. The accuracy of this technique can reach a few tens of microns. Therefore, it permits to resolve an optical wavelength. We have recalled the principle of two-wavelength interferometry and how it can be link to single-wavelength interferometry. We have presented a state of the art of two-wavelength interferometry and analyzed the sources of error. In particular, we have shown that the relative accuracy of two-wavelength interferometry in the air is limited to 10^{-8} by the uncertainty on the available model of the refractive index.

We present a state of the art of the laser sources for two-wavelength interferometry to highlight the new possibilities offered by the new concept we propose. This concept uses an optical frequency comb as a reference grid to stabilize two lasers over large frequency intervals with high accuracy. Applied to two-wavelength interferometry this technique enables the generation of synthetic wavelength from tens of microns to several meters. Assuming that the number of modes between the two lasers is known, the accuracy on the frequency difference is only limited by the relative accuracy of a radio frequency reference signal feeding the comb. In vacuum, the corresponding synthetic wavelength will be known with the same relative accuracy.

We have integrated a prototype of the source and verified experimentally that it can generate synthetic wavelengths as small as 90 μm. The accuracy of the synthetic wavelength in vacuum is 10^{11}. The calibration of the synthetic wavelength in air is limited by the calibration procedure to an accuracy of 0.2 ppm. With a phase accuracy better than $2\pi/200$, this synthetic wavelength allows to resolve the optical wavelengths and therefore to reach ultimately nanometer accuracy. Using the frequency tuning capacity of the ECLD, the two-wavelength source should enable long distance measurements with very high accuracy by using a chain of highly accurate synthetic wavelengths.

We have proposed a modification of PRIMET to enable the calibration of the interferometer by two-wavelength interferometry instead of the current incremental approach. We have described the corresponding upgrades of the two-wavelength source prototype and of the phasemetre. Based on the experimental results obtained with the prototype, we have shown that three synthetic wavelengths are required to calibrate PRIMET. Finally we give an overview of the problems that are still to be tackled before the establishment of a final design of the upgrade of PRIMET.

References

[ABL+01] Markus-Christian Amann, Thierry Bosch, Marc Lescure, Risto Myllylä, and Marc Rioux. Laser ranging: a critical review of usual techniques for distance measurement. *Optical Engineering*, 40(1):10–19, January 2001.

[B.02] Pécheux B. *Optimisation d'un dispositif interférométrique de mesure de distance absolue utilisant une diode laser à cavité externe continûment syntonisable dans les bandes S et C.* PhD thesis, Université Louis Pasteur, Strasbourg I, 2002.

[BD93] K. P. Birch and M. J. Downs. An updated edlén equation for the refractive index of air. *Metrologia*, 30:155–162, 1993.

[BDS06] L-G. Bernier, G. Dudle, and C. Schlunegger. Federal office of metrology metas, time broadcasting services, hbg time signal transmitter, May 2006. URL http://www.metas.ch/en/labors/official-time/hbg/.

[BF98] Karl-Heinz Bechstein and Werner Fuchs. Absolute interferometric distance measurements applyingg a variable synthetic wavelength. *Journal of Optics*, 29:179–182, 1998.

[BL95] Thierry Bosch and Marc Lescure. *Selected papers on laser distance measurements*, volume 115 of *SPIE Milestone Series*. SPIE Optical Engineering Press, Bellingham, Washington USA, 1995.

[BO79] G. L. Bourdet and A. G. Orszag. Absolute distance measurement by co_2 laser multiwavelength interferometry. *Applied Optics*, 18(2):225–227, January 1979.

[CCL02] Benyong Chen, Xiaohui Cheng, and Dacheng Li. Dual-wavelength interferometric technique with subnanometric resolution. *Applied Optics*, 41(28):5933–5937, October 2002.

[dG91] Peter j. de Groot. Three-color laser-diode interferometer. *Applied Optics*, 30(25):3612–3616, September 1991.

[dGK91] Peter de Groot and Stanley Kishner. Synthetic wavelength stabilization for two-color laser-diode interferometry. *Applied Optics*, 30(28):4026–4033, October 1991.

[DHH94] Rainer G. Dorsch, Gerd Häusler, and Jürgen Herrmann. Laser triangulation: fundamental uncertainty in distance measurement. *Applied Optics*, 33(7):1306–1314, March 1994.

[DSLG98] S. Dubovitsky, D. J. Seidel, D. Liu, and R. C. Gutierrez. Metrology source for high-resolution heterodyne interferometer laser gauges. In Robert D. Reasenberg, editor, *Astronomical interferometry*, volume 3350, pages 973–985. SPIE, 1998.

[DSZ98] René Dändliker, Yves Salvadé, and E Zimmerman. Distance measurement by multiple-wavelength interferometry. *Journal of Optics*, 29:105–114, 1998.

[DTP88] René Dändliker, R. Thalman, and D. Prongué. Two-wavelength laser interferometry using superheterodyne detection. *Optics Letters*, 13(5):339–341, May 1988.

[GBR81] C. W. Gillard, N. E. Buholz, and D. W. Ridder. Absolute distance interferometry. *Optical Engineering*, 20(1):129–134, January 1981.

[GC97] Anatol N. Golubev and Alexander M. Chekhovsky. Absolute distance interferometry with two-wavelength fringe visibility measurement. *Optical Engineering*, 36(8):2229–2232, August 1997.

[GMD94] E. Gelmini, U. Minoni, and F. Docchio. Tunable, double-wavelength heterodyne detection interferometer for absolute distance measurements. *Optics Letters*, 19(3):213–215, February 1994.

[Har91] P. Hariharan, editor. *Selected papers on interferometry*, volume 28 of *SPIE Milestone Series*. SPIE Optical Engineering Press, Bellingham, Washington USA, 1991.

[IKO98] K. Imai, M. Kourogi, and M. Ohtsu. 30-thz span optical frequency comb generation by self-phase modulation in an optical fiber. *IEEE Journal of Quantum Electronics*, 34(1):54–60, 1998.

[KS02] Th. Kinder and K-D. Salewski. absolute distance interferometer with grating-stabilized tunable diode laser at 633nm. *Journal of Optics A: Pure and Applied Optics*, 4:364–368, November 2002.

[LDP+03] O. P. Lay, S. Dubovitsky, R. D. Peters, J. P. Burger, S.-W. Ahn, W. H. Steier, H. R. Fetterman, and Y. Chang. Mstar: a submicrometer absolute metrology system. *Optics Letters*, 28(1):890–892, June 2003.

[LE00] Mats G. Löfdahl and Henrik Eriksson. Resolving piston ambiguities when phasing a segmented mirror. In Breckinridge & Jacobsen, editor, *UV, optical and IR space telescopes and instruments VI*. SPIE, 2000.

[LE01] Mats G. Löfdahl and Henrik Eriksson. Algorithm for resolving 2π ambiguities in interferometric measurements by use of multiple wavelengths. *Optical engineering*, 40(6):984–990, June 2001.

[Lui01] Andre N. Luiten, editor. *Frequency measurement and control: advanced techniques and future trends*, chapter Generation and metrological application of optical frequency combs, page 295. Topics in applied physics. Springer Berlin / Heidelberg, 2001.

[MA96] Vered Mahal and Ady Arie. Distance measurements using two frequency-stabilized nd:yag lasers. *Applied Optics*, 35(16):3010–3015, June 1996.

[Mat81] Hirokazu Matsumoto. Infrared he-xe laser interferometry for measuring length. *Applied Optics*, 20(2):231–234, January 1981.

[Mat84] Hirokazu Matsumoto. Synthetic millimeter-wave signal generation for length measurement. *Applied Optics*, 23(7):973–974, April 1984.

[Mic93] Albert A. Michelson. Comparison of the international meter with the wavelength of the light of cadmium. *Astronomy ans Astrophysics*, 12:556–560, 1893.

[PPB92] J. M. Payne, D. Parker, and R. Bradley. A rangefinder with fast multiple range capability. http://www.gb.nrao.edu/ rcreager/GBTMetrology/documentation/gbtmemo/gbtmemo73.html, January 1992. updated version of GBT Memo 73 which was originally published in February of 1992.

[Sal99] Yves Salvadé. *Distance measurement by multiple-wavelength inteferometry.* PhD thesis, Université de Neuchâtel, July 1999. Chapter 6.

[SD00] Yves Salvadé and René Dändliker. Limitations of interferometry due to the flicker noise of laser diodes. *Journal of the Optical Society of America A*, 17(5):927–932, May 2000.

[SDM02] Achim Schumacher, Nicholas Devaney, and Luzma Montoya. Phasing segmented mirrors: a modification of the keck narrow-band technique and its application to extremely large telescopes. *Applied Optics*, 41(7):1297–1307, March 2002.

[SFIT91] Zoran Sodnik, Edgar Fisher, Thomas Ittner, and Hans J. Tiziani. Two-wavelength double heterodyne interferometry using a matched grating technique. *Applied Optics*, 30(22):3139–3144, August 1991.

[Wal87] C. J. Walsh. Measurements of absolute distance to 25 m by multi-wavelength co_2 laser interferometry. *Applied Optics*, 26(9):1680–1687, May 1987.

[WCSC02] Arno A. Wielders, Bertrand Calvel, Bas L. Swinkels, and Patrick D. Chapman. Metrology concepts for a space interferometer: Smart-2. In Shao, editor, *Interferometry in space*, volume 4852, pages 268–278. SPIE, 2002.

[Wya71] J. C. Wyant. Testing aspherics using two-wavelength holography. *Applied Optics*, 10(9):2113–2119, September 1971.

[YOI+99] Shuko Yokoyama, Jun Ohnishi, Shigeo Iwasaki, Katuo Seta, Hirokazu Matsumoto, and Norihito Suzuki. Real-time and high-resolution absolute-distance measurement using a two-wavelength superheterodyne interferometer. *Meas. sci. technol.*, 10:1233–1239, 199.

[ZSD96] E. Zimmermann, Y. Salvadé, and R. Dändliker. Stabilized three-wavelength source calibrated by electronic means for high-accuracy absolute distance measurement. *Optics Letters*, 21(7):531–533, April 1996.

[ZZL99] Yang Zhao, Ting Zhou, and Dacheng Li. Heterodyne absolute distance inteferometer with a dual-mode hene laser. *Optical Engineering*, 38(2):246–249, February 1999.

Conclusion

PRIMA, the forthcoming instrument of the VLTI, will soon be operated at the Paranal observatory. In order to detect extra-solar planets it requires a stable and accurate internal metrology system called PRIMET. The key element of the performance of this laser interferometer is the accuracy and stability of its wavelength which is used as a yardstick. This dissertation addressed the design, test and characterization of frequency stabilized laser sources for PRIMET.

In Part I, we have introduced the Phase-Referenced Imaging and Micro-arcsecond Astrometry facility in the larger framework of the VLTI. The basic principle of single-wavelength interferometry is recalled and highlights the need for frequency stabilized laser sources. A summary of the design of PRIMET has been included in relation with the technical implications of the specifications of the system. We used this general introduction to justify the analysis of the two problems tackled by this thesis.

In Part II, we described the characterization and improvement of the absolute frequency stabilization of the Nd:YAG laser used by PRIMET.

Laser interferometry requires the calibration and the stabilization of the laser wavelength on an absolute reference. PRIMET Nd:YAG laser is stabilized using the Pound-Drever-Hall method on an absorption line of iodine at 659.5 nm after frequency doubling of the laser light. We demonstrated theoretically and experimentally that periodically poled lithium niobate fulfills the specifications for the second harmonic generation. We measured the absorption spectrum of iodine in the laser frequency tuning range and designed the iodine cell for the Nd:YAG frequency stabilization system.

After integration of the frequency stabilization system by the Institute of Micro-technology of Neuchâtel, we have modified the control loop to use a second frequency actuator. It prevents the first actuator from reaching saturation which permits to keep the control loop closed over at least several weeks instead of typically half an hour. Furthermore, we have calibrated the error signal. Thus, the error signal can be used to estimate the stability of the laser frequency.

In order to measure accurately the performance of the absolute frequency stabilization system, we have used a self-referenced optical frequency comb generator as an independent frequency sensor. This allowed me to measure the optical frequency of the stabilized Nd:YAG laser with a relative accuracy better than 10^{-12}. The standard deviation of the frequency noise in closed loop over the bandwidth 0.5 mHz - 8 kHz is better than 1.87 MHz to be compared to 2.27 Mhz required by the specifications. Nevertheless, we have shown that the system performance is limited by detection noise. We have identified the sources of this noise and reduced them when feasible. We have calibrated the Nd:YAG wavelength with the optical frequency comb. The mean wavelength in vacuum is λ_{NdYAG}=1.319,176 μm corresponding to the frequency $\nu_{\mathrm{Nd:YAG}}$=227.257,330,6 Thz. The repeatability of the laser locking frequency is better than 100 kHz over one week.

In spite of the absolute reference provided by an atomic transition, the locking frequency may be changed after the transport and the integration of the system at the Paranal observatory. Furthermore, aging of the system components or variations of the environmental conditions may alter the locking frequency on the long time scales (several years) required by the most demanding observations. Therefore we have investigated the possibility to calibrate the Nd:YAG wavelength with a reference interferometer available at the observatory. We have shown experimentally that such a calibration cannot reach the required accuracy of 10^{-8}. Therefore, the system will be calibrated after integration with a self-referenced optical frequency comb.

In Part III, we have addressed the problem of the upgrade of PRIMET from incremental distance measurements to absolute distance measurements.

A state of the art of optical distance measurements showed that only single-wavelength interferometry associated to multiple-wavelength interferometry allows to measure without ambiguity the OPD of the interferometer over its full range. Applied to PRIMET this technique would reduce the calibration time from tens of minutes to a few seconds. The principle of two-wavelength interferometry and its link to single-wavelength interferometry is presented. A state of the art of the the laser sources is included. It shows that current sources often emit synthetic wavelength within a limited range and with a low accuracy.

We describe a new concept of frequency comb referenced two-wavelength laser source based on the use of an optical frequency comb. This comb is used as a reference grid to stabilize two lasers over wide frequency intervals with high accuracy. Applied to two-wavelength interferometry this technique enables the generation of synthetic wavelength from tens of microns to several meters. Assuming that the number of modes between the two lasers is known, the accuracy on the frequency difference is only limited by the relative accuracy of a radio frequency reference signal feeding the comb. In vacuum, the corresponding synthetic wavelength will be known with the same relative accuracy. In air, we demonstrated that a correction should be applied in order to take the refractive index difference at both wavelengths into account. Nevertheless, we have verified experimentally that the two-wavelength source can generate synthetic wavelengths as small as $90\,\mu$m with an accuracy better than 0.2 ppm. With a phase accuracy better than $2\pi/200$, this synthetic wavelength allows to resolve the optical wavelengths and therefore to reach finally nm accuracy. Using the frequency tuning capability of the ECLD, the two-wavelength source should enable long distance measurements with very high accuracy by using a chain of highly accurate synthetic wavelengths.

We proposed an upgrade of PRIMET which requires only little modification of the current two-wavelength laser source and phasemeters. Three synthetic wavelengths are enough for this absolute PRIMET to enable the calibration of the interferometer over its maximum stroke with nanometer accuracy.

Continuation of this work Currently, the incremental PRIMET is part of a set-up used to test extensively the fringe sensors of PRIMA in laboratory. PRIMA shipment and integration at the Paranal Observatory is scheduled for early 2008. The integration and testing of the instrument is expected to last one year. Therefore, the instrument should be available for observations in 2009.

Concerning PRIMET, the stability and accuracy of the Nd:YAG absolute frequency stabilization is foreseen to be tested after its integration at the Observatory with a self-referenced optical frequency comb in partnership with Menlo Systems. No mean of periodically calibrating the wavelength is expected to be used.

The development of an absolute PRIMET will be pursued with the goal of presenting a preliminary design review before the end of 2006. Moreover, the knowledge acquired in absolute distance measurement may be useful in the development of the new large scale project of ESO: the construction and operation of an extremely large telescope of diameter up to 60 m. In that framework, absolute distance measurement with nanometer accuracy over several tens of meters may be required for alignment of optical parts. Due to its intrinsic high stability and tuneability, the concept of two-wavelength source proposed in this thesis could be used as a basis of such distance measurement systems. Finally, the first generation of space interferometers, scheduled to be launched in the next decade, may open a new field of application for this concept.